ZÁPADOČESKÁ UNIVERZITA V PLZNI
FAKULTA STROJNÍ

DISERTAČNÍ PRÁCE

2021 Omid Khalaj, M.Sc., Ph.D.

ZÁPADOČESKÁ UNIVERZITA V PLZNI

FAKULTA STROJNÍ

Studijní program:N2031 Strojní inženýrství

Studijní obor: 3911V016 Materiálové inženýrství a strojírenská metalurgie

DISERTAČNÍ PRÁCE

Mechanické chování expandovaného polystyrenu (EPS) za statického a cyklického zatěžování

Mechanical behavior of expanded polystyrene (EPS) under static and cyclic loading

Autor: **Omid Khalaj, M.Sc., Ph.D.**

Školitel: **Prof. Dr. Ing. Bohuslav Mašek, Ph.D.**

Konzultant specialista: **Dr. Ing. Hana Jirkova**

Akademický rok 2020/2021

PROHLÁŠENÍ O AUTORSTVÍ

Předkládám tímto k posouzení disertační práci zpracovanou na téma:

Mechanické chování expandovaného polystyrenu (EPS) za statického a cyklického zatěžování / Mechanical behavior of expanded polystyrene (EPS) under static and cyclic loading

Prohlašuji, že jsem předloženou práci vypracoval samostatně, dle Studijního a zkušebního řádu Západočeské univerzity v Plzni, pod odborným dohledem školitele a s použitím odborné literatury a pramenů uvedených v seznamu, který je součástí této práce.

V Plzni dne:..... .....

Podpis autora

PODĚKOVÁNÍ

Především bych rád poděkoval vedoucímu disertační práce panu prof. Dr. Ing. Bohuslavu Maškovi, Ph.D. a konzultantce pani Dr. Ing. Haně Jirkové, Ph.D. za cenné rady, které mi poskytli během realizace této práce. Mé poděkování patří také všem kolegům z laboratoře experimentálního tváření a metalografické laboratoře a pracovníkům katedry materiálu a strojírenské metalurgie. Dále bych rád poděkoval vedoucímu experimentální a modelovací laboratoře technologické univerzity Khajeh Nasir Toosi (KNTU), panu prof. Dr. Seyed Naser Moghaddas Tafreshimu a všem jeho týmům za podporu rozsáhlých zkoušek.

Autorská práva

ANOTACE

AUTOR	Khalaj, M.Sc., Ph.D.	Omid
STUDIJNÍ OBOR	Materiálové inženýrství a strojírenská metalurgie	
VEDOUCÍ PRÁCE	Mašek, Ph.D.	Prof. Dr. Ing. Bohuslav
PRACOVIŠTĚ VEDOUCÍHO	ZÁPADOČESKÁ UNIVERZITA V PLZNI	
DRUH PRÁCE	**disertační**	
NÁZEV PRÁCE	Mechanické chování expandovaného polystyrenu (EPS) za statického a cyklického zatěžování	

Fakulta: Strojí
Katedra: Materiálové inženýrství a strojírenská metalurgie
Rok odevzdání: 2021

Počet stránek (A4 a ekvivalentů A4)

Celkem	110		**Textová část**	80		**Grafická část**	30

STRUČNÝ POPIS ZAMĚŘENÍ, TÉMA, CÍL POZNATKY A PŘÍNOSY	
KLÍČOVÁ SLOVA	

SUMMARY

AUTHOR	Khalaj, M.Sc., Ph.D.	Omid
FIELD OF STUDY	Materials Engineering and Engineering Metallurgy	
SUPERVISOR	Mašek, Ph.D.	Prof. Dr. Ing. Bohuslav
INSTITUTION	UNIVERSITY OF WEST BOHEMIA IN PLZEN (UWB)	
TYPE OF WORK	**dissertation**	
TITLE OF THE WORK	Mechanical behavior of expanded polystyrene (EPS) under static and cyclic loading	

Faculty: Mechanical Engineering
Department: Materials Engineering and Engineering Metallurgy
Submitted in: 2021

Number of pages (A4 a eq. A4)

Totaly	110		**Text part**	80		**Graphical part**	30

BRIEF DESCRIPTION TOPIC, GOAL, RESULTS AND CONTRIBUTIONS	
KEY WORDS	

KURZFASSUNG

AUTOR	Khalaj, M.Sc., Ph.D.	Omid
STUDIENFACH	Materials Engineering and Engineering Metallurgy	
BETREUER	Mašek, Ph.D.	Prof. Dr. Ing. Bohuslav
INSTITUTION	UNIVERSITÄT WESTBÖHMEN IN PILSEN	
ART DER ARBEIT	**dissertation**	
TITEL	Mechanisches Verhalten von expandiertem Polystyrol (EPS) unter statischer und zyklischer Belastung	

Fakultät: Maschinenbau
Katheder: Materials Engineering and Engineering Metallurgy
Abgeben: 2021

ANZAHL VON SEITEN (A4 a eq. A4)

Total	110		**Text teile**	80		**Grafik**	30

KURZBESCHREIBUNG	
SCHLÜSSELWÖRTER	

Table of Contents

List of Figures

List of Tables

Glossaries

a	Radius of loading plate
D_{10} (mm)	Diameter of soil particles at which 10% of the sample's mass is comprised of particles with a diameter less than this value
D_{30} (mm)	Diameter of soil particles at which 30% of the sample's mass is comprised of particles with a diameter less than this value
D_{50} (mm)	Diameter of soil particles at which 50% of the sample's mass is comprised of particles with a diameter less than this value
G_s	Specific gravity of soil
γ_d (kN/m^3)	Dry unit weight of soil layer
γ_s (kN/m^3)	Unit weight of soil
ϕ (degree)	Soil internal friction angle
C (kPa)	Soil cohesion
E (MPa)	Young's modulus of soil in elastic analysis
K_1	First calibration parameter for nonlinear analysis
K_2	Second calibration parameter for nonlinear analysis
D (mm)	Diameter of the loading plate
u (mm)	Embedment depth of geocell layer
h_s (mm)	Thickness of soil layer
h_{gt} (mm)	Thickness of the upper EPS geofoam layer
h_{gb} (mm)	Thickness of bottom EPS geofoam layer
γ_{gb} (kg/m^3)	Density of the bottom EPS geofoam layer
γ_{gt} (kg/m^3)	Density of the upper EPS geofoam layer
P_t (kPa)	Magnitude of transferred pressure on top EPS layer
σ_C (kPa)	Compressive strength of EPS geofoam (measured at 10% strain in EPS sample test)
d (mm)	Joint separation distance between EPS blocks

SR	Ratio of transferred pressure on EPS geofoam to the compressive strength of EPS ($p_t/\sigma c$)
δ_S (mm)	Settlement of the loading surface/plate from tests or simulation
δ_g (mm)	Settlement on top of EPS geofoam layer from simulation
RSGS	Ratio of loading plate settlement to the settlement calculated on top of EPS geofoam layer ($\delta s/ \delta g$)
$\delta_{r.m.n}$ (mm)	Surface settlement of reinforced system at loading stage "m" and load cycle "n".
$p_{r.m.n}$ (kPa)	Vertical stress at point of interest at loading stage "m" and load cycle "n".
P_s (kPa)	Stable pressure threshold of EPS geofoam.
P_t (kPa)	Pressure transferred on EPS geofoam.
X	Reinforcement status (r for reinforced and u for unreinforced).
n	Number of load cycles, the cycle number is reset to 1 for the first cycle of the second, more highly loaded, stage (1, 101 and 400 indicate the first cycle of both loading stages, last cycle of first loading stage and the last cycle of second loading stage, respectively).
M_R (MPa)	Resilient modulus
m	1 and 2 for the first and second loading stages (applied pressures of 275 and 550 kPa to loading plate), respectively
IF_p	Improvement factor for comparison of reinforced and unreinforced transferred pressures
IF_δ	Improvement factor for comparison of reinforced and unreinforced settlements
υ	Poisson's ratio
Δ (mm)	Resilient deflection under the loading plate

Abstract

Nowadays, development of constructions and infrastructures has been moved to marginal areas due to population growth and thus, variable ground conditions might be encountered frequently along civil projects. With the growing needs for new constructions, novel methods are studied to enable quicker construction of embankments. As a solution, Expanded Polystyrene (EPS) geofoams are frequently used for a broad range of civil engineering, mining and agricultural applications. Performance of EPS geofoam systems is mainly dependent on the overlying soil thickness, density of EPS geofoam layers, thickness of EPS layers and the type and amplitude of applied pressure. Considering reduction in overburden and accelerating construction, EPS geofoam has served as an ultra-light weight material however, studies that consider the effect of these parameters as well as mechanical properties of EPS geofoams are rare, or in some cases non-existing.

To investigate the effect of these factors, a series of small-scale as well as large-scale tests were carried out under static and cyclic loading which then, accompanied with numerical analyses (for the static loading condition). The static small-scale tests were performed by using universal testing machine however the large-scale tests were carried out using special testing box. The box dimensions were 2200x2200 mm in plan and up to 1400 mm in height and loading plate dimension was 300 mm. The repeated loading was applied as 100 cycles of 275 kPa pressure, followed by 400 cycles of 550 kPa pressure (equivalent to 39 kN), with 10 second time per each load application. EPS densities of 14.4 to 28.8 kg/m^3 were tested and gravelly sand was used as the overlying layer.

The uniaxial test results show that a cylindrical shape might have an advantage over the cubic shape due to more uniform pressure distribution on the top and bottom surfaces of the samples. Also, the train rate, can influence both elastic modulus and compressive strength of the EPS geofoam. The results during static loading indicated that increasing soil thickness from 300 to 600 mm reduced settlements by up to 65% and provision of reinforcement could cause up to 54% reduction in surface settlements. Numerical analyses signified that increasing the vertical gap between EPS blocks from 0 to 5 mm substantially increased surface settlement in the unreinforced pavement, though settlements due to gaps were almost diminished by using reinforcement. Under repeated loading, the rut depths reduced by 13.5% and 40.8% with increasing the soil thickness by 33% and 100% from 300 mm, respectively. Increasing thickness of the overlying denser EPS geofoam layer beyond 200 mm (and simultaneous decrease of bottom EPS thickness) would only result in a 20% decrease in the peak settlements at the final loading cycle. EPS density can be reduced to a minimum of 19.4 kg/m^3, provided that 600 mm thick soil layer is used.

Keywords: EPS geofoam, Uniaxial test, plate load tests, lightweight fill, construction, pavements

1 Preface

1.1 Introduction

Geofoam is the generic name given to lightweight blocks of expanded polystyrene (EPS) or extruded polystyrene (XPS). The main purpose of EPS geofoam is to provide lightweight material fill used in highway or railway construction and bridge abutments. Additionally, other areas of application for EPS geofoam includes pipe and culvert protection, thermal breaks (insulation), wave barrier systems, etc. A close view of EPS geofoam is shown in Figure 1-1.

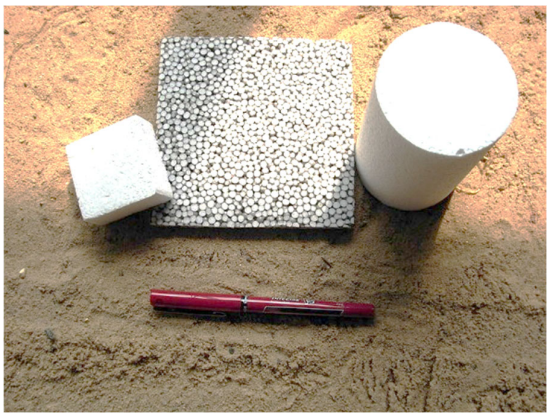

Figure 1-1: Close view of EPS geofoam

The material structure in EPS geofoam consists of abundant open-ended air bubbles that are attached, bonded, or fused together, and sometimes might be bundled together, which is manufactured from the extrusion process of raw polystyrene beads. The individual tubes might have simple random geometric shapes in their cross section (circle, ellipse, hexagon, octagon, etc.), which might averagely vary from less than 1 mm to a few millimeters. When bundled together, the composite resembles a honeycomb in its overall cross section assembly, hence its name – “geocomb”. At the moment, geocomb is only produced from rigid polymers (polypropylene and PVC) materials (Geofoam, n.d.). In this section, first a brief history of EPS geofoam is presented and then, some of the manuals for design with EPS geofoam are introduced.

1.2 Background

The first application of EPS geofoam was in embankments around Flom Bridge in Oslo, Norway at 1972 for reducing settlements. Preceding the installation of EPS geofoam, 20-30 cm of settlement occurred annually in this area, severely damaging the existing road pavements. With the successful outcome of the Oslo geofoam project, a series of international conferences have been started to extend the knowledge, disseminate research, share new application and discus case histories. The first conference of these series was held in Oslo at 1985 (Geofoam, n.d.) [1].

Since then, there have been many successful applications of EPS geofoam in civil engineering projects around the world, mostly due to the advantages it possesses as a lightweight fill. For example, over 1,300,000 m^3 of geofoam was used in 2,000 projects in Japan between 1985 and 1987. These applications include runway fill embankment in Japanese airports, demonstrating geofoam's capability for sustaining heavy and repeated pressure applications. The first use of geofoam in the United Stated took place in 1989 on Highway 160 between Durango and Mancos where a landslide happened due to rain fall and destroyed part of the highway as a consequence. To prevent similar events, geofoam was utilized to stabilize highway side slopes along suspected areas. This method reduced the total cost of the project by 84% compared to conventional renovation techniques.

Figure 1-2 displays a number of EPS geofoam blocks carried to construction. Note the use of weighted anchors to prevent the blocks from being blown around in the wind.

Figure 1-2: EPS geofoam blocks at a construction site

From 1997 to 2001, the largest geofoam project took place in the United States Interstate 15 in Salt Lake City, Utah. Approximately 100,000 m^3 geofoam was used in order to minimize relocation and remolding operations within the project with a total saving around $450,000. Likewise, geofoam was applied in bridge abutments and approaches to increase its base stability. With the achievements of EPS geofoam usage for the I-15 project, Utah Transit officials incorporated geofoam embankments for their light rail (i.e., TRAX) and commuter rail lines (i.e. FrontRunner).

In another project, and the largest one in North America up to 2012, a new highway segment was built in Quebec, Montreal area with 625,000 m^3 of geofoam (from 2009 to 2012). Since 2016, the new elevated Highway 15 and Turcot interchange in Montreal have used a vast amount of geofoam. This brief introduction indicates that the usage of EPS geofoam in civil engineering projects is continuously increasing and it is becoming required for professionals to increase their knowledge regarding this material.

Production of expanded polystyrene is comprised of two processes, pre-expansion, and molding. In the pre-expansion stage, the polystyrene beads are placed in a container and heated to a temperature between 80ºC and 110^{o}C by steam. The result of this process (also called "pre-puff") are polystyrene beads expanded to approximately 50 time larger than their original size. The new polystyrene spheres are then cooled so as to enable their

stabilization process during the next several hours. Subsequently, the pre-puffs are sent into molds and heated by steam for further expansion or possible softening. At this stage, EPS blocks are formed and in the following, they are released from the mold and left for several days to "season". This process must be done to let the blowing agent used in the manufacturing process to diffuse out of the geofoam structure. This allows dimensional changes and swelling related to the completion of the cooling process. The complete procedure is represented in Figure 1-3 [2].

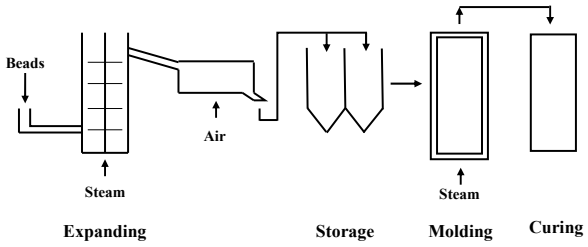

Figure 1-3: Production procedure of EPS geofoam [2]

1.3 Applications

EPS geofoam has been used successfully in a variety of projects including backfill for retaining walls, bridge abutments and as subgrade for roads and highways worldwide [3, 4]. Many countries including, but not limited to, Norway, Sweden, USA, Japan and Turkey have benefitted from ultra-light weight of EPS in a variety of projects. For use as a fill material, EPS geofoam provides a number of advantages for replacing soil. These include:

(a) Low density (circa 1% of soil), which reduces both dead and seismic loads,

(b) Readily cut into variety of shapes,

(c) Easy to install,

(d) Desirable physical and mechanical properties [5].

As the unit weight of EPS geofoam ranges around a typical value of 1% of a conventional soil's unit weight, it helps to reduce dead load, as well as seismic loads, on structures. It can be handled easily and quickly compared to common construction materials (e.g. soil). These attributes greatly assist in speeding up the rate of construction and delivering projects much faster and, therefore, increasing the economic efficiency of the project. Besides these benefits, EPS also contributes to a lighter design of nearby structures (retaining walls, culverts etc.) because of a very low Poisson's ratio and its energy dissipation characteristics (owing to its very low density). A detailed discussion on the benefits of EPS geofoam, plus a detailed characterization is presented by several researchers [4, 6, 7]. Figure 1-4 and Figure 1-5 show practical applications of EPS geofoam blocks in road construction for N201 road in Netherlands and 100 South Street in USA.

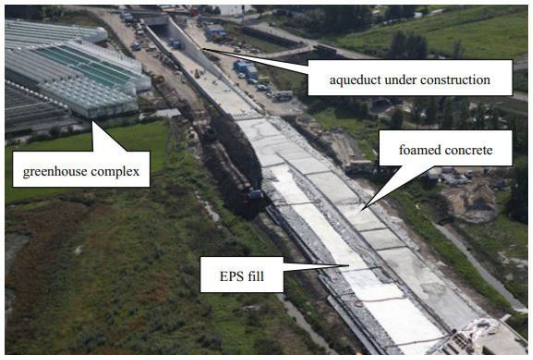

Figure 1-4: View of the N201 road embankment during construction with EPS geofoam [8]

Figure 1-5: Construction of 100 South Street and I-15 with EPS geofoam. Note the proximity of operations with houses and power lines [9]

Despite the application of EPS geofoam over the last 50 years [10], research on the use of EPS geofoam in construction is still ongoing, with improved guidelines and specifications being developed [2, 7]. There are still knowledge gaps that need further investigation; these are introduced in the next sections. Furthermore, road embankments supported on EPS geofoam blocks might face failure or early reduction in the performance due to inappropriate design or usage of EPS or even inefficient load distribution system [11].

Prior to entering the main discussion, a brief overview on typical EPS geofoam applications in construction including road construction and widening, bridge abutments, culverts and pipes and retaining structures and a few case histories related to road construction with EPS geofoam are presented in the following.

1.3.1 Road construction

Today, the need for new roads and highways is growing and many of these infrastructures are built where soil might be incapable of tolerating additional loads. Among various construction techniques and materials available to address these cases, a proficient method would be to use innovative lightweight material (e.g. EPS geofoam) to reduce surcharge and bridge sensitive existing utilities, which accelerates project speed at the same time. Thus, the loading on the underlying soils and nearby structures decrease, as EPS geofoam is much lighter than ordinary soil material (1-2% of soil density). The compressive strength of EPS is sufficiently high to withstand secondary and interstate highway traffic

loads. Furthermore, EPS geofoam is easily handled and does not require special machinery which speeds up construction procedure. Unlike common fill materials that come with complicated QA/QC testing during construction, EPS geofoam production is an engineered procedure and is delivered on site tested QA/QC already [4].

As shown in Figure 1-6, a typical EPS geofoam road section from top to bottom includes: placing a layer of compacted sand at the base of the road section to adjust desired level configuration and free draining construction surface. Below this, EPS geofoam blocks are placed in a staggered manner to prevent vertical joints from aligning in subsequent vertical locations. Moreover, a layer of geotextile could be employed to separate EPS blocks from the overlying soil layer. This separation layer improves the performance of the pavement with two functions. One of them is reinforcing mechanism and the other is increasing the durability of EPS geofoam by avoiding soil particles from damaging EPS surface during and after construction. Depending on the situation, hydrocarbon resistant geomembrane, geogrid, geocell with soil fill, soil cement, pozzolanic stabilized materials or a reinforced concrete slab could be used instead of geotextile. For example, when only fuel spill is a concern, a hydrocarbon resistant geomembrane would be the proper selection. If additional protection against traffic overstressing is required, a reinforced concrete load distribution slab (RCLDS) can be employed to avoid overstressing and hydrocarbon attack simultaneously. Another benefit of RCLDS is its ability to support other anchored structural elements such as tilt-up panel walls, impact barriers, light and power poles, etc. Another examples of using EPS geofoam in road construction are provided in Figure 1-7 [4].

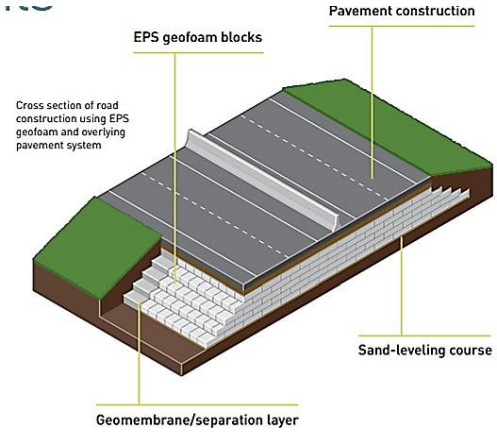

Figure 1-6: Graphic representation of EPS geofoam used for road construction [4]

Figure 1-7: Borman Expressway (Gary, Indiana) reconstruction using EPS geofoam fill [4]

1.3.2 Road widening

Road widening (Figure 1-8) often requires extra fill material which can be expensive and time- consuming. The traditional embankment construction method in these cases involves placing and compacting of subsequent thin layers of soil. When EPS geofoam is considered, the need for compaction and QC/QA procedures is eliminated, reducing construction time and the impact of nearby roads and buried utility lines. The compressive strength of EPS geofoam is high enough to withstand traffic forces without imposing excessive loading to the underlying soil or adjacent structures.

Several lifeline infrastructures including high-pressure gas lines, water mains and communication cables are present in the vicinity of road widening project (parallel or transverse to road); which have to remain in service during construction procedure. In some circumstances, the settlement caused by placing conventional fill soil material would have generated extra stresses or strains in buried utilities. These problems have been solved to a great extent by using EPS geofoam in the backfill. As a brilliant outcome, the I-15 reconstruction project received 2002 ASCE Outstanding Civil Engineering Achievement Award. The decision of the jury was based on the fact that by using EPS geofoam, the completion time of the project was halved and $32 million was saved [4].

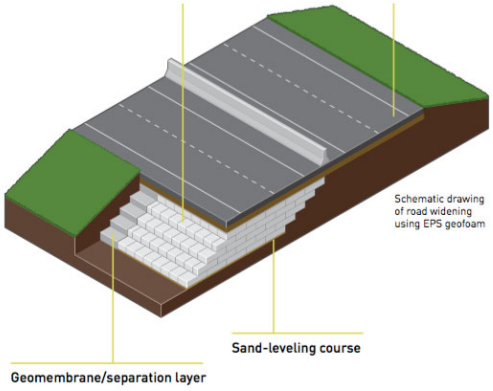

Figure 1-8: Graphic representation of EPS geofoam used for road widening [4]

1.3.3 Bridge supports

Application of EPS geofoam in construction of bridge abutment fills has several benefits; EPS geofoam can impede underlying soil from overstressing imposed the traffic load with its high compressive strength (Figure 1-8). As a result, the differential settlement between bridge/approach fill, construction costs and maintenance costs are reduced. Because of the much lighter weight of EPS compared to soil, the lateral forces of the backfill applied to the abutment walls, foundations and other retaining structures are considerably decreased; which means a great saving for construction of these structures that do not need to withstand significant static/dynamic lateral forced anymore. In the reconstruction project of York Bridge in Washington State, presence of compressible peat and clays soil on the west bank of the Sammamish River led the designers to adopt EPS geofoam to construct the west approach of the bridge. With this method, the potential settlement at the bridge approach the need for relocation of existing lifelines was almost eliminated [4].

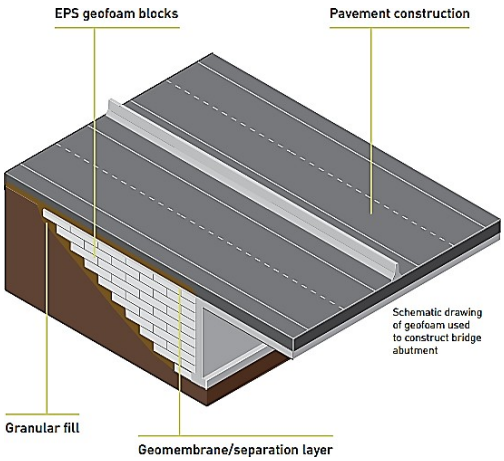

Figure 1-9: Graphic illustration of EPS geofoam used in bridge abutments [4]

1.3.4 Retaining walls and structures

As mentioned for bridge support structures, EPS geofoam can address a similar benefit to retaining structures by the same lateral pressure reduction mechanism. As the density of EPS geofoam is much lower than soil, the horizontal pressure from active soil zone acting on the wall or retaining structure decreases significantly compared to the cases backfilled with soil, thus letting much less robust structure. In addition to static loads, the lower mass of EPS backfill leads to generation of lower earthquake forces on the structure. For sites with shallow ground water and loose soils, proper drainage systems must be installed to avoid development of hydrostatic stress and buoyancy forces on EPS geofoam. A schematic view of EPS geofoam used behind retaining walls is shown in Figure 1-9. EPS geofoam retaining wall backfill for West Virginia University student housing project, Morgantown, West Virginia is presented in Figure 1-10 [4].

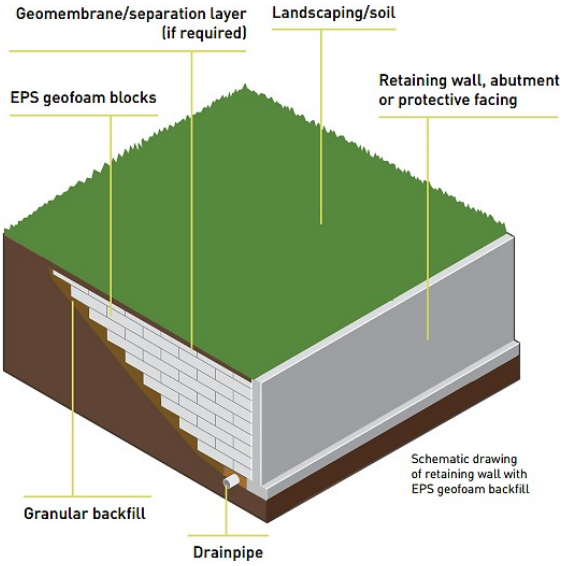

Figure 1-10: A typical view of EPS geofoam for retaining structures [4]

Figure 1-11: West Virginia University student housing project (Morgantown, West Virginia) with EPS geofoam retaining wall backfill [4]

1.3.5 Culverts, pipelines and buried structures

Development plans sometimes require placement of an infrastructure over present underground utility lines and structures that are not originally designed to sustain such an overstressing. In these conditions and instead of strengthening or reinforcing, a set of EPS geofoam blocks could be placed over or adjacent to the existing utilities to prevent the increase in the applied load. A typical overview of such system can be seen in Fig. 1-11 [4].

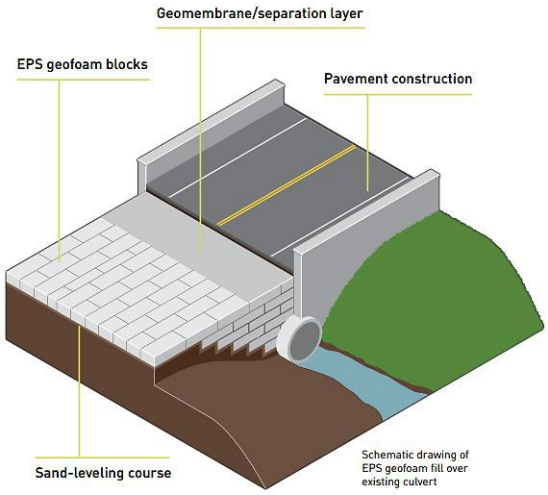

Figure 1-12: Typical overview on the application of EPS geofoam in pipe protection [4]

1.4 Design Manuals

As mentioned earlier, most typical applications of EPS geofoam in the civil engineering industry include road construction and widening, bridge abutments, culverts and pipes and retaining structures; these will be discussed further in the next sections. Based on these applications, several design manuals have been prepared for various areas of EPS geofoam application. The Swedish standard (1987) and the Norwegian standard (1992) are two of the pioneers which tried to provide minimum requirements for safe and reliable performance of

pavement foundations supported on EPS geofoam blocks. Although they seem to involve basic design parameters (e.g. thickness of soil layer), they merely discussed performance of EPS geofoam per se, or as a part of a pavement foundations.

Following those efforts, Stark (2004) summarized the research on EPS geofoam embankments into a conclusive design procedure, incorporating a systematic approach; called "Guideline and Recommended Standard for Geofoam Applications in Highway Embankments", [7]. This guideline is the most complete reference for designing EPS embankments and considers internal stability, external stability, seismic stability, hydrostatic uplift etc. The mentioned document comes with a supplementary guideline called "Geofoam Applications in the Design and Construction of Highway Embankments", [12]. This reference provides comprehensive details regarding response of EPS geofoam material, concepts of the design methodology, external and internal stability concepts, design examples, construction practices, Quality Control (QC) / Quality Assurance (QA) issues and a few case histories. This guideline can be addressed as the most detailed reference presenting design concepts and procedures for designing EPS geofoam embankments (at least based on the available research up to 2004). At the end of this guideline, some of the future (of course according to the research available at that time period) research topics are also listed, among which using soil reinforcement methods is also addressed.

Most recent reference is "Ground Modification Methods Reference Manual" that mostly presents a summary and guide to previous resources [13]. They show that geofoam is suitable for a wide range of geologic conditions, although the costs might be up to threefold of the conventional fill materials (without considering installation costs), as shown in Table 1-1. Furthermore, "Use of ultra-lightweight geofoam to reduce stresses in highway culvert extension" by Sun et al (2005) provides insight in the area of utility protection [14]. Regarding slope stability design, "Guidelines for geofoam applications in slope stability projects" by Arellano et al. (2011) is also available [15]. It is worth mentioning that research on EPS geofoam is still ongoing and these guidelines may be updated in the future.

Table 1-1: Comparison of conventional lightweight fill in projects [13]

Material	**Total Cost***
Traditional Soil Fill	$563K
Pumice Rock	$633K
EPS-block Geofoam	$1,145K
Expanded Shale Clay	$490
Wood Chips	$545K
Tire-derived Aggregate	$334K

* *Total cost based on material, transportation and longevity costs, does not include installation costs or contractor's overhead and profit*

1.5 Case histories

Three interesting case histories demonstrating special uses of EPS geofoam in construction projects related to road pavement foundations is described here.

1.5.1 Manchester railway bridge replacement

In north-west of England, on the western edge of Manchester, Bridge 193 over a historic, but now empty, channel of the River Irwell channel which had long-term maintenance problems. It was decided to replace it with a new embankment to be built under the old bridge so that the railway could remain open during the works. Geotechnical investigations showed a relatively shallow water table with a variety of complications (including a thick layer of weak soil, layers of soap-works waste, dredging deposits, arsenic and other dangerous substances) as listed in Table 1-2. A schematic side view of the bridge and project conditions is shown in Figure 1-13. Furthermore, with a work room less than 10 m under the bridge, most of the rehabilitation methods were not suitable. EPS geofoam was found to be a good solution for the following reasons: much less disturbance was caused to the ground and less headroom was needed compared to a piled foundations and other solutions [16]. In particular, the contaminated ground could be left safely in place, without being disturbed and without being significantly stressed. Either might have caused contaminants to spread while excavation would have been extremely costly due to the need to take the contaminated soil to a licensed hazardous waste dump.

Table 1-2: Main problems at project site [16]

Type of Constraint	Description
Construction	Deep layers (up to 8m thick) of weak and compressible soils, soft clay silts and soap works waste – High water table
Contamination	Soils and groundwater were chemically contaminated
Client Requirement	Railway had to be kept operational throughout construction, except for 100-hour possession period

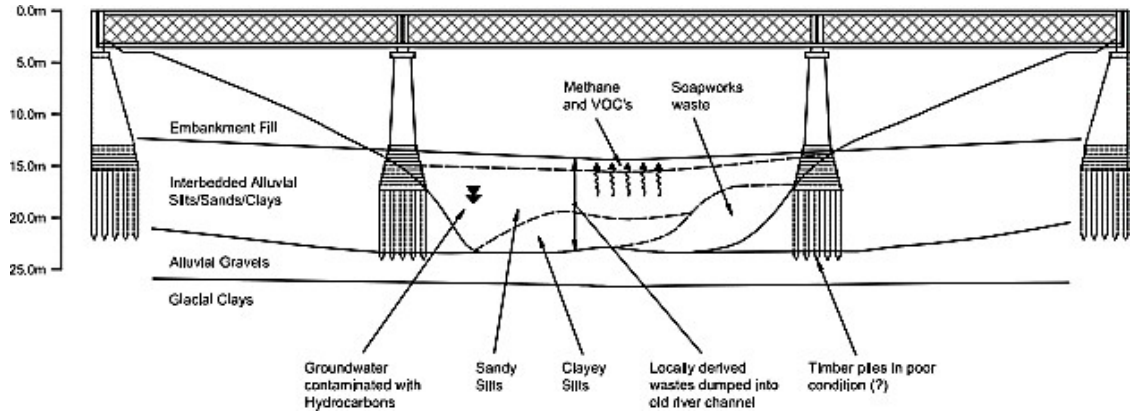

Figure 1-13: Schematic side view of the old bridge and underground conditions [16]

1.5.2 First application of EPS geofoam for road embankment in Turkey

EPS geofoam was used for roadway embankment construction in Turkey in 2017 for the first time. The construction site involved two 2.2 m diameter water pipes placed at 3.8 to 5.6 m below the embankment foundation level. With the help of EPS geofoam, additional cost for relocation of these water mains within a complicated and busy urban environment was prevented and the possible damage to these utilities due to conventional fills was minimized. Furthermore, this method did not cause any interruption in the water service during construction (see Figure 1-14). The EPS embankment was carefully instrumented and monitored for possible distress or deformation during construction and for a period of ten months after opening to traffic. It was observed that the measured parameters remained within the safe and allowable limits [17].

Figure 1-14: Construction area of the EPS geofoam embankment [17]

1.5.3 Watford junction replacement station platform

At Watford Junction station in the UK, on one of the major rail lines north from London, a timber-supported platform needed replacement. The existing platform was supported on concrete sleepers placed more-or-less directly on the ground surface. Electrical or telecommunication cables were fixed to the timber supports. Cutting the cables and rewiring would have necessitated temporary closure of the rail line due to the need for the replacement wires to be tested to check that none of the signal interlocking had been compromised. To install foundations for the replacement platform compliant with modern structural requirements would also have necessitated closure of the rail line. For these reasons brick- built, precast concrete, steel framed or glass-reinforced-plastic framed solutions were all rejected in favor of EPS blocks with precast concrete capping to provide the surface. The EPS was faced in fire-resistant covering. The cables which were simply moved sideways into cut- outs made in the EPS. The existing catenary and lighting posts were retained and the EPS cut to go around them, avoiding any need to provide new earthing connections. In this way the platform was replaced in 48 hours at the Christmas period when the rail network is non- operational. A picture of a similar platform is shown in Figure 1-15.

Figure 1-15: Installation of a replacement platform, similar to that at Watford, using geofoam

1.6 Problem statement

As mentioned, design and construction of road embankments might involve significant challenges. Dead weight of the embankment fill generates long-term settlements in the subsoil that might require expensive pre-loading with wick drains. In extreme cases a bridge with limited soil improvement at the foundation intervals might be required. Additionally, sourcing and movement along existing highway networks by many trucks is associated with noise, dust, emissions and congestion for a lengthy period. By introducing lightweight materials, such as EPS geofoam, the construction industry can overcome many of the mentioned difficulties and resolve further issues [3, 6, 18-20]. Despite solving most of the above problems, there has been a few failure events (excessive settlement, rutting etc.) related to improper usage or design of an EPS system in a highway – where the misunderstanding about the behavior of EPS in that application was determined to be the main reason. Failures in pavements including EPS geofoam might have led to many designers avoiding its application despite the great features it can provide [11]. Hence, similar to other novel methods, evaluation of unknown (or less known) aspects of designing and building EPS geofoam subgrades seems to be essential. This has created a motivation for the current study with the aim of producing a better understanding and elimination of current shortcomings.

It has been noted that to enable widespread usage of EPS geofoam and to update current standards, further research considering various loading conditions and improvement methods is required in this area [2]. Moreover, approximately 80% of roads are unpaved in the world and most of them are low-volume [21]. Around 20% of pavement failures are due to insufficient structural strength, which might arise during construction or service period of pavements supported on EPS geofoam [22]. Proper measures for improving overall strength, reducing costs and decreasing repair necessities should be provided to overcome narrow resources for repair, keeping and recovery of low-volume roads [21, 23].

Application of EPS geofoam in construction practice is rising continuously, as its valuable features are becoming evident more than ever. However, a true cost-effective approach with respect to real behavior of EPS in actual conditions is nearly neglected by existing guidelines [12]. As the required volume of EPS for highway construction is very high, reducing the density of EPS even if it is a minor reduction, contributes to a huge reduction in the overall cost of the project. The above discussion suggests that implementation of EPS geofoam should be done with more consideration and further research is postulated regarding a safe and efficient design.

The growth rate in this technology can only be sustained where methods to enhance its use and to overcome failure are in place. With regard to the latter, early rutting (and possibly tension cracking) of overlying pavement surfaces have been observed [11]. This may be attributed to lack of support from the underlying EPS geofoam [24], which can result in punching of concentrated loads into the EPS geofoam due to inefficient load spreading above the EPS layer. This phenomenon might be due to the collapse of the foam bubbles giving it, in effect, a negative Poisson's ratio [25]. EPS geofoam contrasts with common soil backfills: its Young's modulus is comparable to very soft soils, its compressive strength is lower than most soils, it has different visco-elastic and visco-elasto-plastic behavior under cyclic loading [26, 27] and it has differing stress-strain response, with a wide range of plastic strain sustained under loading [3, 28]. Furthermore, EPS geofoam is more expensive compared to soil or common low-density materials, thus its consumption (in terms of bulk density) has to be minimized. By utilizing appropriate methods, e.g. as investigated in this study, the load applied on the pavement surface may be handled such that the stress applied to EPS geofoam remains within a safe margin.

1.7 Objectives

With the above background, a series of experimental tests planned to find out the exact behavior of EPS blocks prior to large scale complex tests. The results from this series may be later use to make a numerical analysis for further prediction of EPS behavior using in different constructions. Besides, a number of large-scale tests were accomplished to find out the exact behavior of EPS blocks, soil and the full road section comprised of soil layer over several layers of EPS block under application of repeated loading. Sample sized tests on cylindrical EPS geofoam blocks by uniaxial repeated and static test will also conduct to characterize the behavior of EPS geofoam. It would be worthwhile to characterize the effectiveness of geocell reinforcement on improving the performance of pavement foundation supported on EPS geofoam blocks. Considering previous research and preliminary evaluations prior to main tests, several factors (e.g. reinforced and unreinforced soil thickness, EPS density, etc.) were found out to be essential and need further investigation. The main parameters that were measured for performance evaluations include surface settlements and the transferred pressure intensity on EPS geofoam; with their diagrams plotted for discussions and elaborations.

A summary of the key objectives of the experimental program using small scale model can be described as:

- Exploration the characteristic of EPS Geofoams under different loading conditions,
- Evaluation of pressure distribution with depth of EPS embankments,
- Exploration of performance of EPS embankments compared with soil embankments,
- Assessment of effects of EPS size, density, strain rate and loading conditions

With cooperation of Khajeh Nasir Toosi University of Technology, a large-scale experimental test also performed to achieve the following goals:

- Assessment of effects of repeated loading intensity, soil and upper EPS layer thickness, EPS density (stiffness) and thickness of EPS block layers on surface settlement, resilient modulus and transferred pressure on EPS geofoam blocks,
- To determine the simultaneous effect of soil thickness on the behavior of pavement foundations resting on EPS geofoam,
- To determine the effect of soil layers over EPS geofoam, and,
- To describe the effect of EPS densities on the performance of EPS pavements overlaid by geocell reinforced soil.

To achieve these, a series of uniaxial tests as well as full-scale static and repeated plate load tests were conducted. In addition to the experimental tests, a shortened Finite Element analysis used to assist with better understanding of mechanisms, and interpretation of experimental results.

1.8 Research limitations and outline

This study is placed within material aspect of EPS geofoam pavement foundation and application of geofoam for increasing the performance of such foundation systems. The basis of research is on large scale plate load tests performed on one type of EPS geofoam (originated from one specific molder), one type of soil, one loading frequency and one loading plate size. Therefore, the results might be subject to change if different materials, loading frequency or dimensions are used. As the main framework of this research is experimental, the numerical modeling is very basic and simulations are limited to static loading. The constitutive model used for EPS geofoam is very simple, future research should consider robust constitutive models for evaluation of EPS geofoam behavior. Nevertheless, the observed trends are not expected to dramatically change for similar configurations to those used here. Future research can extend this work to assess other possible factors including soil type, loading frequency and reinforcement type and the presented results could assist in future numerical or analytical developments.

2 Literature Review

2.1 Introduction

According to the previous chapter, soil and EPS geofoam are the major elements of the pavement foundation systems in this study. First, a short review of soil behavior under repeated loading is presented in Section 2.2. Then, selected research on EPS geofoam foundations is introduced in Sections 2.3. After reviewing production method of EPS geofoam in section 2.3.1, a review of general properties of EPS geofoam and the most important guidelines for design and construction with EPS geofoam are presented in Section 2.3.2 and 2.3.3, respectively.

2.2 Soil

To address the mechanism involved in the soil behavior (unsaturated) subjected to repeated loading, the deformation of granular material under traffic loading can be simply categorized into recoverable (resilient) and residual deformation (see Figure 2-1). Resilient response demonstrates the load bearing ability of the pavement structure and the residual strain response is representative of the long term performance and rutting phenomenon in the pavement [29].

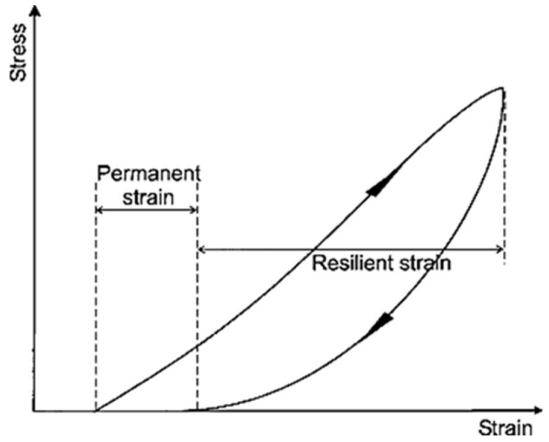

Figure 2-1: Residual and resilient deformation in soil under one loading cycle [29]

These behaviors originate from the inter-particle and particle properties of soil medium. The exact nature of aggregate deformation mechanisms during load repetitions is not fully understood yet, but three main mechanisms can be postulated: consolidation, distortion, and attrition. These mechanisms are the result of soil compaction, sliding/rolling (for rounded aggregate) or bending (for flat aggregate) and particle crushing, respectively. Combination of these mechanisms in the microscopic level leads to volumetric, shear and simultaneous occurrence of these deformation modes [29]. Effect of important relevant factors on the resilient and residual responses are discussed in the following.

2.2.1 Resilient response

While many factors affect the resilient behavior of granular pavement material, stress parameters have the most significant effect. It has to be noted that the load duration and frequency of loading has insignificant or no influence on the resilient behavior of granular soils. Yet the resilient modulus of the granular material is considerably dependent on the confining pressure and sum of the principal stresses. With increase in the confining stress and sum of principal stresses, the resilient modulus considerably increases. It has been shown that with increase in the confining stress from 20 to 200 kPa, resilient modulus increased by 500%. However, under constant confining stress, the resilient modulus is practically unaffected or slightly decreases by the magnitude of the deviator or shear stress, provided that plastic deformations do not increase significantly. The investigation on the effect of stress history and loading cycles have showed that slight changes might appear due to progressive densification and rearrangement of the soil particles. Other observations have shown that after approximately 100 cycles of the same stress (up to 25000 repetitions), the effect of stress history is almost omitted, again if the applied stress is not large enough to generate excessive residual deformation in the pavement material [29].

2.2.2 Residual strain response

Residual strain accumulation is inversely dependent upon confining pressure and directly related to the magnitude of deviator stress. In fact, some form of deviatoric to confining pressure ratio governs the granular soil behavior under repeated loading. However, the failure of granular material under repeated loading is a gradual process and does not occur suddenly like static loading, therefore ultimate shear strength is not completely relevant when such incremental behavior is encountered. In real condition, stress orientation affects the behavior, but it is not fully understood yet. With rotation of the principal stress direction under real loading condition, some sort of densification might occur in the soil and result in reduction of the residual strain rate with increasing load cycles, consequently causing a reduction in the proportion of residual strain to resilient deformation. The magnitude of shear stress is influential in this process. While some observations indicate constant increase in the residual deformations of the pavement under repeated loading (for instance linearly with logarithm of the number of load cycles), others indicate that an equilibrium state is achieved after about 1000 load cycles, such that a limit value can be defined for the accumulation of plastic strains. This equilibrium is more likely to occur when the applied stress is sufficiently low [29]. With inclusion of geocell reinforcement, residual deformations reduce and resilient modulus increases with increasing loading repetitions [30].

2.2.3 Shakedown concept

In pavement design practice, the residual deformation of each layer should be limited to zero or very small values. Studies have shown that when the applied stress ratio is small ($\Delta\sigma1/\sigma3$, where $\sigma1$ is vertical pressure and $\sigma3$ is the radial pressure), the residual deformations might finally get into an equilibrium state (residual strain growth stops with further load repetitions). With increasing the additional (deviator) stress ratio, the growth in

residual deformation continues and finally results in failure. To prevent the onset of residual deformations, the applied stress level must be limited to the value associated with resilient response. The critical stress level that distinguishes between stable and unstable behavior of pavement is marked as “shakedown limit” [31]. Considering granular material behavior under various load levels, there major type of behavior (based on the ranges observed in Figure 2-2) can be identified in Figure 2-3: (A) Plastic shakedown, (B) Plastic creep and (C) Incremental collapse.

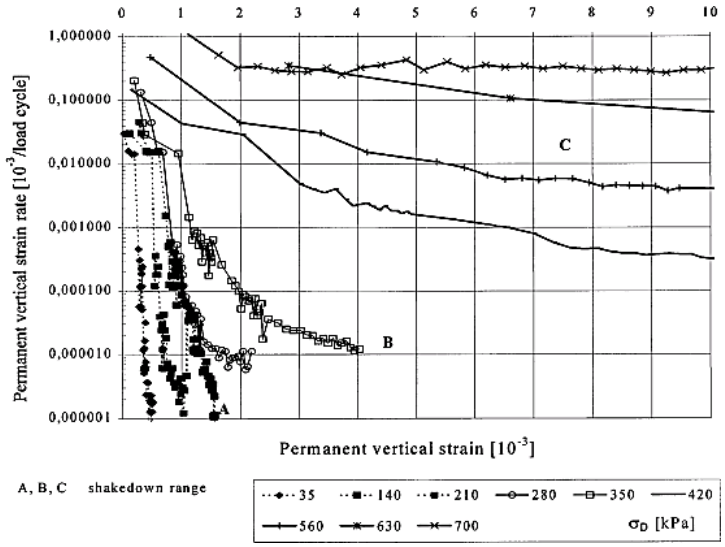

Figure 2-2: Variation of residual vertical strain rate with residual vertical strain [31]

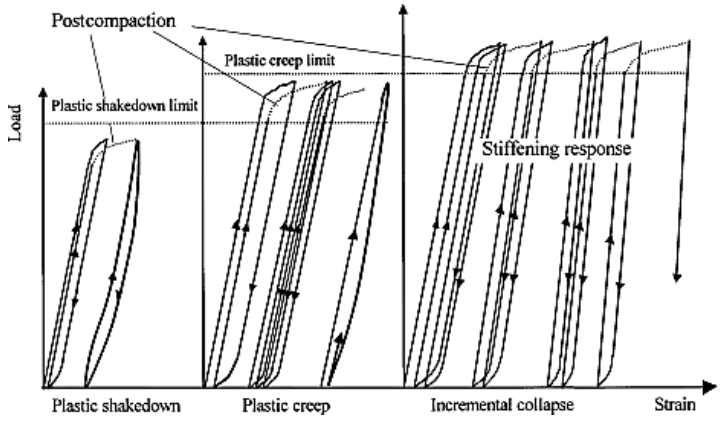

Figure 2-3: Classification of granular material response under repeated loading [31]

Plastic shakedown occurs when rate of plastic deformation gradually decreases and accumulation of residual deformation stops after a certain number of load applications, leading to a final constant strain value. On the other side, incremental collapse involves progressive increase in plastic deformation with load repetitions and the strain rate decreases very slowly, or not at all. This behavior results in generation of ruts (and finally, failure) in the pavement. Plastic creep behavior places between these two ranges: the rate of plastic deformation which was initially high, reaches to a constant value (an approximate

linear increase in residual deformation). In microscopic scale, no or slight particle breakage happens. While plastic creep and incremental collapse are associated with particle wear damage and total particle breakage, respectively. These behaviors are dependent on the material and loading level. Incremental collapse must be avoided, while the other two responses could be acceptable [31].

2.3 EPS geofoam

2.3.1 Production of EPS geofoam

Production of expanded polystyrene is comprised of two processes, pre-expansion, and molding. In the pre-expansion stage, the polystyrene beads are placed in a contained and heated to a temperature between 80ºc and 110ºc by steam. The result of this process is polystyrene beads (also called “pre-puff”) expanded to approximately 50 time larger than their original size. The new polystyrene spheres are then cooled so as to enable their stabilization process during the next several hours. Subsequently, the pre-puffs are sent into molds and heated by steam for further expansion or possible softening. At this stage, EPS blocks are formed and in the following, they are released from the mold and left for several days to “season”. This process must be done to let the blowing agent used in the manufacturing process to get out of the geofoam structure. This allows dimensional changes and swelling related to the completion of the cooling process. The complete procedure is represented in Figure 2-4 [2].

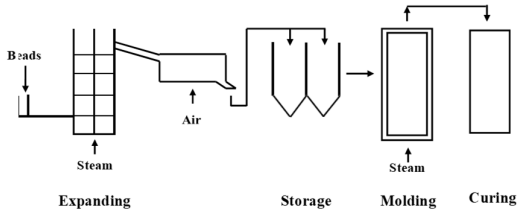

Figure 2-4: Production procedure of EPS geofoam [2]

After the production is complete, the blocks are cut and trimmed (due to improper molding) prior to transportation. In trimming, thin pieces of material is sliced off from one or more faces of EPS geofoam blocks to establish a maximum specific tolerance of ±0.5 in flatness, squareness, length, width or thickness in EPS blocks. Since calculations of design guidelines are based on the full contact on the full-faces area of EPS blocks and there will be horizontal gaps between untrimmed blocks, the actual stresses will be underestimated and localized stress concentration will occur. As a consequence, excessive total and differential settlements are generated and leads to serviceability failure when untrimmed blocks are used. Besides, improper molding might involve concavity in blocks and in excessive cases, water may pond on the blocks and absorbed by them. Subsequently, the unit weight of the blocks increases and cause excessive pressure that might generate extra settlement and pavement reconditioning. In addition, large EPS blocks are cut into two or more portions to meet the size requirement of particular projects [2].

2.3.2 Properties of EPS geofoam

The engineering properties of EPS geofoam can be categorized into three main groups: physical properties, static properties and dynamic/cyclic properties. Standard procedures for characterizations exist; some of these are currently available as listed in Table 2-1:.

Table 2-1: Standards related to EPS geofoam and its application

Standard No.	**Description**
ASTM D 7180-05	Standard Guide for Use of Expanded Polystyrene (EPS) Geofoam in Geotechnical Projects
ASTM D 6817-17	Standard Specification for Rigid Cellular Polystyrene Geofoam
ASTM C 578-19	Standard Specification for Rigid, Cellular Polystyrene Thermal Insulation
ASTM D 1622-08	Standard Test Method for Apparent Density of Rigid Cellular Plastics
ASTM D 1621-00	Standard Test Method for Compressive Properties of Rigid Cellular Plastics

In the following sections, the most important characteristics of EPS geofoam are described.

2.3.2.1 EPS Density

Because density of EPS material is very low (as little as 0.01 of commonly used fill materials, see Table 2-2), it is an exceptional fill material. The engineering properties of expanded polystyrene including Young's modulus and creep behavior are directly associated with its density. Therefore, it is essential to use the appropriate EPS density in specific applications.

Table 2-2: Density range for typical lightweight fills [2]

Lightweight Fill Type	**Range of Density (kg/m^3)**
Geofoam (EPS)	12-35
Foamed concrete	335-770
Wood fiber	550-960
Shredded tires	600-900
Expanded Shale and Clay	600-1040
Fly-ash	1120-1440
Boiler Slag	1000-1750
Air Cooled Slag	1100-1500

For instance, the optimum value of EPS density in highway embankment construction is typically in the range between 16 and 32 kg/m3, although densities up to 100 kg/m3 are sometimes used where high strength, exceptional load spreading and/or low compressibility are required [16]. EPS geofoam is manufactured in typical densities around the world according to the local standards [2]. According to ASTM C 578-19 and ASTM D 6817-17, some of these typical values are provided in Table 2-3.

Table 2-3: EPS geofoam densities [2]

ASTM C 578 Type	Density (kg/m^3)	ASTM D 6817 Type
I	15	EPS15
II	22	EPS22
VIII	18	EPS19
IX	29	EPS29
XI	12	EPS12

2.3.2.2 Typical stress-strain behaviour

A typical stress-strain curve of EPS geofoam under static loading is displayed in Figure 2-5. The figure generally consists of four distinguishing parts including: zone 1: an initial linear elastic response, zone 2: yielding, zone 3: linear + work hardening, and zone 4: nonlinear + work hardening [7]. To define the initial elastic limit and compressive strength of EPS geofoam, the stress at 1% and 5% (or more commonly 10%) strain is taken into account [5].

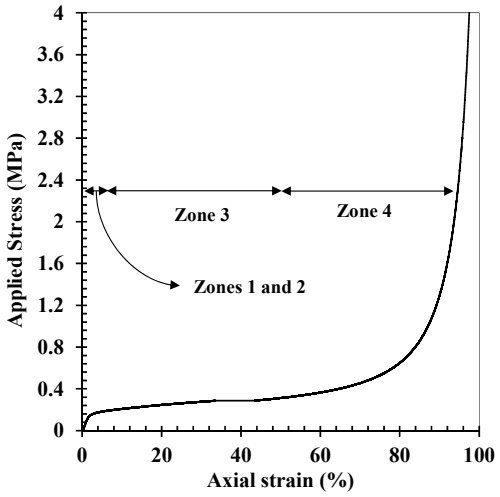

Figure 2-5: Typical stress-strain curve of EPS geofoam

2.3.2.3 Young's modulus and Poisson's ratio

Young's modulus and Poisson's ratio of expanded polystyrene is typically obtained from uniaxial compression tests on 50 mm samples of EPS geofoam according to ASTM D 1621-00,

EN 826, and ISO 844. As mentioned, these parameters are directly related to the density of EPS geofoam. However due to the absence of a standard test procedure, a widely accepted relation between EPS density and its elastic parameters does not exist in the current literature [7].

According to Figure 2-6 and supposing that the EPS is of proper quality, an average of the linear empirical equations between EPS density and initial Young's modulus of EPS (E_{ti}) can be presented as Equation 2-1:

$$E_{ti} = 450\,\rho - 3000 \qquad \textit{Equation 2-1}$$

Where E_{ti} has units of kPa and ρ = EPS density in kg/m^3.

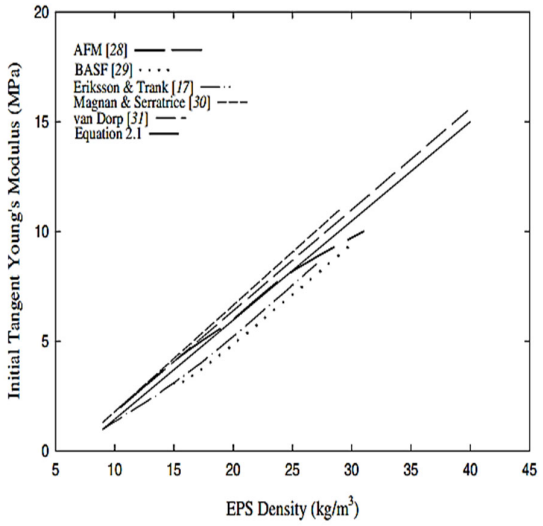

Figure 2-6: Variation of initial Young's modulus with EPS density [7]

To estimate Poisson's ratio of EPS geofoam, the following Equation 2-2 is suggested by EDO-EPS of Japan:

$$\upsilon = 0.0056\rho + 0.0024 \qquad \textit{Equation 2-2}$$

Where, υ = Poisson's ratio of EPS ρ = Density of EPS (kg/m^3).

However, Poisson's Ratio values are highly variable with strain level as, once cells in the foam start to break, the polymer walls contract and the EPS volume decreases and can even result in an apparent negative value!

2.3.2.4 Compressive strength

The compressive strength of EPS is a significantly important parameter due the predominant mode of loading (i.e. compression) in geotechnical applications. As previously mentioned, the compressive stress sustained at 10% strain is taken as the compressive strength of EPS by ASTM standards (see Table 2-4 for typical values). At this stress level, the EPS geofoam crushes one-dimensionally into solid particles and a general rupture failure does not take place. Note that there is nothing fundamental about a strain level of 10

percent (or 5 percent for that matter) in Table 2-4. except that it is located after the initial yielding region of the EPS.

Research indicates that the compressive strength of EPS does not correlate directly to the creep behavior. Therefore to prevent long-term consequences of permanent loading, it is suggested that the designers keep the applied pressures in the elastic range, which is defined as 1% of compressive strain in a rapid loading test [2].

Table 2-4: EPS geofoam compressive strength [2]

Physical Property	EPS12	EPS15	EPS19	EPS22	EPS 29	EPS39
Compressive Resistance at 1 % Strain (kPa)	15	25	40	50	75	103
Compressive Resistance at 5 % Strain (kPa)	35	55	90	115	170	241
Compressive Resistance at 10 % Strain (kPa)	40	70	110	135	200	276
Flexural Strength (kPa)	69	172	207	240	345	414

The compressive strength of EPS geofoam grows linearly with increasing EPS density, hence the following suggested correlation (Equation 2-3):

$$\sigma_{c10} = 8.82\,\rho - 61.7$$ *Equation 2-3*

where σ_{c10} = compressive strength (defined at 10% compressive strain) in kPa and ρ = EPS density in kg/m^3.

2.3.2.5 Shear strength

The shear strength of EPS geofoam is categorized into two separate types, internal and external shear strengths. The internal shear resistance is related to the resistance against sliding along planes that may develop inside the material while the external shear strength is associated with the resistance of the interface between EPS blocks, or the sliding resistance occurring at the contact surface of EPS geofoam and other materials. Research has shown that the internal shear strength of EPS geofoam is directly related the density of the EPS geofoam. As the density is increased, the shear strength is increased. To obtain internal shear resistance, the rapid loading method on the EPS geofoam specimen is adopted until reaching the maximum shear stress. The shear strength at the EPS/EPS contact surface could be approximated using the traditional Mohr-Coulomb formulation shown in Eq. 4-4. It is obvious that the shear strength depends on the vertical pressure at the interface of the blocks, originated from surcharge loads and weight of the EPS blocks. If additional shear strength is needed, special connectors might be utilized to limit relative lateral movement of the blocks [2].

$$\tau_e = \sigma_n \tan \phi$$ *Equation 2-4*

where

τ_e = external shear strength at the EPS/EPS contact surface (kPa)

σ_n = vertical pressure produced at the EPS/EPS interface (kPa)

ϕ = interface friction angle between EPS blocks (degrees)

The test procedure introduced by ASTM D5321-19 is recommended for determination of interface friction angle, which is typically between 27° and 32°. The above equation can also be used for calculating the external shear strength at the interface between EPS geofoam and other materials. The friction angle is different in this case; however, a designer can assume 30º for the frictional angle between sand and EPS geofoam. In one study, the friction angles of EPS/geomembrane and EPS/geotextile interfaces were taken to be 55° and 25°, respectively [2].

2.3.2.6 Behavior under cyclic/dynamic loading

Cyclic loading is defined as the loads that are applied, removed and reapplied, e.g. on a pavement, in a relatively rapid and repetitive form. Current research shows that when the amplitude of applied pressure is kept under the elastic stress limit (σ_e), there is:

no residual strain after the removal of the applied stress,

no reduction in the Young's modulus during cyclic loading.

The initial Young's modulus, E0, can be obtained from cyclic uniaxial tests. Trandafir and Erickson (2011) used a loading frequency of 1.5 Hz and various geofoam densities (15–25 kg/m^3), measuring the E0 value (in kPa) at a cyclic axial strain amplitude, εac, of 0.01%. Then, using a regression techniques they obtained the relationship given in Equation 2-5 and illustrated in Figure 2-7 [32].

$$E_0 = 59.93\rho^3 - 1622.8\rho + 15602 \qquad \textit{Equation 2-5}$$

where ρ is the geofoam density expressed in kg/m^3.

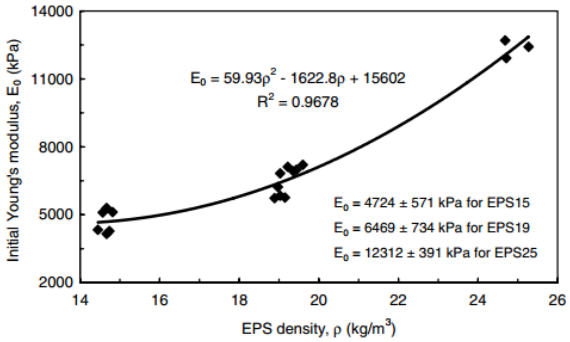

Figure 2-7: Variation of the Initial Young's modulus with geofoam density [32]

However, with increasing the applied pressure beyond the elastic limit, residual deformation and modulus degradation will occur. Degradation in elastic modulus is well demonstrated with the progressive flattening of the loading-unloading curves (see Figure 2-8). This figure is the result of rapid cyclic loading on a 50 mm cubic specimen with density of 13 kg/m^3. The loading amplitude was in the post-yield range, i.e., the applied stress was beyond the elastic stress limit. As can be seen in Figure 2-8, the average of tangential Young's modulus decreases with increase in load cycles and is smaller than the initial tangent Young's modulus. When increasing the strains to very large values (substantially beyond those tolerable in practice), Young's modulus increases [7].

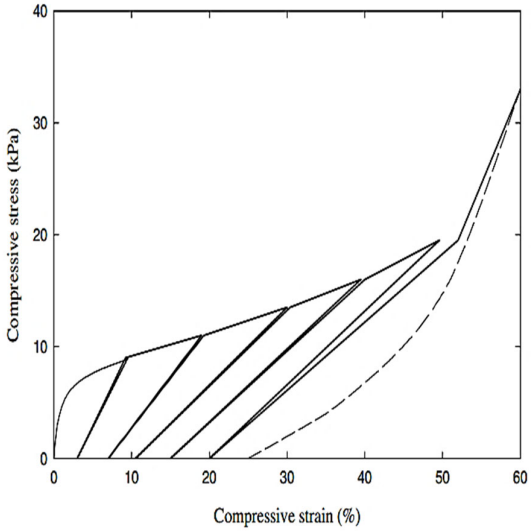

Figure 2-8: Typical stress-strain curve of EPS geofoam subjected to cyclic loading [7]

2.3.2.7 Dynamic characterization

Accepted theory for linking shear modulus, G, and Young's modulus, E, of EPS geofoam has not been developed yet. However, a simplified empirical expression to estimate average properties of cellular foams, based on the theory of elasticity, has been expressed as [33]:

$$G = \alpha \frac{E}{2(1+\upsilon)}$$ *Equation 2-6*

Where υ is Poisson's Ratio, as before.

Based on triaxial test results, values of α vary between 1.5 and 2.2, which include most applications of EPS geofoam. However, more research is required to prove these values. Based on Figure 2-9, with growth in shear strain, shear modulus reduces and damping ratios increase. For shear strains between 10-4 and 10-1%, shear modulus and damping ratio remain almost constant and then vary significantly with further increase ins shear strain [33].

As mentioned in previous sections, shear modulus and damping ratio is closely related to the EPS density (ρ) and the applied confining stress (σ3). Similar to the model derived for clay material, the following equations are obtained to estimate dynamic parameters of EPS geofoam [33]:

$G = (G_{min} - G_{max})\, H(\gamma) + G_{max}$ *Equation 2-7*

$\lambda = (\lambda_{max} - \lambda_{min})\, H(\gamma) + \lambda_{min}$ *Equation 2-8*

$$H(\gamma) = \left[\frac{(\gamma/\gamma_r)^{2B}}{1 + (\gamma/\gamma_r)^{2B}}\right]^A$$ *Equation 2-9*

Where, γ_r is a reference strain at 50% of the maximum shear modulus. A and B are dimensionless parameters dependent of EPS density, estimated from a multilinear fitting method for 24 kg/m^3 ≤ ρ ≤ 32 kg/m^3 and 0 kPa ≤ σ3 ≤ 60 kPa. These parameters are estimated using the following formula [33]:

$$A = -0.99\left(\frac{\sigma_3}{100}\right)^2 + 0.65\left(\frac{\sigma_3}{100}\right) - 0.40\left(\frac{\rho}{10}\right)^2 + 0.22(\rho) - 1.92$$ *Equation 2-10*

$$B = 0.26\left(\frac{\sigma_3}{100}\right)^2 - 0.7\left(\frac{\sigma_3}{100}\right) + 0.40\left(\frac{\rho}{10}\right)^2 - 0.22(\rho) + 3.61$$ *Equation 2-11*

$$\gamma_r(\%) = 0.40\left(\frac{\rho}{100}\right)^2 + 0.26\left(\frac{\sigma_3}{100}\right) - 0.27(\rho) + 5.09$$ *Equation 2-12*

Using the same method, the following expressions are suggested for computation of G_{max} (MPa) and λ_{min} (%) values (maximum shear modulus and minimum damping ratio, respectively) based EPS density and confining stress [33]:

$$G_{max} = 9.62\left(\frac{\rho}{100}\right)^2 - 2.78\left(\frac{\sigma_3}{100}\right) - 4.66(\rho) + 67.03$$ *Equation 2-13*

$$\lambda_{min} = -1.26\left(\frac{\rho}{10}\right)^2 + 0.36\left(\frac{\sigma_3}{100}\right) + 0.69(\rho) - 8.64$$ *Equation 2-14*

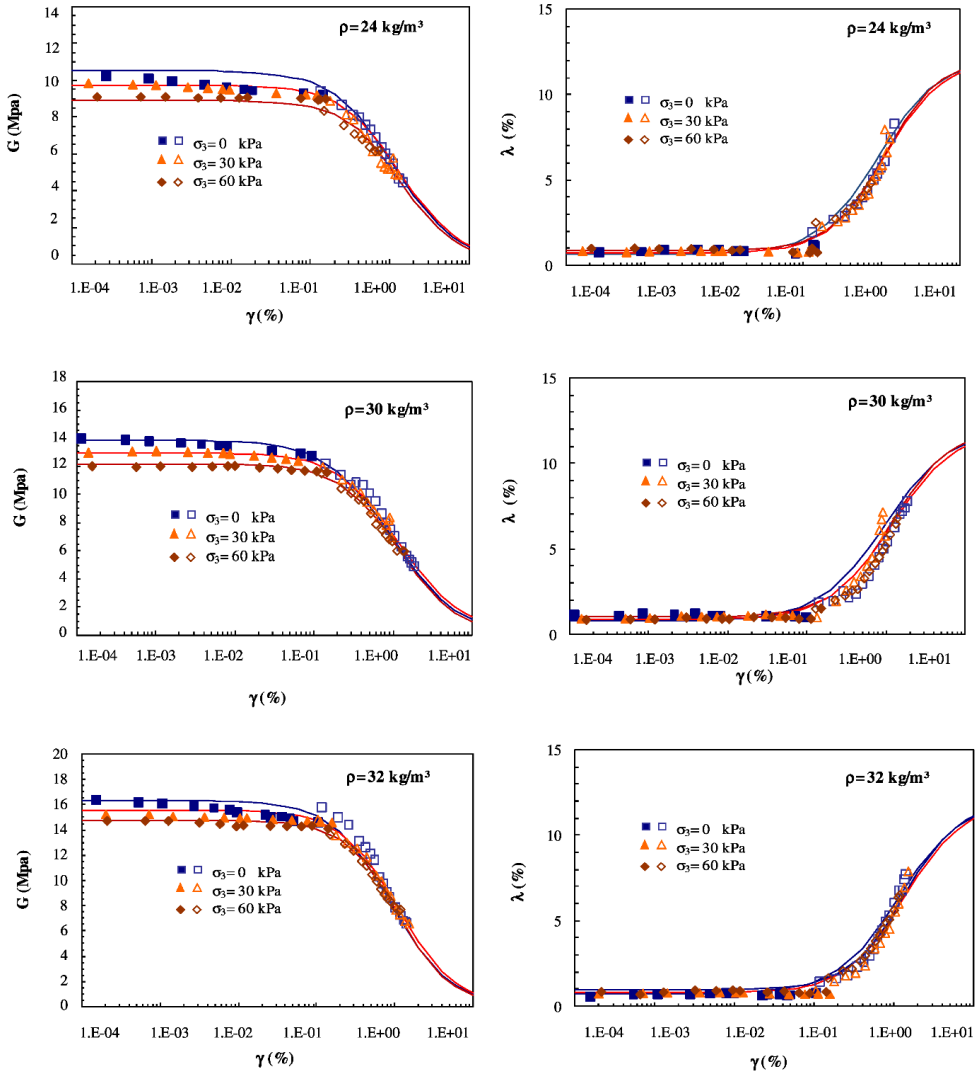

Figure 2-9: Shear modulus and damping ratio curve for EPS from suggested Equations and test results [33]

These equations are used to estimate shear modulus and damping ratio curves based on Equation 2-13 and Equation 2-14. When there is no experimental data in hand, deviator stress-strain curves can be predicted from available literature [33].

2.3.2.8 Creep and time dependent behavior

A permanent dead load applied on to EPS geofoam blocks can trigger creep behavior in an overlying pavement structure after the construction phase. The initial phase of time-dependent creep behavior could start with application of permanent dead load on the pavement structure, closing the gaps between EPS geofoam blocks. The magnitude of such creep deformation is directly dependent on the magnitude of the applied pressure on the pavement. Additionally, it has been shown that once the permanent (continuous loading) exceeds 2% compressive strain limit, creep deformation of EPS geofoam material will start. Designers try to avoid such creep type by keeping the applied pressures within the linear portion of the stress-strain curve of EPS geofoam [2].

Creep behavior of EPS geofoam is determined from testing samples of EPS geofoam. Since smaller samples would overestimate actual strain, the minimum recommended dimension of the specimens is 300 mm to derive an equation for predicting the creep settlement [34]. To use two or three day creep test data for extracting the equation, it is necessary to compare the results of these tests with longer creep test results. Srirajan et al (2001) report that 2 m height with full size block and compressive strength of 100 kPa approximately yielded 1.1% strain during 3 years. 64% of the total strain occurred within the first two days [34].

An empirical Equation 2-15 for total strain (ε) was obtained from tests results performed on 300 mm cubic of EPS20 material. Creep strains would be insignificant for the applied stresses below 25% of the EPS geofoam compressive strength (ε<1%). For operational pressures between 25% and 50 % of strength [34]:

$$\varepsilon = (3\alpha + 0.1) * [(-0.0004D + \beta) * Ln(t) + \gamma] \quad \text{Equation 2-15}$$

where ε = total strain, percent

σ = applied load, kPa

D = density of geofoam, kg/m^3 (12 kg/m^3 - 35 kg/m^3)

t = time, minutes

α, β, γ are parameters as defined below:

$$\alpha = \sigma / (7.5\,D - 41.3)$$

$$\beta = 0.230\alpha - 0.045$$

$$\gamma = -1.95\alpha + 0.985$$

According to this equation, when EPS20 geofoam is subjected to 50% compressive strength, a total strain of 2% would be generated during 50 years. In other words, if the pavement system could withstand 2% long-term creep deformation, a maximum permanent

pressure of 50% of compressive strength would be allowed [34]. Finally, the following issues are notable regarding creep behavior of EPS geofoam:

- EPS Sample size directly affects its creep performance; smaller samples overestimate creep strains due to stress concentration at sample edges and noticeable seating effects,
- For the same applied pressure, denser EPS geofoam demonstrate less creep. The amount of reduction in creep is dependent on the applied stress level. The difference is negligible for the applied pressures around 30% of the compressive strength, while at pressures equivalent to 50 % of EPS compressive strength, the creep can reduce by 25% with an increase in EPS density from 10 to 30 kg/m^3,
- Poisson's ratio reduced with increase in creep strains,
- Using creep tests on large geofoam samples under stress levels up to 50 percent of compressive strength could be indicative of the creep behavior under working loads for geofoam design.

Effect of loading frequency on the plastic yielding of EPS19 under static deviator stress level of 50 kPa and cyclic deviator stresses of 25 and 35 kPa are shown in Fig. 2 6. For both selected cyclic deviator stress amplitudes, plastic strain accumulated under a specific number of cycles is larger for lower cyclic loading frequencies compared to higher loading frequencies [32].

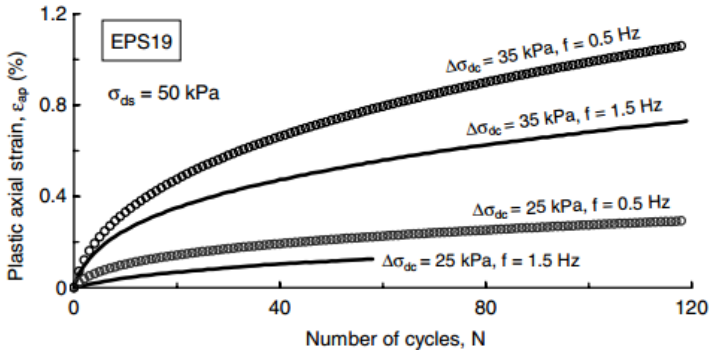

Figure 2-10: Accumulated plastic strain at different cyclic deviator stress amplitudes ($\Delta\sigma_{dc}$) under different loading frequencies (f) [32]

2.3.3 Other important issues

Besides the engineering properties discussed above, there are several issues that must be considered during design and application of EPS geofoam. These include UV protection, fire and solvent risk, environmental hazard, recycling, etc. and are addressed in the following.

2.3.3.1 UV protection

Although EPS geofoam does not deteriorate similar to other geosynthetics products when subjected to ultra-violet light, it is still recommended to protect it from direct sunlight to prevent its surface from becoming yellow after a few weeks. Depending on the geometry

of the EPS geofoam on the site, a suitable type of covering system should be selected. Often a covering will serve several purposes such as excluding light, solvents and water.

2.3.3.2 Solvent risk

If EPS is touched with hydro carbonate solvents (gasoline or diesel oil), it will be dissolved. Therefore, a big concern regarding use of EPS geofoam is potential accidents accompanied by fuel leakage downwards into the ground, thence dissolving EPS geofoam. After any fuel spill, the upper most layer of the foundation must be removed. Therefore, a fuel resistant geomembrane is the proper solution to protect EPS geofoam from such dangers and it should not be placed immediately below the surface construction but at a depth where equipment removing a contaminated covering won't damage it.

2.3.3.3 Fire risk

EPS is a plastic material prone to flammability and burning in fire. Full-scale fire tests in Japan showed that by using 500 mm soil cover on EPS geofoam, melting of EPS is avoided even after a one hour fire of kerosene on a sloped embankment (although thinner soil layers were not investigated). EPS should always be covered, either by soil or by a fire-protective material. Adding fire retardant agents to EPS during production also helps prevent fires from starting, and limits their spread, thereby reducing this this concern.

2.3.3.4 Environmental impact

Using EPS geofoam is beneficial to the environment as it reduces construction time and requires less fuel consumptions compared to when heavier soil material is transferred. However it has to be kept in mind that EPS geofoam is a plastic that obtained from oil and its utilization should be limited to cases where other methods are not efficient.

2.3.3.5 Recycling

To recycle EPS geofoam, it can be crushed and reused in a variety of applications including: lightweight concrete, plastic boards, durable exterior terrace floors, drainage grains, etc. In practice, however, very little is recycled partly due to the lack of a significant market for the material. Of the 377,580 tons of polystyrene produced in the state of California in one year in the early 2000s, only 0.8% was recycled [35]. More recent, anecdotal, evidence suggests that this has changed little since then. Therefore the 'green' credentials of the material referred to above can only be assured where long-lifetime use of geofoam is envisaged.

2.3.3.6 Insulation and permafrost regions

EPS geofoam is a thermal isolative material. Although it may be a secondary function, when EPS geofoam is used in permafrost regions, it can reduce heat transfer to deeper ground levels and prevent melting of the frozen soil, maintaining the bearing capacity e.g. of airport pavement foundations [36].

2.3.3.7 Fixing while placing

The inherent cohesion between EPS blocks might be insufficient in some circumstances. When using EPS geofoam in sloping ground, it might be necessary to keep EPS blocks in place by using barbed plates or other mechanical devices. Additionally, these connectors help EPS blocks fix in their place during seismic events. Of course, these connectors increase

construction costs and their use should be limited to circumstances where sliding or flexing apart are important concerns.

3 Experimental modeling and materials

3.1 Introduction

The materials used in this study include soil and EPS geofoam. The major characteristics of these materials are introduced in following sections, the overall methodology of the research is provided then. In last section, test box and equipment and loading are explained. Later, testing program for the static loading as well as repeated loading are illustrated.

3.2 Material Properties

3.2.1 Soil

The soil used as the upper layer and protective cover over EPS layers was supplied from a quarry near Tehran. Three classes of soil including sand and gravel were brought and mixed, proportionally by weight, to attain the grading diagram shown in Figure 3-1 (ASTM D 6913 / D 6913M-17). This soil is appropriate for use in base and subbase of highways and airports (ASTM D 2940-09) and is classified as a well-graded gravelly sand (SW with about 47% gravel) based on the specifications of Unified Soil Classification System (ASTM D 2487-09).

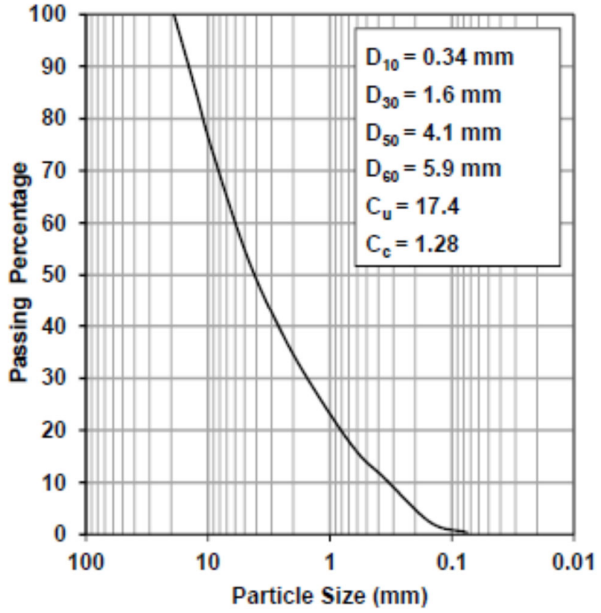

Figure 3-1: Grain size distribution curves for backfill soil (according to ASTM D 6913 / D 6913M-17)

Modified Proctor compaction tests showed that this soil can gain a maximum dry density of 20.42 kN/m^3 (ASTM D 1557-12) at about 5% optimum water content. The soil had a specific gravity (G_s) equal to 2.66 with maximum and mean grain size of 20 mm and 4.3 mm, respectively. Using triaxial compression tests on specimens of soil at a wet unit weight of 19.72 kN/m^3 (equivalent to about 97% of maximum compaction) and moisture content of

5%, the internal friction angle of soil was found to be 40.5º. Further information regarding the soil grading is available in Figure 3-1.

3.2.2 EPS geofoam

EPS blocks were supplied from IZOPOL Dvořák company (a local manufacturer in the Czech Republic). The original block size was 2000×2000×300 mm and it was cut into desired dimensions by using waterjet cutting system. The test method for characterization (e.g. EPS density, compressive strength and elastic modulus) and selection of EPS material will be in accordance with the requirements provided in ASTM D6817-04, ASTM D1621-00. Unconfined static and repeated tests on EPS samples will also performed according to ASTM D1622-08 and a detailed property are shown in Table 3-1.

Table 3-1: Material properties (ASTM D 6817/6817M-17)

Properties	**EPS 15**	**EPS 19**	**EPS 22**	**EPS 29**
Density (kg/m^3)	14.4	18.4	21.6	28.8
Initial elastic modulus, E_i (MPa)	2.5	4	5	7.5
Compressive resistance@1% axial strain (kPa)	25	40	50	75
Compressive resistance@5% axial strain (kPa)	55	90	115	170
Compressive resistance@10% axial strain (kPa)	70	110	135	200

3.2.2.1 Behavior of cylindrical EPS samples

In addition to the main large-scale repeated loading tests, a set of small static and cyclic uniaxial tests were also conducted on 150×300 mm cylindrical specimens of EPS with different densities, in accordance with ASTM D 1621-00. The static tests were performed to measure elastic and plastic limits and the repeated loading tests were also performed to evaluate the response of EPS block under repeated loading.

A thorough understanding of the behavior of EPS per se will provide a great aid to realize the role of EPS in the overall behavior of these pavement systems, and to recognize what happens when EPS blocks are incorporated in conjunction with soil. Previous research is available about the sole behavior of EPS geofoam in static and dynamic/repeated loading conditions [3, 5, 18, 24, 27, 32, 33]. To evaluate the behavior of EPS geofoam used in the current study, unconfined uniaxial static and repeated plate load tests were performed on EPS 15, EPS 19, EPS 22 and EPS 29 (abbreviation of EPS block with densities of 14.4, 18.4, 21.6 and 28.8 kg/m^3, respectively). For the static loading, pressure was applied at a strain rate of 0.001 s^{-1} in order to comply with the condition of fully static loading. With a simple comparison from the results presented in the next section, the strain rate up to the compressive strength of EPS 20 samples is 10% / 84sec (equivalent to 0.0012 1/sec), slightly smaller than 10% / 60sec (equivalent to 0.0017 1/sec) proposed by ASTM D 6817-04. Both of the adopted and standard proposed values are safely placed within static response of EPS geofoam [37]. For repeated tests, each loading application was made during 10 seconds, which is identical to the load application as in the full-scale repeated loading tests. The test setup for evaluation of EPS samples response is shown in Figure 3-2a.

3.2.2.1.1 Static loading

Fig. 3-2b displays the measured stress-strain response of the EPS under static loading. The overall shape of the stress-strain curves is similar to those determined in previous studies, consisting of 4 parts including: an initial linear response, yielding, linear + work hardening, and nonlinear + work hardening [7]. The elastic limit of EPS geofoam is defined as the stress at 1% strain and compressive strength is defined as the compressive stress at 5 or 10 percent strain; the latter is more common [5]. Using this definition, the elastic limit of EPS 15, EPS 19, EPS 22 and EPS 29 are about 8, 22 and 29 kPa and their compressive strengths are about 60, 76, 140, 190 kPa correspondingly.

The subsequent part of the curves (up to about 6~7% strain) is elasto-plastic, comprising a limited amount of plastic strain and therefore, is excluded from the definition of elastic limit. From the elastic part, elastic modulus of the material can be obtained as 3.47, 4.17, 6.93 and 10.28 MPa for EPS 15, EPS 19, EPS 22 and EPS 29 respectively. All specimens were strained up to 90%. At this ultimate point, EPS 15 could tolerate 500 kPa of pressure. EPS 19 showed a resistance of about 650 kPa, EPS 22 showed a resistance of about 950 kPa and for EPS 29, this ultimate resisting pressure was around 1300 kPa.

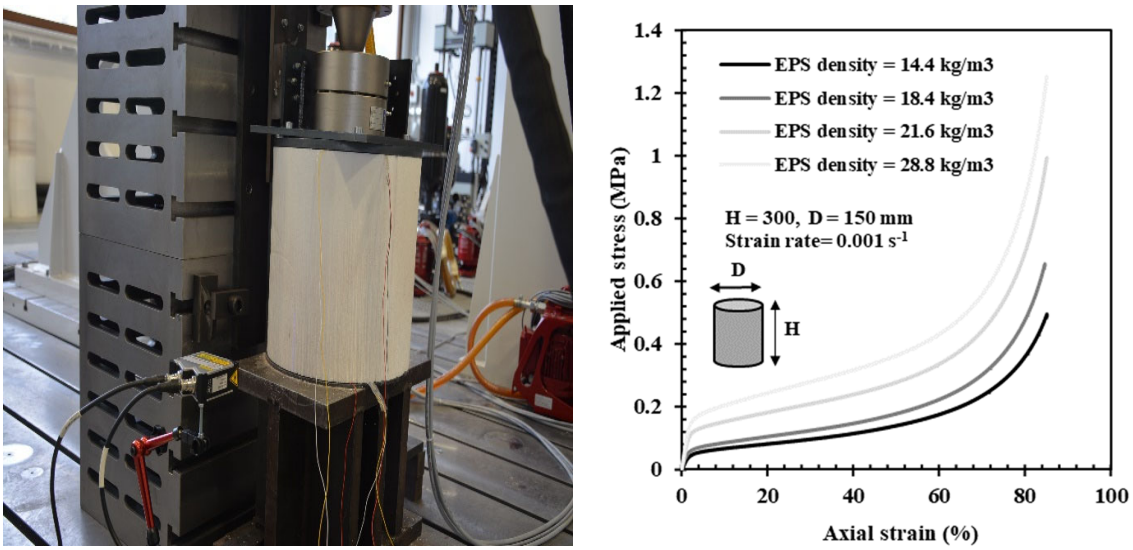

(a) (b)

Figure 3-2: (a) Test setup for uniaxial compression static testing of 150 mm cylindrical EPS 15, 19, 22 and 29 geofoam samples, prior to loading, (b) Stress-strain diagram for static loading on EPS with densities 14.4, 18.4, 21.6 and 28.8 kg/m^3

Horvath (1994) presented a diagram for EPS 21 under short term unconfined axial compression loading. The tests were strain controlled at a rate of 1-20% per minute with 10% per minute as the most common rate. The overall shape of the resulting diagram is very similar to the diagram for EPS 20 derived from current study, however the values show a noticeable difference. For instance, the pressure at 80% vertical strain is 340 kPa in the current tests, while it reaches to about 500 kPa in the mentioned research. A value of approximately 500 kPa is also reported by [38].

Various studies have identified different functions to evaluate elastic modulus and compressive strength of EPS based on their densities. For example, a polynomial function of second order to relate initial Young's modulus of EPS with its density [24]. Stark et al. (2004) concluded that a linear regression would be adequate. They have also suggested a linear function for predicting the compressive strength of EPS from its density. Drawing on the data of Figure 3-2b, Equation 3-1 and Equation 3-2 have been identified respectively to calculate initial Young's modulus and compressive strength of the EPS blocks.

$$E=102.5\,\rho - 1132 \qquad \text{Equation 3-1}$$

$$\sigma_c = 8\,\rho - 7.86 \qquad \text{Equation 3-2}$$

Where E and σc are the initial Young's modulus (kPa) and compressive strength (kPa) of EPS and ρ is density of EPS block (kg/m^3).

The first equation shows a lower initial Young's modulus of EPS geofoam than those presented by Stark et al. (2004). However, the coefficients of the second equation are clearly close to the coefficients of equation introduced by Stark et al. (2004). This indicates that the elastic region of the EPS in the current study is more limited compared to those of similar studies. Hence, the current EPS exhibits a steady transient region from its elastic to its plastic part, while the EPS introduced in other studies shows a sudden transformation from elastic to plastic behavior. In practice, EPS geofoam is seldom designed and evaluated by its elastic modulus, nor is it limited to work in its elastic strain range (1%); but rather, its compressive strength and yield strength (which is also dependent on its compressive strength) are the determining factors for most applications.

3.2.2.1.2 Cyclic loading

To evaluate and quantify the response of EPS blocks under repeated loading, the three densities of EPS were tested under two or three specific repeated pressures with a repetition of 100 cycles. The intensities of the repeated pressure were selected based on the recorded range of pressure values transferred to the top of EPS layer. These values had been logged by the pressure sensor during the mainstream experiments. The response of each density under the selected repeated pressures would this be truly representative of its behavior in the full-scale test; and the conclusions based on these small-scale tests can provide a logical base for interpretation of the overall behavior of the pavement structure in the full scale tests.

Figure 3-3a shows hysteresis curves of EPS 19 under repeated pressure of amplitudes 50, 100 and 150 kPa. It can be observed that EPS 19 shows a stable behavior for repeated pressures up to 100 kPa. When the repeated pressure is 50 kPa, EPS 20 does not strain larger than about 2.3% after 100 cycles; when the repeated pressure is 100 kPa, vertical strain reaches to 4.47%. It should be noted that when the applied pressure is 100 kPa, the value of strain tends to grow slightly during whole loading procedure, however for 50 kPa, it can be assumed to become totally stable after the first few cycles of loading. For both 50 and 100 kPa loading, it is clear that the major portion of residual deformation occurs during the first cycle and strain does not significantly increase after this point. When the applied repeated pressure reaches 150 kPa, EPS 19 turns out to deform very rapidly, such that the vertical

strain increases beyond 20%. When loading continued with additional cycles, total and residual deformations grew even larger.

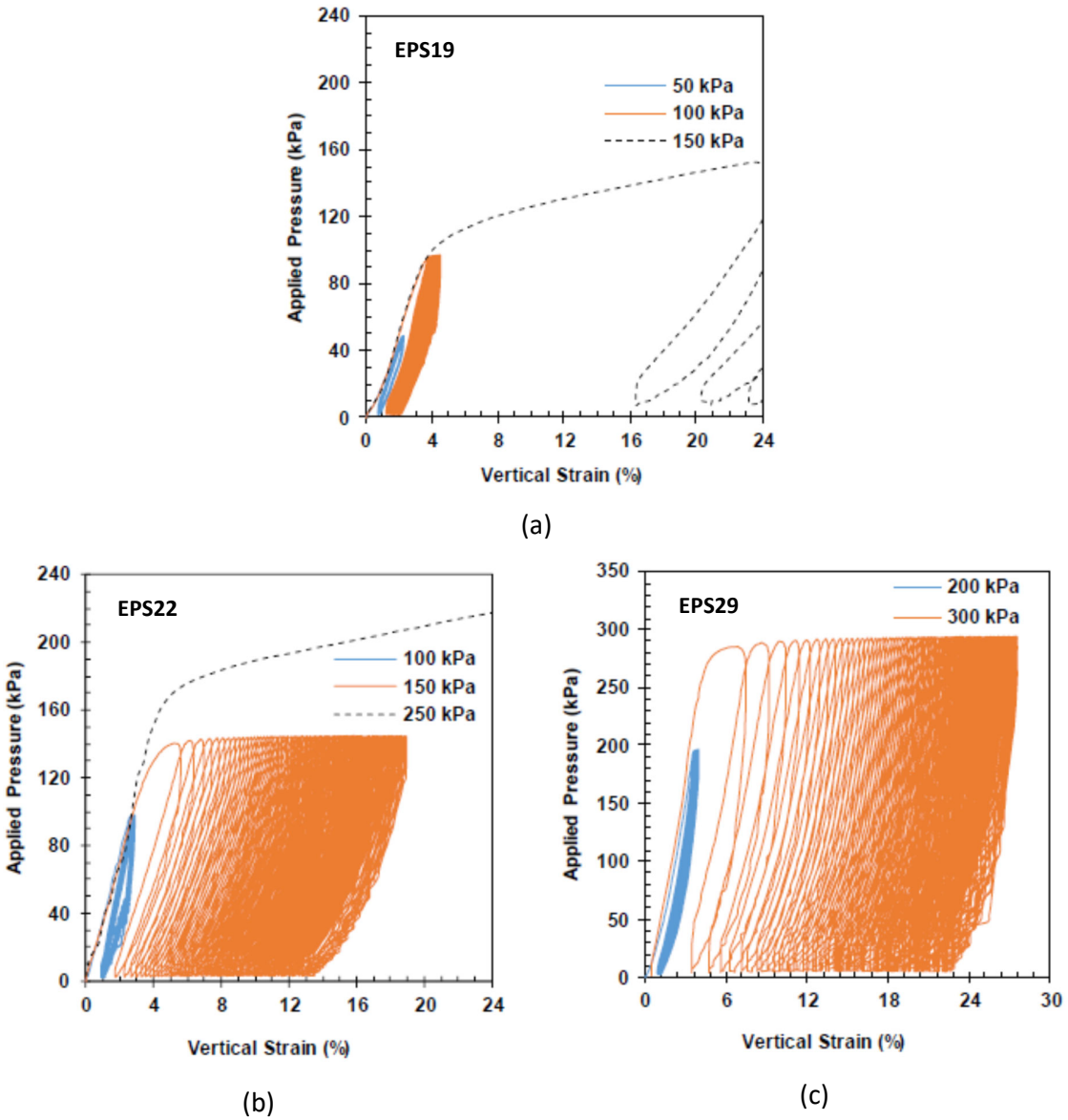

Figure 3-3: Hysteresis response of EPS cubic geofoam sample for (a) EPS 19, (b) EPS 22 and (c) EPS 29

Comparing Figure 3-3a with Figure 3-3b, while EPS 19 shows a maximum strain of about 4.5% at the end of 100 repetition of 100 kPa pressure, this value for EPS 22 is less than 3%. This is reasonable as EPS 22 is stiffer and has a greater yield stress compared to EPS 19. EPS 30 reaches a maximum strain of about 18% after 100 cycles of 150 kPa, whereas EPS 19 deformed severely after the first cycle at this pressure. EPS 29 was not used commonly in the repeated tests, hence only two repeated pressures were picked to assess its response. Figure 3-3c shows that applying 100 cycles of pressure at 200 kPa will generate only a maximum strain as small as 4.3% in EPS 29 after 100 cycles. For EPS 22, the strain under

cycles of this stress is definitely greater than 18% (the value at 150 kPa) according to Figure 3-3b. It is also clear that the strain under this repeated pressure is very stable and does not grow significantly after the first few cycles of loading.

According to Figure 3-4a, EPS 19 strains in a stabilizing manner for repeated pressures of 50 and 100 kPa and deforms very rapidly for a repeated pressure of 150 kPa. Figure 3-4b shows that EPS 22 deforms very rapidly under 150 kPa and does not tend to stabilize even after 100 cycles. This kind of intermediate trend is also expected for EPS 19 between 100 and 150 kPa, which has not been determined exactly here.

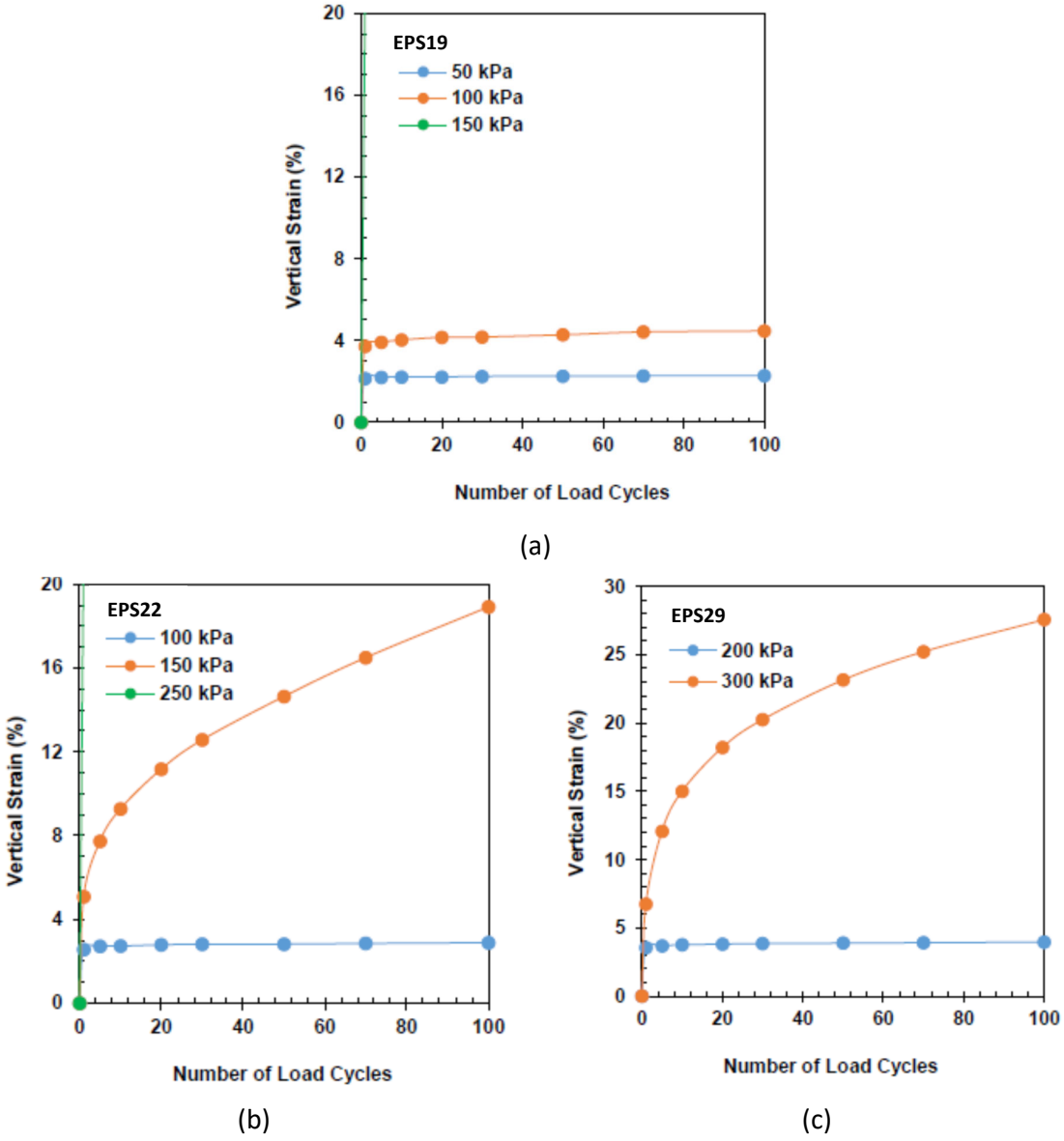

Figure 3-4: Variation of peak vertical strain against the number of load cycle for (a) EPS 19, (b) EPS 22 and (c) EPS 29

When the amplitude of repeated pressure increased to 250 kPa, EPS 30 also exhibited a severely unstable behavior and strained up to 28% after the first cycle of loading. These findings indicate that even though EPS 22 is stronger than EPS 19, it shows a rapidly increasing deformation behavior under repeated pressures larger than 100 kPa. Further tests could be planned with pressures between 100 and 150 kPa to find a threshold for EPS 22, but it was not necessary as the main objective of these small-scale tests was just to obtain an overview about the consequences of using EPS of different densities.

Another important parameter to consider would be the resilient modulus (M_r) of EPS geofoam alone. Figure 3-5 display resilient modulus of EPS 19, EPS 22 and EPS 29 subjected to two different intensities of applied pressure for each EPS density. According to this plot, the resilient modulus of EPS geofoam varies with the amplitude of applied pressure. Considering the stabilized part of the plots (say after 50^{th} cycle) for EPS 19, M_r rises from 3.2 to about 4.1 MPa with increasing the applied pressure from 50 to 100 kPa. Increasing the applied pressure to 150 kPa causes a recession in the resilient modulus to less than 3 MPa during the initial applied loading cycles, prior to failure (not shown on the figure).

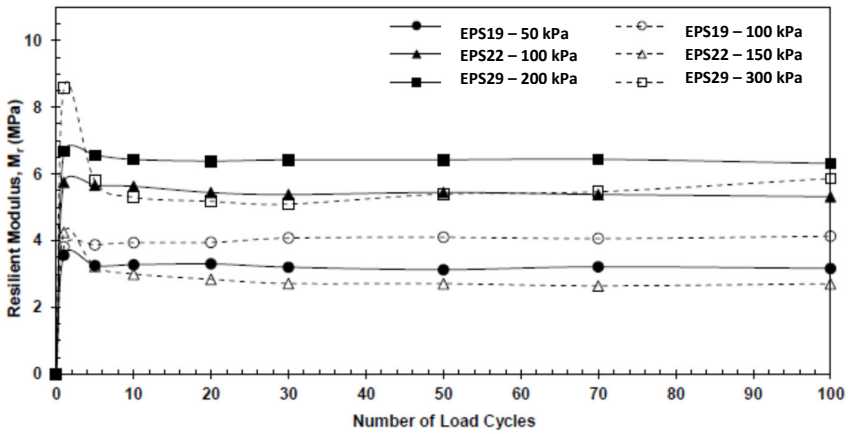

Figure 3-5: Resilient modulus of EPS 19, EPS 22 and EPS 29 under two different amplitudes of applied pressure for each density

This behavior is in agreement with the trend of behavior observed in Figure 3-3 and Figure 3-4 and it can be deduced that as long as the applied pressure is below the stable limit of EPS geofoam, the resilient modulus increases slightly with increase in the applied pressure. With increasing the applied pressure after this limit, an initial jump appears, followed by the typical steady trend as observed when subjected to other pressure values. Besides that, the resilient modulus calculated from repeated tests is generally greater than those obtained from static tests and this value can be considered for design purposes. The inequality of resilient modulus and initial tangent young's modulus resulted from these tests is somehow dissimilar to the reports of Stark et al. (2004), although it is generally expected that resilient moduli values slightly increase with load repetitions. The same observations are also made for the other two EPS densities, as the stable state resilient moduli for the studied deviator stress values for EPS 22 and EPS 29 were 5.5 and 6.5 MPa, and their lower bound moduli were about 2.64 and 5.5 MPa, respectively.

To summarize, tests on small samples of EPS reveal that when EPS is subjected to repeated stresses below a certain limit, the amount of residual deformation is very small, and a major portion of this strain or deformation is resilient. When the repeated pressure values exceed a certain value (around its compressive strength), EPS deforms very rapidly and substantially. This threshold pressure is unique for each EPS density after which the resilient modulus also starts to decrease [32]. According to these outcomes and earlier suggestions in the literature, higher densities of EPS were placed directly under the soil layer and above lower density fill of EPS, in order to provide protection and act as a load spreader to reduce pressure and strains in the main part of the embankment (lower-density EPS).

3.3 Methodology

The basic flowchart of research activities is illustrated in Figure 3-6. In the first stage, available literature were gathered, classified and evaluated, accompanied with limited numerical analyses to determine the key factors involved in the system response. The preliminary large-scale tests were conducted to obtain an initial understanding of the pavement foundation performance. After this stage, the main model tests were performed, and the results were compared. Depending on the range of pressures, EPS samples were tested using uniaxial and triaxial compression tests to accurately assess their engineering properties. Further simplified numerical modeling was also used to help deeper perception of the mechanisms involved. The results were then gathered, interpreted and checked if additional information was required. Finally, the research output was summarized and presented in charts and figures.

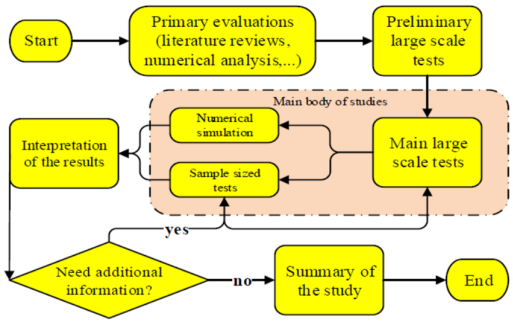

Figure 3-6: Basic flowchart of research activities

3.4 Test components and layout

Various methods have been used for studying the performance of pavement foundations subjected to static and repeated loading. A great number of these studies have implemented well-known evaluation methods, such as plate load test, yet there has been several efforts for introducing novel methods or materials into application [39-53]. For instance, Piratheepan et al. (2012) combined Indirect Diametral Tensile (IDT) and Unconfined Compressive Strength (UCS) tests to estimate cohesion and internal friction angle of conventional granular material stabilized with slag lime and general blend (GB) cement-fly ash. Physical and mechanical properties of marginal lateritic soil and Melamine Debris (MD) blends as a sustainable engineering fill material were studied using Los Angeles

(LA) abrasion and California Bearing Ratio (CBR) and other test by Donrak et al. (2016). Tavira et al. (2018) used plate load and falling weight deflectometer tests to characterize construction and demolition waste (CDW) used as base and subbase materials. Yet, the plate load test still remains a simple and practical method for evaluation of pavement foundation systems, and was also used in this study.

For this research, the large-scale plate load tests simulating real conditions, were performed in a test box, excavated inside the "Research Laboratory of Physical modelling" at the K.N. Toosi University of Technology. The model tests comprise a test box, reaction frames, loading system and measurement equipment (see the schematic view in Figure 3-8).

3.4.1 Equipment

The first series of experimental test will perform in "Regional Technological Institute" at the University of West Bohemia by using a universal hydraulic loading system equipped with high-speed precise data acquisition will use to apply the uniaxial vertical loading. The loading frame which supports the hydraulic cylinder weighs 4.5 tons with a capacity of 32 tons. A hydraulic jack with nominal span and load of 250 mm and 100 kN will use to apply the loading force. The applied load measured by an inline load transducer with a capacity and accuracy of 100 kN and 0.02% which double checked by an oil pressure sensor inside the hydraulic cylinder. The vertical movement of the hydraulic cylinder is controlled by an internal displacement transducer which can control the movement of the hydraulic piston with an accuracy of 0.01%. In order to monitor the side deformation of EPS samples, two laser scanners with measurement span and accuracy of 10 mm and 640 points/profile were installed on the side of the sample, free from the frame movement, to obtain the precise side measurement of the middle part of the samples. The transferred pressure to EPS blocks will measured using four pressure cells; two of them will installed in the middle of the block and the other two on the top of the EPS sample. The pressure cells were made of a thin layer of polyester with a sensing area of 25.4 mm capable of measuring a maximum pressure of 700 kg/cm^2 with an accuracy of 0.01%. The whole system is controlled by the central data acquisition system with a sampling rate of 25 Hz - which covers the precise measurement for static tests. Figure 3-7 shows the real view of the testing system.

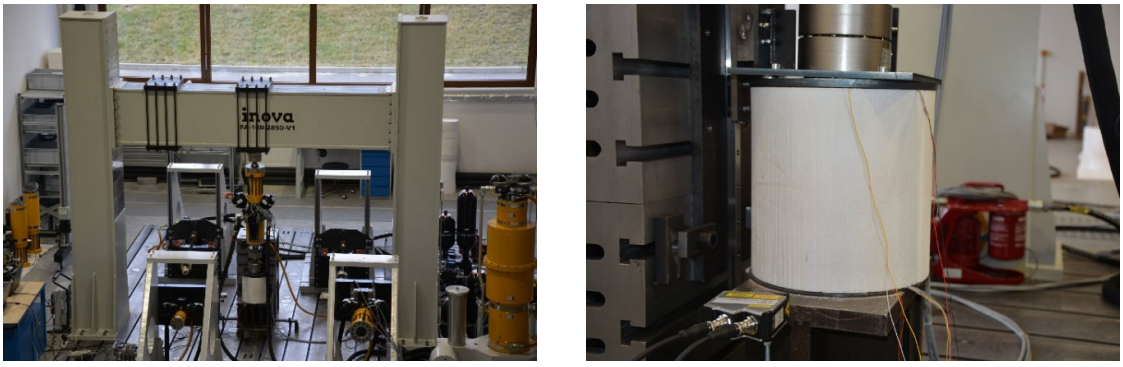

(a) *(b)*

Figure 3-7: Preparation of test setup: (a) Testing equipment, (b) Sample setup

In this study, monotonic and repeated plate load testing was employed to mimic the loading applied by a truck tire as recommended by AASHTO T 221-90 and ASTM D 1195- 09 for soils and flexible pavement components. For this aim, the model pavement sections were constructed in a test box of 2200×2200 mm in plan and 1200 mm (could be increased up to 1400 mm) in depth (see Figure 3-8). The interior sides and bottom of the box were covered with a rough layer of cement-sand mixture and unreinforced concrete, respectively.

In the majority of tests, the failure mechanisms have been observed to be of a similar punching nature and the failure surface does not extend, laterally, to a distance further than 3-4 times of loading plate diameter from the center of loading (i.e. a diameter ≤1.2m). As a confirmation to this observation, if the horizontal plane dimensions of the test box are equal to seven times of the diameter of the loading surface, that would be enough to prevent the effect of side boundaries [54]. In agreement with the observations that will be described later, the box dimensions fulfilled the recommended values by using a horizontal dimension of 7 times of the loading plate which would be 2100 mm in this study [55].

The depth of the box seems to be sufficient, based on the recommendation of a 700 mm deep test box would be sufficient to prevent possible stress redistribution induced from bottom of the box (box depth is ≥1200 mm in this study) [54]. Measurements indicated that the amplitude of pressure transferred to depths below 1000 mm are equal to a negligible portion of the applied stress on the top of embankment. Therefore, the probable rigid boundary effect initiating from the bottom of the test box is insignificant. Tests by Moghaddas Tafreshi et al. (2012) also showed that a minor portion of applied tire pressure on the soil surface will penetrate to levels deeper than 700 mm. Thus, the box dimensions are suitable for avoidance of boundary influences [56].

Along with the above suggestion, DeMerchant et al. (2002) used a 305 mm plate in a 2200 mm width and 860 mm deep test box for studying geogrid-reinforced lightweight material and confirmed that the results were not altered by the side or bottom boundaries [57]. Accordingly, Hegde and Sitharam (2015) found that the pressure dispersion depth (where pressure is ≤10% of the bearing capacity) would be 1.6B and 1B for an unreinforced and a geocell-reinforced soft clay bed, equivalent to 480 mm and 300 mm in this study [58].

In the current research, the main purpose of using EPS geofoam in pavement system is to speed up construction, in which various conditions (from soft to stiff) could be expected at the bottom boundary. However, with the current box height (i.e. 1400 mm), the surcharge stress from EPS geofoam and the stress magnitude beneath the box from the surface applied pressure are negligible, so the rigidity or stiffness of the bottom boundary will have a minor effect on the system response. Thus, the dimensions of the test box employed here are more than sufficient on the basis of previous researchers' results and current rationales.

Considering above description, the second series of test will perform in "Research Laboratory of Physical Modeling" at the K.N. Toosi University of Technology by using physical model simulator (Figure 3-8). The loading frame consisted of a heavy reaction beam, supported on two strong columns (Figure 3-8). A hydraulic jack with capacity of 100 kN and capable of producing monotonic and repeated movements was fixed above the reaction beam. The loading was applied to a rigid steel plate of 300 mm diameter and thickness of 25

mm on the pavement surface through adjustable rigid steel shafts. The rigid steel plate is representative of the tire of a common truck and exerts the load from hydraulic jack to the surface of the pavement. It should be noted that the loading plate and pavement section dimensions were selected near real scale (according to equivalent tire dimension recommended by other researchers [59]), therefore scale effect is negligible present in this study.

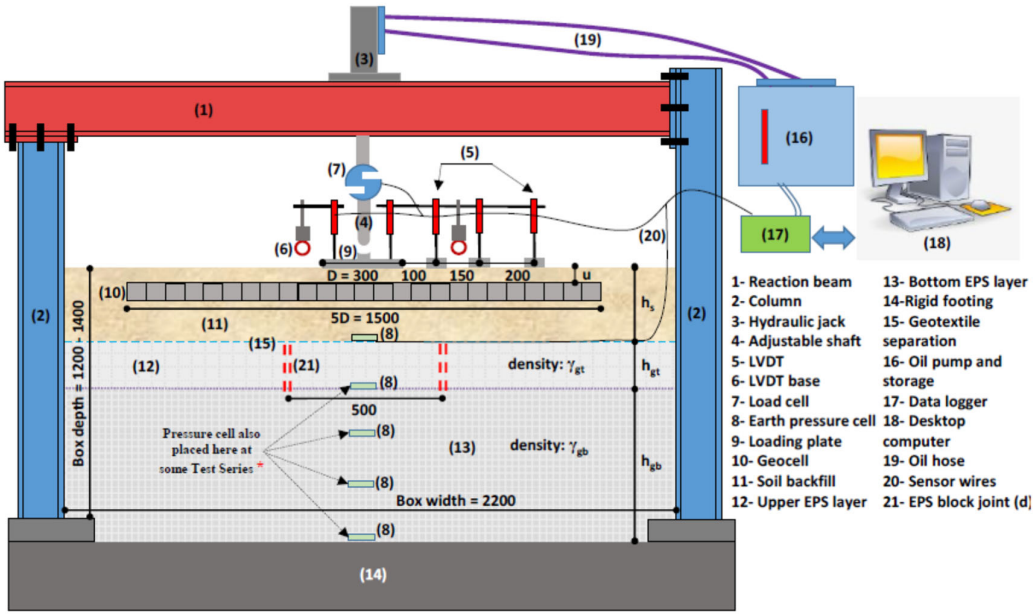

Figure 3-8: Schematic view of the testing apparatus (not to scale) and test parameters (units in mm), for geocell reinforcement

In general, two important loading types for the EPS geofoam bed could be identified: (1) Static Loading: In some circumstances, heavy trucks move very slowly along the still unpaved work platform, the magnitude of the applied pressure on the overlying soil or EPS geofoam is relatively high, (2) Repeated Loading: a large number of repeated traffic load with considerably lower amplitude (due to pressure dispersion effect of the asphalt layer) is applied on the overlying soil layer placed on EPS geofoam (low-amplitude repeated loading).

Although the dominant type of loading on the pavements of airports, logistic terminals, container terminals, parking lots, industrial areas and storage areas is long term static or impact loads, the type of loading encountered during pavement construction is short term static loading which might cause sudden rupture or failure when the extreme loads are applied during construction. On the other hand, during service period and when the low-amplitude repeated loading is applied, a steady state (elastic or plastic shakedown) is accessible. Thus, in addition to the necessity for evaluation of the structural strength of these foundation systems during the mostly demanding phase (the first loading type), further investigation is required on their performance during the service life of the pavement foundation (the second loading type).

Regarding the repeated loading for the second loading stage, AASHTO T 221-90 and ASTM D D1195-09 both allow application of repeated plate load cycles so as to evaluate airport and highway pavements. ASTM D 1195-09 suggests the use of static plate loading, with a few load repetitions, on soils and unbound base and subbase materials for evaluation and design of highway and airport flexible pavements. Although the number of vehicles passes will definitely exceed these values by a large margin, the pressure on the unbound layers will be greatest, and most critical, in the construction phase of the road, when the covering materials are at their thinnest (or even absent). At such a stage, Powell et al (1984) showed that 500 axle passages are a likely maximum.

To simulate the critical loading that might be applied to a road surface, Brito et al. (2009) suggested applying repeated pressures of 400 and 800 kPa on an approximately 300 mm diameter plate (as shown for super single tire in Figure 3-9a) [59]. Although, EPS geofoam is rarely used in unpaved roads, Brito's pressure values are impractical in the case EPS embankments [7] and, for the present study, must be reduced to allow for the stress distribution that would be provided by the thickness and stiffness of the pavement's asphalt layer. Using KENPAVE software and assuming 50 mm asphaltic layer with Young's Modulus of 2.5 GPa, the pressure amplitudes can be reduced to 275 and 550 kPa respectively to represent the stress passed down to the top of the soil layer. Thus, in the present study, two loading stages adopted for the repeated loading study:

(1) A first stage of loading comprising 100 applications at 275 kPa, which is followed by

(2) A second stage with 400 repetitions of 550 kPa pressure (Figure 3-9b).

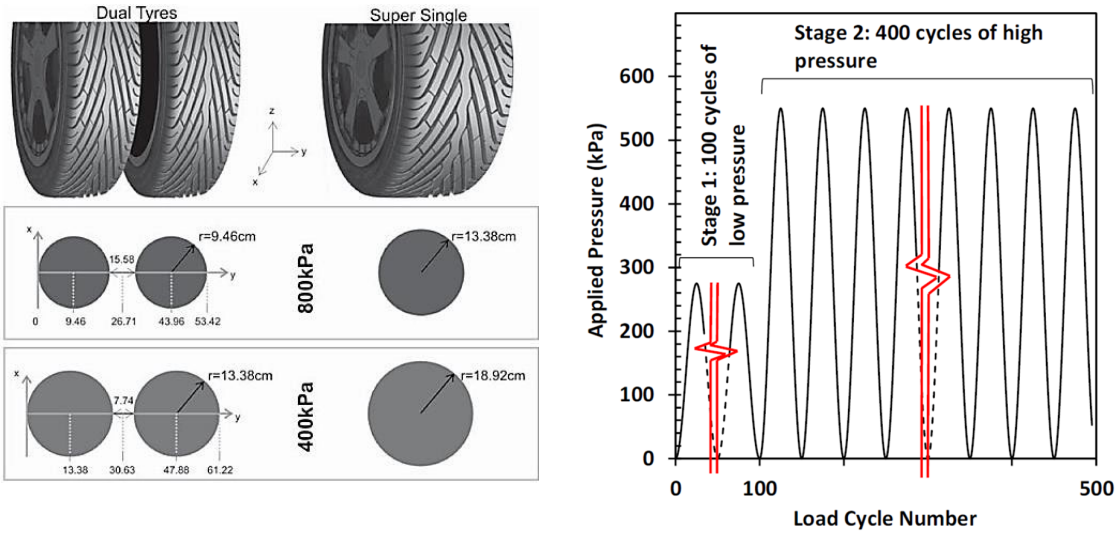

(a) (b)

Figure 3-9: (a) Equivalent wheel radius and pressure (Brito et al., 2009), (b) Schematic illustration of loading pattern including: stage 1, including 100 repetitions of 275 kPa repeated pressure and stage 2, including 400

In agreement with the reality encountered as explained above, only applied 100 cycles of 550 kPa pressure to evaluate deformation of geocell-reinforced recycled asphalt pavement bases subjected to repeated loading [60]. Similarly, Sun et al. (2015) who applied

100 cycles of pressure at various loading increments up to 700 kPa to investigate the performance of geogrid-stabilized unpaved roads under repeated loading [61]. Therefore, evaluation of pavement foundation performance using a several load cycles is widely used by various researchers.

Although the rate or frequency of loading might have a direct effect on the response of EPS embankments, a wide range of frequencies (e.g. 0.01~10 Hz) have been implemented by previous researchers for this purpose [55, 62-64]. Gonzalez-Torre et al (2015) concluded that high frequency loading does not affect the pavement significantly and the lower the frequency, the higher impact will the loading have. Additionally, Peralta (2010) signified that for soil loading with frequencies between 0 to 1 Hz, the effect of inertia is negligible and the loading type would be repeated, rather than repeated-dynamic or dynamic (see Table 3-2 for classification) [65]. In this research, due to limitation of loading system, each pressure application was made in sinusoidal form during 10 seconds (equivalent to 0.1 Hz), the low range of the frequencies adopted by the mentioned research.

Table 3-2: Classification of repeated loading of soils [65]

Repeated Loading of Soils	Repeated	Repeated-Dynamic	Dynamic
Frequency	0 to 1 Hz	1 to 10 Hz	>10 Hz
Inertia	No (negligible)	Yes (relevant)	Yes (Relevant)
Strain accumulation	Predominantly plastic	Plastic and elastic	Predominantly elastic

3.4.2 Measurement system

The measurement system of the large-scale repeated plate load test is shown in schematically in Figure 3-8. Two LVDTs were placed above the rigid plate and the settlements of the loading surface were measured and the average values was used. To obtain an approximate sketch of the deflection basin in some of the tests, two additional LVDTs were also placed at 100 mm and 150 mm away from the edge of the loading plate in a few tests. The LVDTs had an accuracy of ±0.01% at their full range (75 mm). A S-shaped load cell was placed between hydraulic jack and the rigid plate to control the amplitude of applied load. The capacity of the load cell was 100 kN and its accuracy was ±0.01%. In all of the experiments, an earth pressure cell of 1 MPa capacity with accuracy of 1 kPa was placed above the upper layer of EPS geofoam (between soil layer and EPS bed) to read the amplitude of the pressure transferred to the top of the EPS layers. In such type of pavements, the amplitude of pressure transferred on top of EPS layer would have an acute influence on pavements' performance [66] and is considered as an important part of design procedures [7]. The transferred pressure to lower depths was considered negligible and thus, the pressure at deeper levels of EPS bed was only measured in a few tests. It is also worth mentioning that all of the sensors and pressure cell were calibrated using proper calibration method to ensure the accuracy of the recorded data. The sensors were connected to a data logger, and the measured data were sent to a computer, which saves and presents data for future analyses.

3.4.3 Backfill preparation and test procedure

The initial stage was to fill the test box with EPS geofoam blocks. Zou et al. (2000) found that size and lateral restraints have no significant effect on the performance of geofoam blocks [67]. Making use of this finding, the blocks were ordered to be prepared as 1000×500 mm in plan and 100 or 200 mm in height in order to have flexibility in replacing deformed or damaged blocks with more intact ones, to minimize disposal costs and to provide longer life spans for the current testing material. A few tests were also repeated by replacing some of the larger EPS blocks but the results did not show a noteworthy difference.

The blocks must be placed in tight arrangement together, to prevent increased settlements originating from gaps between the EPS blocks [67, 68]. EPS blocks were located at bottom of the test pit with minimum lateral (horizontal) gap between them. Yet a slight gap is unavoidable in most cases, although, it will not affect the overall performance of the section, as reported by [67]. The blocks were leveled properly and differential surface alignments were minimized. Adjacent blocks were investigated for any unbalanced vertical alignment or varied surface levels. Any surrounding voids at the corners were also filled and leveled by smaller pieces of EPS. Reaching a perfect surface in terms of surface smoothness and flatness is almost impossible, but maximum effort was made to establish such a condition. For placing the subsequent layers of EPS geofoam, the direction of the longest side of the blocks was aligned perpendicular to those of the underlying blocks, so as to form an integrated mass of EPS, and minimize relative vertical displacement of the blocks due to unleveled seating [7]. The lateral boundaries condition would have a negligible effect on the results. This is primarily due to the very low Poisson's ratio of EPS geofoam [25, 27], which prevent lateral deformation and subsequent stressing on box sides. Furthermore, the box dimensions are adequate to prevent boundary effect for a single loading plate, as discussed earlier. However to comply with real embankment conditions [7], any remaining gaps between EPS blocks and test box wall were filled with smaller pieces of EPS geofoam. Fig. 3-9a displays the test box after preparing the EPS bed.

The selected height of 100 or 200 mm for EPS blocks also helped to examine the effect of EPS density and thickness at the subsequent layers. To this aim, the blocks in each layer were replaced with the desired density and height, so an appropriate order of blocks were formed from top to bottom of the test box (see Figure 3-8). It is a well-known practice [7] to place a layer of higher density EPS as the uppermost layer, in order to control excessive local deformation or failure of EPS, directly below the pressurized zone of overlying soil [7], while the major portion of subgrade is constructed with a lower density EPS in order to reduce costs. In other words, a balance has to be established between cost and the maximum allowable rut depth of the pavement surface. This approach was also used in the current study, and the majority of test sections comprised a top layer of EPS with a higher nominal density (e.g. 30 kg/m^3) than the remainder of the EPS (e.g. 20 kg/m^3) as shown in Figure 3-8. The test box after placement and arrangement of the first layer of EPS blocks is illustrated in Figure 3-10a.

Observations during the current tests have showed that even a 10~20 mm vertical gap between EPS layers can be extremely destructive and translate into a twofold to threefold increase in the rut depth on the pavement surface, compared to tight placement of the

blocks. Therefore, it is important to place EPS blocks with great accuracy to avoid such negative consequences. More details on the requirement on the layout and placement of EPS blocks can be found in ASTM D 7180-05.

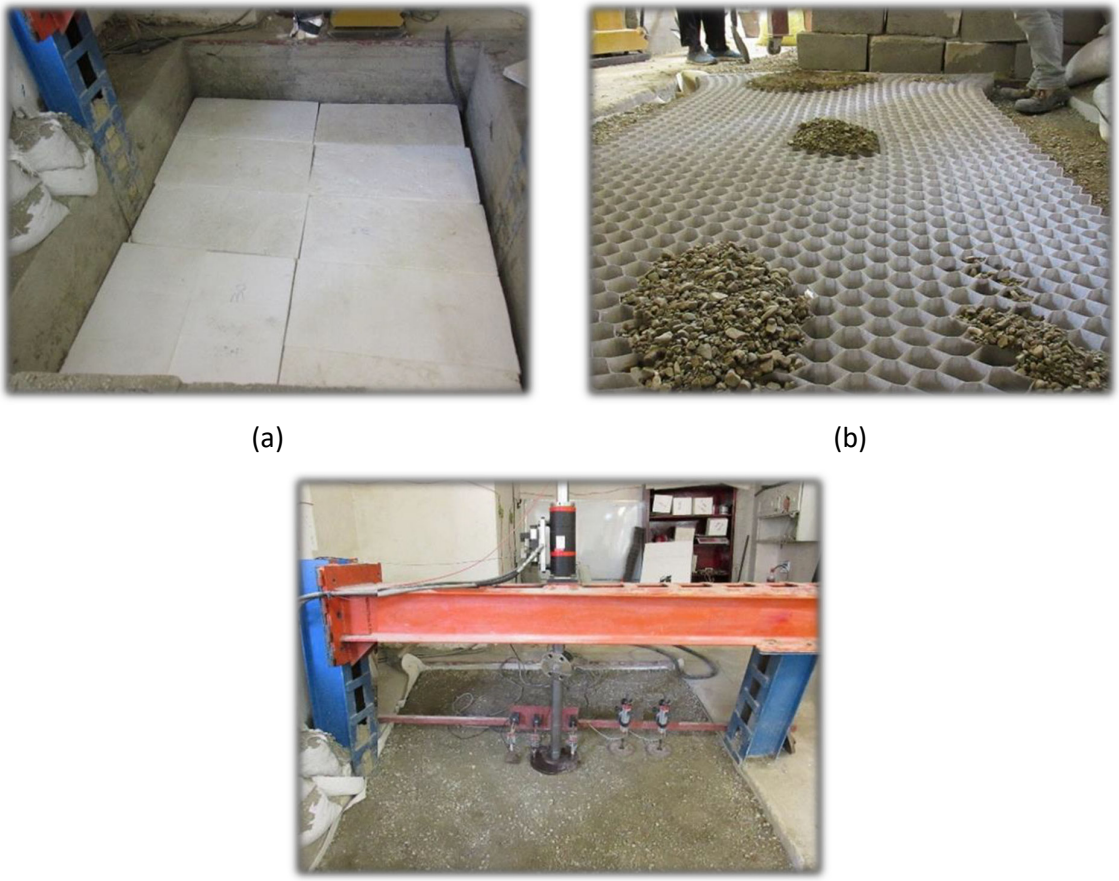

(a) (b)

(c)

Figure 3-10: (a) Placement of EPS geofoam blocks inside test box, (b) Preparation of geocell-reinforced mattress and, (c) Completed test installation prior to loading including reaction beam, loading plate, hydraulic jack, load cell and LVDTs

No connection or adhesive was used between EPS geofoam blocks due to expensiveness for practical applications. Barrett and Valsangkar (2009) have reported about the effectiveness of connectors on the shear resistance of geofoam blocks [69]. They performed shear tests on blocks with no connection, blocks with barbed plate connectors and blocks with polyurethane adhesive. They applied different normal pressures on the blocks with each of the connection methods and compared their shear resistance. The results revealed that barbed plates had little influence on the shear resistance between blocks; rather they might impose a slight reduction in the initial shear resistance between the blocks under repeated loading. However, they did not affect peak shear resistance between the blocks. Polyurethane adhesive could lead to an up to twofold increase in the shear resistance by eliminating horizontal sliding of blocks. Using such adhesives is not a practical approach for real projects and hence was not considered in the current study. Barbed plate connectors

were not used either, in order to eliminate their potential destructive effect on the surface of geofoam blocks.

After completion of the placement of EPS geofoam layers, a geotextile sheet with 16 kN/m strength was placed over EPS bed to separate it from soil, as recommended by Stark et al. (2004) [7]. The importance of the covering geotextile is due to the soft texture of EPS geofoam, which is sensitive to damage when directly in touch with any soil that has a rough nature. Soil particles tend to indent the surface and possibly destroy EPS blocks by eroding EPS particles away from the block. The geotextile used in these tests is not supposed to contribute to the performance of the pavement system. The reason is that the geotextile placed in a non-optimum depth, far enough from the effective stress bulb of the loading plate. Furthermore, the geotextiles sheet was installed without any pre-tensioning to reduce possible activation of its reinforcing mechanisms. Finally, the geotextile was present in all of the tests, hence its effect on the final results (if any minor effect) would be identical.

Then, the soil was transferred into the test box by means of hand shovels, spread and leveled to reach a pre-determined thickness. This pre-compaction thickness was determined, by trial and error, to be approximately 120 mm for unreinforced pavements. A 450 mm wide walk-behind vibrating compactor was used across to compact the leveled soil until it reached the desirable thickness of 100 mm for unreinforced pavements. The influence depth of the compacter was between 50 to 100 mm, as reported by the manufacturer. Thus, passage of the compactor over a soil layer with thickness of 100 mm would not have influenced compaction of the bottom layers. To ensure that soil has reached its ultimate state of compaction, each layer was compacted with at least 5 passes of the compactor with the compactive effort kept approximately the same for each layer.

According to Moghaddas Tafreshi et al. (2014), the optimum installation depth of geocell (u) is 0.2 times the diameter of the loading plate (u/D = 0.2) [70]. Hence, with a loading plate diameter of 300 mm in this study, the optimum depth of geocell mattress becomes u = 60 mm. For this reason, the final compacted layer above the geocell and the geocell layer itself had thicknesses of 60 and 100 mm, respectively. Thus, for reinforced pavements with total soil thicknesses of 400, 500 and 600 mm, the remaining thickness of soil below geocell mattress would be 240, 340 and 440 mm, which were divided, nominally, into 2×120, 3×113 and 4×110 mm layers, respectively. The width of geocell mattress was selected as approximately 5 times the diameter of loading plate in accordance with other's findings [55, 70]. Figure 3-9b shows a view of the placement of geocell in the test box. Figure 3-9c shows the completed test installation including reaction beam, loading plate, hydraulic jack, load cell and LVDTs.

In-situ density tests (according to ASTM D 1556-07) and water content tests were performed at random intervals to guarantee the consistency of the soil condition during the experimental program. The measurements showed that the degrees of compaction achieved were almost equal for both unreinforced and reinforced pavements at the same depth. Water content was maintained close to the optimum water content (5%) with a maximum of 0.25% deviation. Density tests revealed that the maximum achievable dry density (compaction) varied across the vertical profile of the compacted soil, changing from a minimum lower value in the soil layer just above EPS blocks and rising to larger values with

increase in soil thickness. In other words, the maximum obtainable density was found to be a function of the height of soil placed above the EPS geofoam and reinforcement status of the soil layer.

Because of the low mass of EPS blocks and their vibrations, the dry density of the first soil layer (adjacent to EPS bed) could not go beyond 18.7 kN/m^3 (equivalent to 91.5% of maximum compaction). The second and third layer of soil could ultimately reach 19.1 kN/m^3 and 19.4 kN/m^3 (equivalent to 93.5%, 95% compaction levels, respectively. The maximum dry density of the fourth layer and beyond was 19.6 kN/m^3 (96% of maximum compaction). For the fifth and sixth layers of soil, when needed, dry densities higher than 19.6 kN/m^3 were almost unreachable. As will be discussed later, this trend is a consequence of the lower stiffness support provided by the EPS. However, inside the geocell the density could be expected approximately 2-4% lower in the unreinforced soil [70]. The difference can be explained in terms of the geocell wall friction and multiple geotextile boundaries against which uninterrupted packing becomes impossible. Based on the above configuration and symbolization.

3.5 Testing program and parameters

For simpler interpretation of the results, the main test program is categorized into three sections and each part is subsequently discussed in three separate section. The first category discusses the results under static loading for small scale test. The second category is allocated to the results of static loading on the complex material in large scale model and third category is devoted to the result of repeated loading in large scale model.

The performance of the pavement was evaluated in terms of depth of ruts generated on the pavement surface and in part, by the transferred pressure to the top of upper EPS layer. Large scale repeated plate load tests were planned to evaluate the effect of the overlying soil layer thickness (h_s), the thickness of the upper and bottom EPS layers (h_{gt} and h_{gb}, respectively), the density of the upper and bottom EPS blocks (γ_{gt} and γ_{gb}, respectively). Preliminary tests and numerical analysis showed that the compacted soil thickness (h_s), density of the upper EPS layer (γ_{gt}) and density of the bottom EPS layers (γ_{gb}) are the factors having the most significant effect on the response of these pavements (see Fig. 3-8a for definition of parameters) - the subscripts “s”, “g”, “t” and “b” stand for soil, geofoam, top and bottom, respectively. For simpler representation, density of the subsequent layers is shown as EPS γ_{gt}/γ_{gb} from here. For example, EPS 29/22 indicates the use of the upper EPS layer and bottom EPS layers with density of 28.8 and 21.6 kg/m^3 (Table 3-1), respectively.

Regarding the selection of soil thickness and EPS layers, further discussion would be useful. Gandahl (1988) and PRA (1992) had proposed using a minimum of 300-400 mm thickness for the overlying soil layer [71], while Stark et al. (2004) has suggested increasing the minimum thickness of the overlying pavement (including soil layer and asphalt/concrete slab) to 610 mm [7]. Due to the limitation of the depth of test box in this study, a typical thickness of 400 mm has been used in the tests. Another reason for selecting such a low thickness was so as not to conceal the effect of remaining factors which might, otherwise, have been too small to be readily observed. Furthermore, a great advantage of geocell

reinforcement would be to decrease thickness of the overlying soil layer, consequently reducing construction duration and costs. As previously stated, one of the objectives of this study is to characterize pavement foundations overlaid by thinner soil (i.e. 400 and 500 mm) that contains a geocell layer. Therefore, the thicknesses of the overlying soil layer used in this study is (almost) in accordance with others varying from 400 to 600 mm [7, 71].

Stark et al., (2004) recommended that at least two layers of EPS geofoam with typical thickness of 610 mm to 1000 mm be used to prevent shifting of the blocks under traffic loads [7]. As the thickness of EPS blocks were 200 mm in the current study, 3 to 4 layers of EPS have been used to comply with the recommended number of layers. In order to check the repeatability of the test results, a few tests were repeated in each Test Series to ensure that there was no significant change in the test procedures during the experimental program. A close match between results of the repeated tests with a maximum difference of 4-6% was observed. Mean results are discussed hereafter.

3.5.1 Small scale uniaxial tests

The testing program was designed in a way that the most important parameters which affect the behavior of EPS could investigated. The program is divided into five Test Series to check the effects of H/D (height to diameter of the sample), strain rate, Sample diameter (D) and EPS density (γ) on the stress-strain behavior and the side deformation of the EPS samples. These series will help to understand the mechanical properties of EPS geofoam itself which then should consider in the combination of other construction materials. Table 3-3 shows a summary of the testing program.

Table 3-3: Test program for small scale uniaxial tests

Test Group	No. of tests	Sample diameter (D)	Height (H)	H/D ratio	EPS density	Strain rate	Purpose of tests
		mm	mm		kg/m^3	s^{-1}	
A	20	100, 200, 300	300, 600	1, 2	14.4, 18.4, 21.6, 28.8	0.001, 0.01, 0.1	Preliminary tests to check the performance of sensors and system
B	4	150	150, 180, 240, 300	1, 1.2, 1.6, 2	28.8	0.001	Effect of sample height to diameter (H/D)
C	9	300	300	1	14.4, 18.4, 21.6	0.001, 0.01, 0.1	Effect of loading strain rate
D	9	100, 200, 300	100, 200, 300	1	18.4	0.001	Effect of EPS sample diameter (D)
E	8	300, 150	300	1	14.4, 18.4, 21.6, 28.8	0.001	Effect of EPS sample density (γ)

Tests in group A were carried out to check the performance of the loading system, loading frame, all the transducers, measuring and control system. All sizes and densities of samples were used to check the compatibility of the test system at different strain rates. The repeatability of the tests shows less than 2% difference, which confirms that the whole loading and measuring system works properly. Tests in group B were carried out to investigate the effect of Height on Diameter (H/D), of EPS samples with density of 28.8 kg/m^3. The diameter of the samples was 150 mm with various sample heights (150, 180, 240

and 300 mm) to achieve different H/D ratios equal to 1, 1.2, 1.6 and 2. The loading was applied with a constant strain rate of 0.001 s^{-1} to simulate a drained situation (static loading) which gives enough time for the internal air and water to leave the sample and achieve zero pore air and water pressure during the tests.

Tests in group C were carried out to investigate the effect of strain rate on the behavior of the stress-strain curves of EPS. The loading was applied with different strain rates of 0.001, 0.01 and 0.1 s^{-1} up to the maximum available span/load capacity of the hydraulic loading system. The sample height and diameter were 30 cm (H/D = 1) with various densities of EPS (14.4, 18.4, 21.6 kg/m^3). Tests in group D were carried out to investigate the effect of the change in the diameter of the EPS samples. The diameters of the samples were 10, 20 and 30 cm for this test series. One of EPS density (18.4 kg/m^3) and H/D ratio equal to 1 were chosen. The constant strain rate of 0.001 s^{-1} to simulate the drained situation gives enough time for the internal air and water to leave the sample and make zero pore air and water pressure during the tests. In Test Series E, samples with densities of 14.4, 18.4, 21.6, 28.8 kg/m^3 were tested to identify the effect of EPS density. Sample diameters were 15 and 30 cm with H/D = 1 and the strain rate was 0.001 s^{-1}. As well as all these measurements, the relaxation of all the samples after the tests was manually measured at different time intervals up to 6 months after the tests to investigate the short and long-term elastic and plastic deformation of the EPS samples.

3.5.2 Large scale static loading

For main static tests, a total number of 7 independent tests in two Test Series were planned to study the effect of most influencing factors mentioned in Table 3-4.

Table 3-4: Test program for large scale static plate load tests

Test Series	Soil cover thickness, h_s (mm)	Density of upper EPS layer, γ_{gt} (kg/m^3)	Density of bottom EPS layer, γ_{gb} (kg/m^3)	Type of loading	No. of tests	Purpose of the test
1	300	28.8	28.8	Static	4+8[a]	To evaluate the effect of soil thickness
	400					
	500					
	600					
2	400	28.8	21.6	Static	3+3[a]	To determine the effect of EPS density at subsequent layers
		21.6	21.6			
		21.6	18.4			

[a] Indicates the number of tests which have been repeated two or three times to ensure the accuracy of the test data. For example, in test Series 2, a total of 6 tests were performed, including 3 independent tests plus 3 replicates.

In Test Series 1, pavement installations with soil thicknesses of 300, 400, 500 and 600 mm were tested to identify the effect of overlying soil cover thickness (h_s). Density of the upper and bottom EPS layers were 28.8 kg/m^3 in this Test Series. In Test Series 2, density of the upper EPS layer (γ_{gt}) and bottom EPS layer (γ_{gb}) were reduced to 21.6 and 18.4 kg/m^3 investigate the response of the pavements with lower EPS densities.

3.5.3 Large scale repeated loading

The main unreinforced repeated plate load tests comprised six series as described in Table 3-5. In Test Series 1, repeated plate load tests were performed on soil backfill (with no EPS block) with two compactions to determine how density of compacted soil can influence stiffness and settlements. In Test Series 2, the amplitude of applied pressure was varied to discover its effect on the settlements of pavement sections including soil and EPS layers. Test Series 3 was performed to determine how pressure dissipates with depth in the EPS body. As only one pressure cell was available during the experimental program, the pressure sensor had to be placed at depths of 400, 600, 800, 1000 and 1200 mm below the loading surface in separate tests, therefore, Test Series 3 had to be repeated 5 times. In Test Series 4, the effect of soil thickness was investigated. Test Series 5 consisted of experiments to evaluate the influence of the thickness of the upper (denser) EPS layer and finally, Test Series 6 focused on assessing the effect of the upper EPS density on the performance of the pavement. A total of 19 independent test were performed to achieve the required data for analysis of each factor.

Table 3-5: Test program for large scale repeated plate load tests

Test Series	h_s (mm)	h_{gt} (mm)	h_{gb} (mm)	γ_{gt} (kg/m^3)	γ_{gb} (kg/m^3)	Soil density (kN/m^3)	Repeated pressure (kPa)	No. of Tests	Purpose of the Test
1	1200	-	-	-	-	18.7, 19.6	275-550	2+3*	To evaluate behavior of soil backfill
2	400	200	600	21.6	18.4	18.7 to 19.6**	400-800	1+2*	To determine the effect of applied pressure amplitude
3	400	200	600	21.6	18.4	18.7 to 19.6**	275-550	5*** +4*	To determine the stress distribution in depth of EPS geofoam
4	200	600	400	21.6	18.4	18.7 to 19.6**	275-550	4+5*	To evaluate the combined effect of soil and upper EPS layers thickness
	300	500							
	600	200							
	700	100							
5	400	100	700	21.6	18.4	18.7 to 19.6**	275-550	4+4*	To recognize the combined effect of upper and bottom EPS layers thickness
		300	500						
		400	400						
		600	200						
6	400	200	600	28.8	28.8	18.7 to 19.6**	275-550	3+2*	To specify the influence of EPS density
				21.6	21.6				
				18.4	18.4				

* *Indicates the number of tests which have been repeated two or three times to ensure the accuracy of the test data. For example, in test Series 6u, a total of 5 tests were performed, including 3 independent tests plus 2 replicates.*

** *Density of soil layers vary from 18.7 to 19.6 (kN/m3) from bottom to top of soil cover*

*** *Due to insufficient number of available pressure cells, one test was repeated 5 times with placing the pressure sensor at the indicated depths (400, 600, 800, 1000 and 1200 mm below the loading surface in separate tests)*

4 Behavior of EPS Backfills under Static Loading

4.1 Introduction

This section discusses the performance of unreinforced and geocell reinforced pavement foundations on EPS geofoam under static loading as well as uniaxial test result for evaluation of EPS mechanical properties. In Sections 4.2, 4.3 and 4.4 the experimental and numerical results (section 4.5) are presented, respectively. The Test Series used in this Section are based on Table 3-3 and Table 3-4 for mechanical properties of EPS as well as static loading in unreinforced and geocell reinforced installations.

4.2 Experimental procedure

As discussed, the current research is intended to provide an understanding of the mechanical behavior of Expandable Polystyrene (EPS) subjected to monotonic compression loading with different strain rates. A series of uniaxial tests were carried out on cylindrical EPS geofoam specimens with different ratios of height (H) to diameter (D), different diameters (D) and different densities varying from 14.4 kg/m^3 to 28.8 kg/m^3. All the samples were cut from the middle part in order to place the pressure cells to monitor the pressure distribution within the EPS block. In addition, a laser sensor was used to measure the side deflection of the EPS samples to obtain a better understanding of the behavior of EPS geofoam. The EPS blocks used in this study were produced by the company IZOPOL Dvořák, s.r.o. (a local manufacturer in the Czech Republic) with 4 different densities (Table 3-1) which were cut into cylinders using a water-jet (Fig. 1a). The dimensions of the samples were chosen to investigate the effect of the ratio of diameter to height (H/D) within different diameters (D) of samples (Figure 4-1b), as well as other effects described as follow.

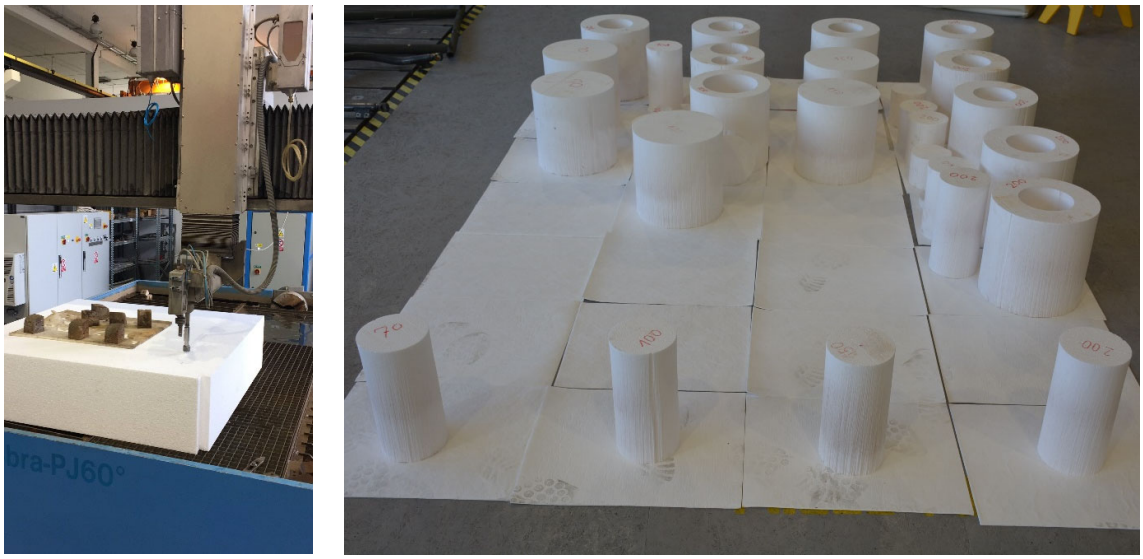

(a) (b)

Figure 4-1: EPS samples preparation: (a) Water jet for cutting the samples, (b) Different sizes of samples cut by water jet

4.3 Small scale tests

Preliminary tests of Test Series A were carried out to check various components of the loading and measurement systems under different loading conditions. Each dimension and density of the EPS blocks in Table 3-1 was prepared from 6 layers of EPS geofoam blocks (Fig. 3a). Pressure cells were placed between the EPS blocks to find out if it was necessary to use more pressure cells in different layers of EPS geofoam (Figure 4-2b). The results show that with an increasing number of EPS layers, the efficiency of the whole testing system is reduced. Due to a lack of lateral support for the EPS blocks, a buckling mode of failure appears with increasing load which leads to instability of the system. This phenomenon certainly affects the results and causes a different pressure distribution between adjacent blocks throughout the height of the arrangement of the EPS blocks. Besides this, the results show that the cubic shape of the EPS samples might induce varied stress distribution on the blocks, thus, the cylindrical sample shape was chosen for the rest of the tests.

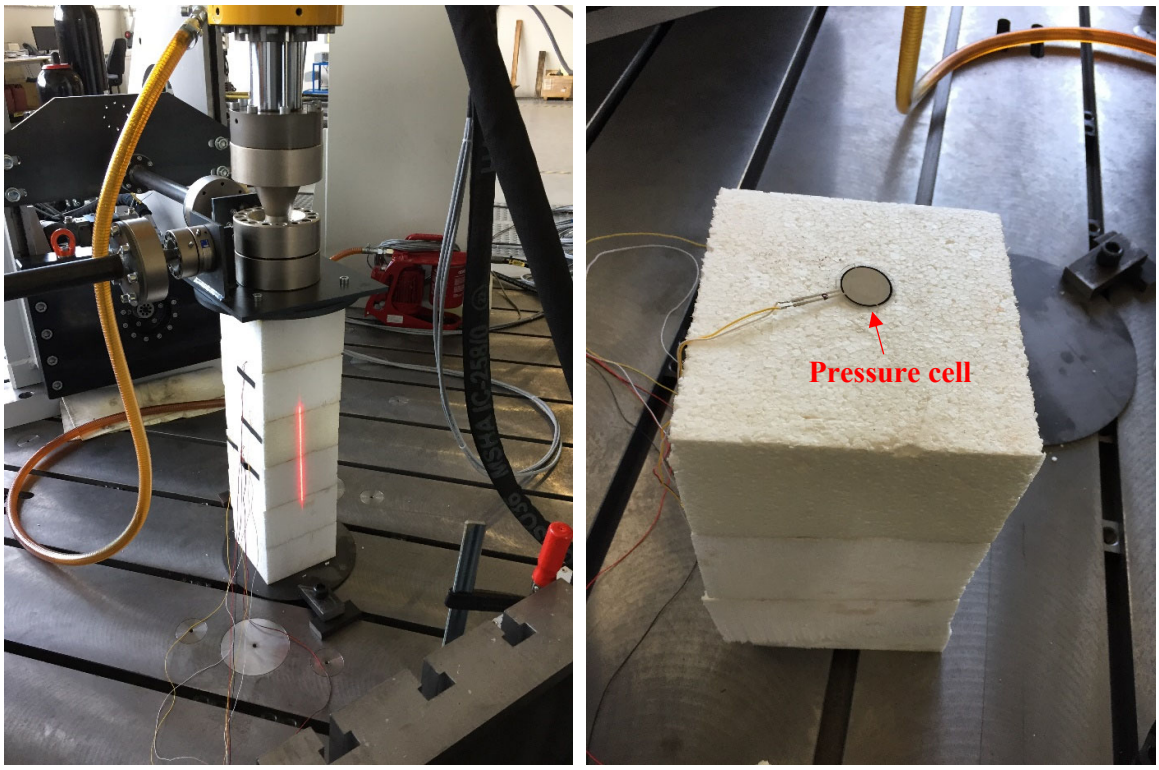

Figure 4-2: Measurement devices installed on EPS samples: (a) Different layers of EPS placed in the loading jack, (b) Pressure cell placed on top of the EPS sample

4.3.1 Effect of height to diameter ratio (H/D)

Test Series B was planned to investigate the effect of EPS sample height or H/D at a specific diameter (D) on the stress-strain behavior of the EPS blocks. The results from Test Series A had shown that increasing the number of EPS layers to increase its height with a constant diameter results in buckling and instability of the blocks. Thus, in this Test Series

single EPS blocks with H/D of 1, 1.2, 1.6 and 2 were tested. The density of EPS was 28.8 kg/m^3 and the strain rate was 0.001 s^{-1}. Figure 4-1 shows the stress-strain curve of EPS geofoam with H/D ratio of 2. Previous research [7] showed that a typical stress-strain curve of EPS geofoam under uniaxial compression loading consists of the following parts: 1) Initial linear behavior, 2) Yielding, 3) Linear-work hardening and 4) Nonlinear with work hardening response. A similar behavioral classification can be made on the stress-strain curve obtained from our tests, as shown in Figure 4-1. However, zones 1 and 2 span a much smaller portion of the figure, and hence are not separated.

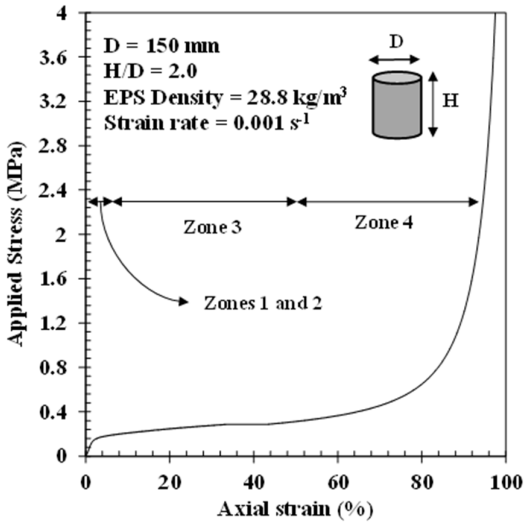

Figure 4-3: Typical stress-strain curve for EPS samples

Fig. 5 shows the result of the uniaxial compression test with a strain rate of 0.001 s-1 on the EPS blocks with a density of 28.8 kg/m3 and different H/D ratios. With increasing H/D ratio, the linear work-hardening zone (zone 3) significantly increases according to Figure 4-4a. Thus, at a specific ultimate stress (say 5.5 MPa in this study), the final strain for H/D=1, 1.4, 1.6 and 2 is approximately 45%, 55%, 75% and 97%, respectively. As tests were performed under stress-controlled conditions, the taller samples (with larger H/D) buckle faster and thus the strains are much larger on reaching a specified magnitude of applied pressure. Additionally, Figure 4-4b demonstrates the stress-strain curves of the sample for up to 10% strain. It is evident that samples with smaller ratios of H/D sustain slightly larger compressive stress compared to taller specimens at this range of strains. The ultimate deformation of shorter and taller EPS samples depicted in Figure 4-5a and Figure 4-5b also suggests that the shorter samples have been compressed evenly along their vertical dimension while the taller samples have experienced bending (visible on the right side of the sample) due to premature buckling. Therefore, taller EPS samples are more likely to demonstrate buckling type failure mechanisms and reduced compressive strength.

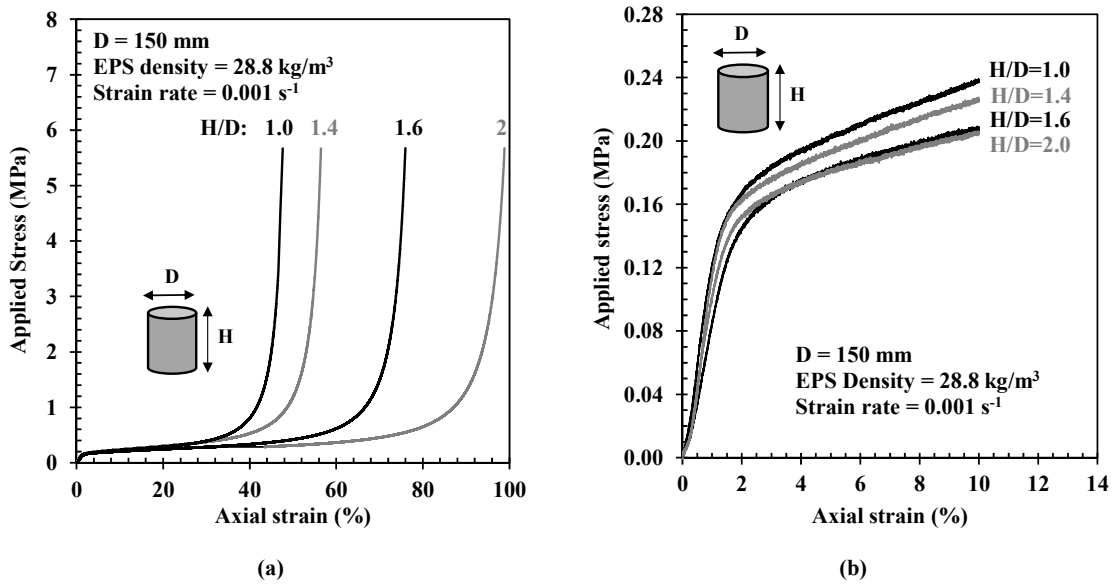

Figure 4-4: Stress-strain curve: (a) for different H/D ratios up to maximum compression, (b) for different H/D ratio up to 10% strain

Figure 4-5: Deformation and failure mechanisms: (a) Regular sample deformation occurring for lower H/D, (b) Buckling-form deformation occurring at larger H/D

4.3.2 Effect of strain rate

In Test Series C, three strain rates of 0.1, 0.01 and 0.001 s^{-1} were selected to evaluate the effect of loading speed. The samples' height and diameter were 300 mm and the EPS density was 14.4, 18.4, 21.6 kg/m^3. Previous observations by Trandafir et al. (2010) showed that the behavior of EPS geofoam is greatly dependent on the rate of loading [27]. According to Figure 4-6a, EPS geofoam exhibits larger compressive strength with increasing strain rate and the difference in the compressive strength between the selected rates increases with increasing strain amplitude. It can be understood that, as the strain rate increases, the increment of increase in the compressive strength of EPS samples gradually decreases.

When the rate of applied pressure is slow, EPS bubbles have enough time to deform and eventually destruct under pressure. As the loading rate increases, the bubbles are forced to contract evenly under the confinement and a smaller number of them might become damaged (comparable to what happens to saturated soil during consolidation). Thus, when pressure is applied in a gentle manner, more EPS bubbles are destroyed and therefore a lower compressive strength is observed. The described mechanism seems to be more valid for lower density EPS geofoam, as the bubbles are larger. The structure of denser EPS geofoam consists of less air and thus might be less sensitive to the loading rate, but this requires further investigation. Figure 4-6b shows the stress-strain response up to 10% strain under the same condition. It is evident that the above discussion is also applicable up to these strain levels.

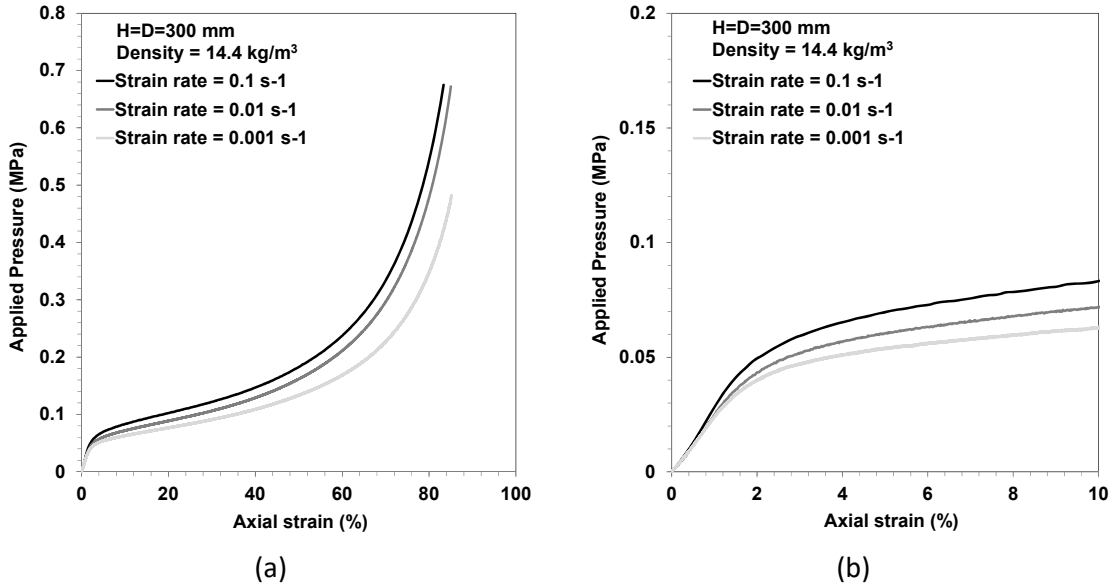

Figure 4-6: (a) Stress-strain curve at different strain rates on various densities of EPS samples with height and diameter of 300 mm (b) The stress-strain curve up to 10% strain under similar condition

Figure 4-7a displays the variation of Young's modulus for different densities of EPS geofoam with the strain rate. Obviously, the higher density EPS shows a larger elastic modulus, and the elastic modulus increases as the strain rate increases. Contrary to the observations made on the whole stress-strain plots, the influence of the strain rate on the Young's modulus of the EPS samples increases with increasing EPS density. This might be because the elastic moduli are obtained from the elastic region of the plots, which are not affected by the bubble's interaction phenomena on the overall plots (Figure 4-6). When the EPS material is elastic (1% strain), the governing influential factor depends on the EPS material itself. It can be concluded that when EPS geofoam is expected to work under elastic conditions, the Young's moduli of the higher density EPS is more dependent on the strain rate, while beyond the elastic limit, lower density EPS would be more sensitive to the loading rate.

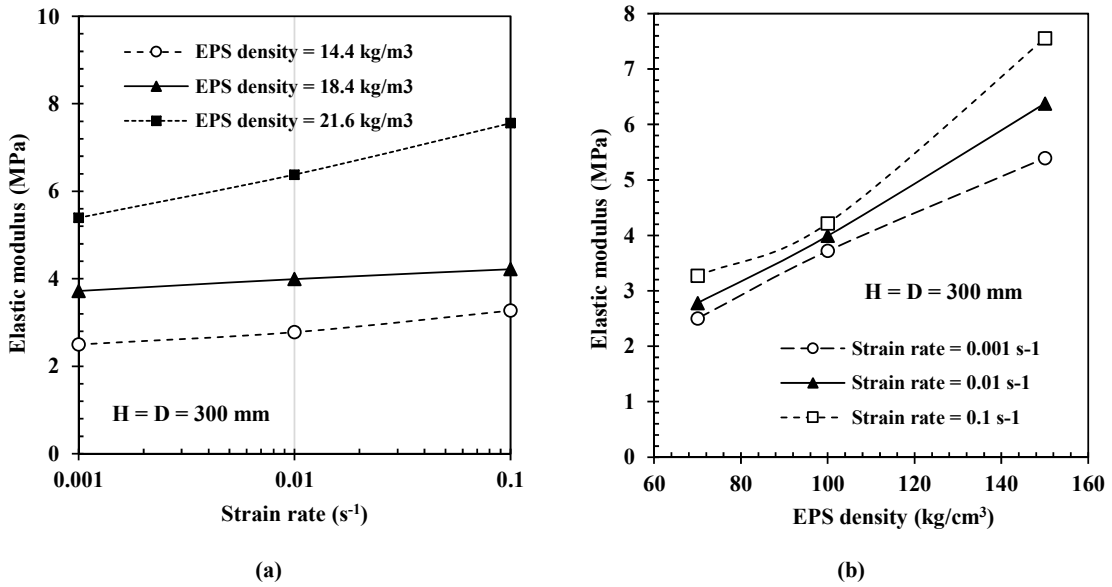

Figure 4-7: Variation of EPS geofoam elastic modulus with: (a) strain rate for different densities of EPS, (b) EPS density at various strain rates

4.3.3 Effect of sample size

In this Test Series, the effect of sample size on the stress-strain response of EPS geofoam is investigated. EPS samples with diameters 100, 200 and 300 mm (representing small, medium and large size) with H/D ratio of 1 were selected and loaded at a rate of 0.001 s^{-1}. From Figure 4-8, it can be seen that the overall stress-strain response of EPS geofoam samples with varying size does not have a significant difference and all the samples behave in similar ways. However, this observation seems to be invalid if certain parts of the stress-strain plots are compared.

The initial part of the stress-strain curve in Figure 4-8 (up to 10% strain) was extracted and displayed in Figure 4-9a to evaluate how these curves differ at the most important strain range (e.g. ranges of elastic modulus and compressive strength). It is evident that the compressive resistance of the larger samples increases with a larger slope, and such samples have shown greater resistance, thus the Young's moduli of larger samples are greater than the smaller samples. Newman et al (2010) also discovered that the elastic modulus of the EPS geofoam sample increases as the sample size increases, thus the moduli of EPS used in the numerical analyses could be selected up to a few times higher than the moduli obtained from testing the small samples [72]. Figure 4-9b shows the variation of elastic moduli vs. the diameter of EPS samples. Using a second order polynomial equation, the dependency of elastic modulus on the sample diameter can be expressed as:

$$E = 0.00004D^2 - 0.0049D + 1.547 \qquad \textit{Equation 4-1}$$

Where E stands for elastic modulus (MPa) and D is the sample diameter (mm). It should be noted that this equation is derived for EPS 100 at a loading rate of 0.001 s^{-1} and can be used to estimate the elastic modulus for the range of diameters used in this study (i.e. 100-300 mm). Although some research have investigated the effect of sample size [1], no such

relation is developed yet. Negussey and Anasthas (2001) have reported that increasing sample size from 50 to 600 mm can increase Young's modulus by 112% [73]. However, in this study, increasing sample size from 100 to 300 mm caused about 220% increase in Young's modulus. Therefore, a final generalization on this issue needs further studies.

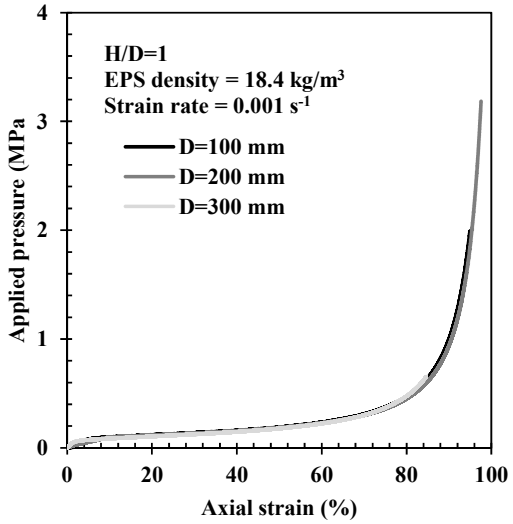

Figure 4-8: Overall stress-Strain curve for different sizes of EPS samples with H/D = 1, density of 100 and loading rate of 0.001 s^{-1}

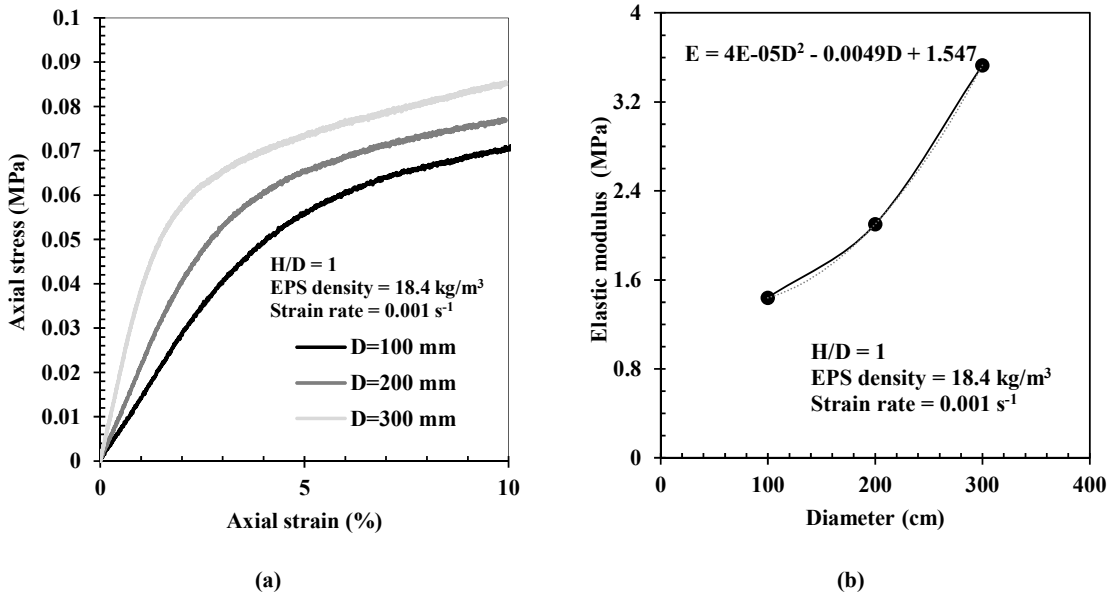

Figure 4-9: Effect of sample size: (a) Stress-strain curve for different sizes of EPS samples with H/D = 1, density of 100 and loading rate of 0.001 s^{-1} for up to 10% strain, (b) Variation of elastic modulus with sample diameter for EPS density of 18.4 kg/m^3 at H/D=1

4.3.4 Effect of EPS density

In Test Series E, the effect of EPS density on the stress-strain behavior and the Young's modulus of EPS samples is investigated. For these tests, the height and diameter of the EPS samples was 300 mm and the rate of loading was 0.001 s^{-1}. Figure 4-10 shows the overall stress-strain curves for various densities of EPS geofoam. As expected, the compressive resistance of EPS geofoam increases with increasing EPS density. EPS with densities 14.4 and 18.4 kg/m^3 are very close in terms of mechanical properties, thus their stress-strain plots move adjacent to each other over a large of portion of strains. The plots of different densities vary at an almost constant difference from 50% strain up to the end of loading. The final compressive pressure (at about 90% strain) sustained by EPS with densities 14.4, 18.4, 21.6 and 28.8 kg/m^3 are approximately 0.5, 0.65, 0.95 and 1.3 MPa, respectively.

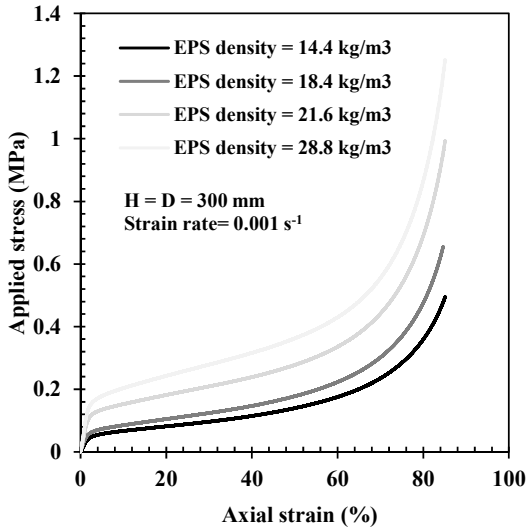

Figure 4-10: Stress-Strain curve for different EPS densities at H=D=300 mm and strain rate of 0.001 s^{-1}

Figure 4-11 shows the variation of Young's moduli for the tested EPS densities and a possible linear fit for the H/D=1 and H/D=2 cases. It should be noted that the Young's modulus for 14.4 kg/m^3 EPS density is slightly larger than the estimated value calculated from the equation obtained from larger densities. However, the upper and lower boundary equations (H/D=2 and H/D=1, respectively) for estimating the elastic moduli based on the EPS density can be expressed as:

$$E=0.5\rho-4.32 \quad \textit{Equation 4-2}$$

$$E=0.46\rho-4 \quad \textit{Equation 4-3}$$

In which ρ (kg/m^3) and E (MPa) stand for EPS density and elastic modulus, respectively.

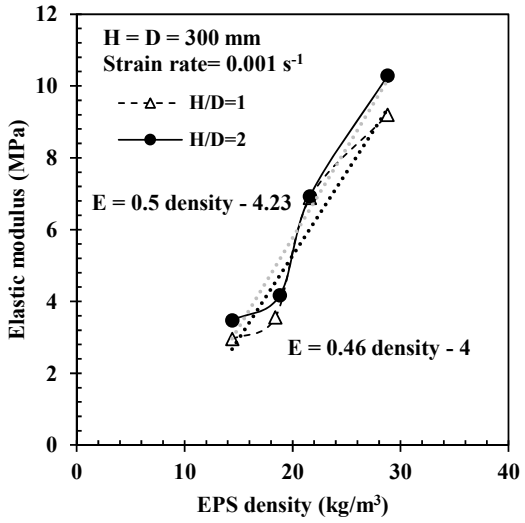

Figure 4-11: Variation of Young's modulus vs. EPS density of samples with H/D=1, 2 and strain rate of 0.001 s^{-1}

4.4 Large scale tests

As discussed, the behavior of pavement foundations underlain by EPS geofoam requires deeper investigation when subjected to short-term, high-amplitude static loads during construction. Yet, beyond the long-term static or impact loading encountered in paved areas (e.g. airports) and repeated loading during service life of roads, the response of such pavement foundations subjected to high-amplitude static loading, temporarily applied during construction phase, is still a concern and needs further investigation and proper improvement techniques.

For EPS geofoam embankments, settlement of the loading surface/plate (δs) and amplitude of the pressure transferred onto EPS blocks (pt) are critical design factors. In this section, the settlement of loading plate (with D = 300 mm) was normalized to the diameter of loading plate in percent (100×δs/D with D = 300 mm) and the measured pressure transferred on EPS geofoam bed was normalized to the compressive strength of EPS geofoam (σc) with the following relation:

$$SR = \frac{P_t}{\sigma_c}$$ *Equation 4-4*

Where SR stands for "Stress Ratio". Therefore, increasing the value of SR from zero to 1.0 means that the transferred pressure on the EPS block is increased from zero to σ_c; hence the maximum compressive strain in EPS geofoam has approximately reached 10% (criteria for commencing plastic strains – compressive strength) and large plastic deformations occur. If SR exceeds 1.0, plastic deformation has occurred in EPS geofoam.

4.4.1 Effect of soil layer thickness

In Test Series 1, four soil thicknesses (i.e. hs = 300, 400, 500 and 600 mm) were considered. Density of the upper and bottom EPS layer were both 30 kg/m^3 and the thicknesses of the upper and bottom EPS layers were 200 and 600 mm, respectively (total of

800 mm). Figure 4-12a presents the surface settlement (δs/D in %) against the applied pressure on the surface for different soil thicknesses. It is evident that for hs = 300 mm, the surface settlement is markedly larger on the whole loading range and with increasing soil thickness, surface settlements reduce. On the first half of loading procedure (say up to 400-500 kPa), the surface settlements increase with an approximately linear trend for all of the case. After this point, the settlement for hs = 300 mm diverges with a greater rate (so is the case hs = 400 mm, but with relatively lower rate). Considering the transferred pressures ratios on EPS (SR values) for the applied pressure of 500 kPa (Figure 4-12b), the values of SR for soil thicknesses of 300 and 400 mm are approximately 0.9 and 0.6, respectively. SR reaches 1.0 for hs = 300 mm at the applied pressure of 570 kPa and it is lower than 1.0 for all of the other cases at the whole range of applied pressures. Thus, by approaching the transferred pressure to the compressive strength of EPS (defined at 10 % strain), excessive strains (up to 10%) are generated in the EPS material, which results in the failure of soil layer above it and subsequent large settlements on the pavement foundation surface. For hs = 500 and hs = 600 mm, the SR values at 800 kPa applied pressure are less than 0.7 and 0.35, respectively; which far away below 1.0. It is evident that when the overlying soil thickness is ≥400 mm, the transferred pressure on EPS is within the compressive strength of EPS and the surface settlements do not grow at a considerable rate.

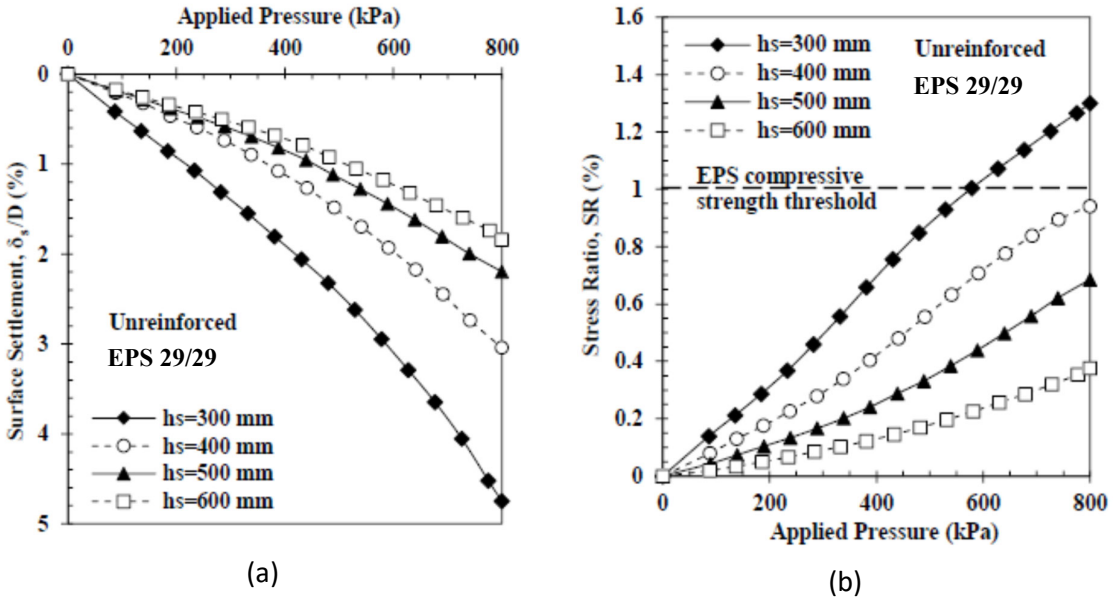

Figure 4-12: (a) Variation of surface settlement vs. applied pressure, (b) Variation of transferred pressure ratio (SR) vs. the applied pressure, for the different thicknesses of unreinforced soil layer placed on EPS 40/40 pavement foundations

4.4.2 Effect of EPS density

To evaluate the effect of EPS density, four arrangement of EPS on the subsequent EPS layers (i.e. EPS 29/29, EPS 29/22, EPS 22/22 and EPS 22/19, the first and second number represent density of upper and bottom EPS layers in kg/m^3, respectively) was considered in Test Series 2. Thickness of the upper soil layer (h_s) was selected equal to 400 mm in this set of tests. Although Stark et al. (2004) has suggested using 610 mm for the unreinforced soil

thickness, Gandahl (1988) and PRA (1992) had suggested 300 and 400 mm soil thickness, respectively. As will be shown in the next section, this thickness would be sufficient when geocell reinforcement is incorporated. As shown in Figure 4-13a, the surface settlement for EPS 40/40, EPS 40/30 and EPS 22/22 cases varies almost linearly with increase in the applied pressure. The case of EPS 22/19 also shows the same behavior up to applied pressure of ~500 kPa. After this point, the settlement increases with an increasing rate and reaches to 13.4% on the applied pressure of 800 kPa. Whereas the surface settlements at the 800 kPa pressure are about 5.7%, 3.8% and 3% for EPS 22/22, EPS 29/22 and EPS 29/29 cases. As shown in Figure 4-13b, the values of SR for EPS 29/29 remain below 1.0 for the whole range of loading amplitudes, while for EPS 29/22, EPS 22/22 and EPS 22/19, SR exceeds 1.0 at about 700, 650 and 580 kPa applied pressure, respectively. For EPS 22/19 cases, SR increases steadily while approaching 1.0 and also beyond this point; likewise, the surface settlement also increases rapidly (see the bending of the plot for EPS 22/19 after 550 kPa applied pressure in Figure 4-13a). Therefore, if EPS 22/19 is considered to be used without soil reinforcement, the magnitude of the surface applied pressure should not exceed 580 kPa.

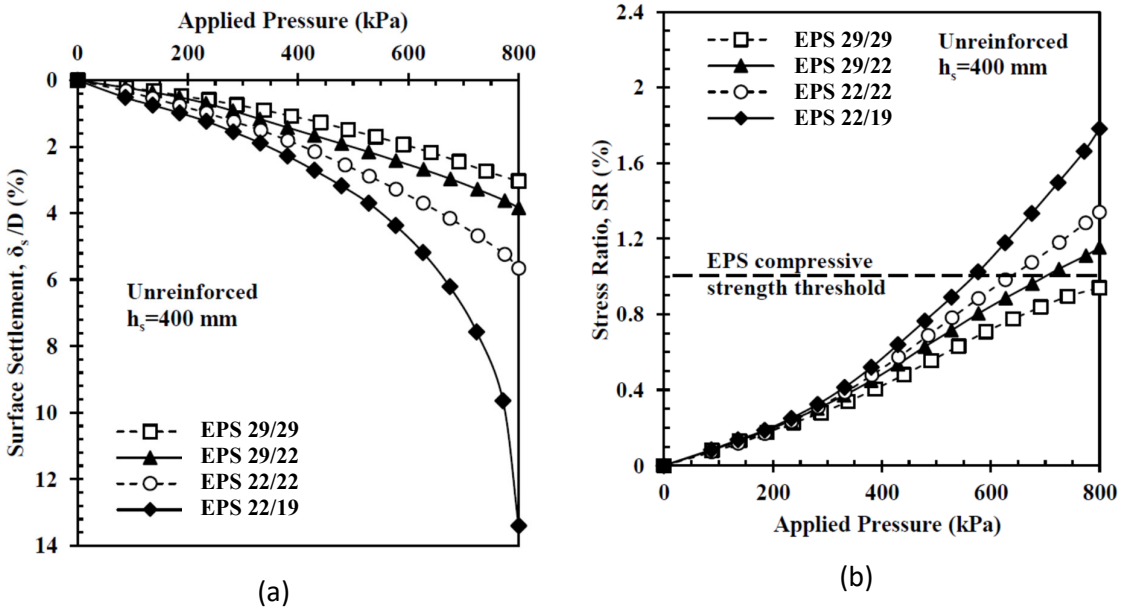

Figure 4-13: (a) Variation of surface settlement vs. applied pressure, (b) Variation of transferred pressure ratio (SR) vs. the applied pressure, for unreinforced soil thickness of 400 mm placed on different densities of upper and bottom EPS layers

4.5 Numerical Analysis

To provide further understanding on EPS geofoam behavior, numerical modelling was carried out and presented in this section. There are several numerical (and of course numerically implemented analytical methods) for addressing the behavior of EPS geofoam material [6, 26, 74-77]. Hazarika (2006) introduced a constitutive model for EPS geofoam under large-strain and rapid loading. The model encompasses the size and shape factors and the density of EPS geofoam. The yield function is defined by taking EPS as a von Mises type material, and considering the isotropic hardening approach Wong and Leo (2006) established a simple elastic-plastic hardening constitutive model using a series of triaxial

tests on EPS samples with the confining pressures ranging from 0 to 60 kPa. The model includes six rheological constant parameters depending on the isotropic elastic behavior, the first yield stress, the hardening rate, and the flow rule and the dilatancy behavior. Neither the time dependency (creep) nor the size and shape factors of the EPS specimens are not addressed in this constitutive model.

A common method is LCPC (Laboratoire Central Ponts et Chaussees) [78], which is simplified form of the Findley approach (Findley et al., 1989) as:

$$\epsilon_t=(\frac{\sigma}{Eti})+at^n \quad \text{Equation 4-5}$$

$$a= 0.00209\left(\frac{\sigma}{\sigma y}\right)^{2.47} \quad \text{Equation 4-6}$$

$$n= -0.9\ log_{10}[1-(\frac{\sigma}{\sigma y})] \quad \text{Equation 4-7}$$

$$\sigma_y= 6.41\gamma-35.2 \quad \text{Equation 4-8}$$

$$E_{ti}= 479\ \gamma-2875 \quad \text{Equation 4-9}$$

in this equation Eti (kPa), γ (kg/m^3) and σy (kPa) are initial tangent Young's modulus, density and yield strength of EPS geofoam, respectively. In this model, the strain values are directly related to the imposed stress and the density of EPS geofoam [77]. Effect of loading time on the behavior of EPS geofoam is considered in the LCPC model. Chun et al. (2004) introduced a hyperbolic model in which the behavior of EPS material is based on the principal stress, principal strain, confining stress and the density of EPS block. This model is represented as follows:

$$\sigma_1= a\epsilon_1^{b}{}_{(\%)}/ (c+ \epsilon_1^{b}{}_{(\%)}) \quad \text{Equation 4-10}$$

$$a= -60.955+9.843\gamma+0.339\sigma_3 \quad \text{Equation 4-11}$$

$$b= 1.135+0.042\gamma-0.008\sigma_3 \quad \text{Equation 4-12}$$

$$c= -0.437+0.102\gamma-0.002\gamma^2+0.011\sigma_3-0.00039\gamma\sigma_3 \quad \text{Equation 4-13}$$

In this equation, ϵ1 (%), σ3 (kPa) and γ (kg/m^3) are the major principal strain, confining stress, and the value of the density, respectively. The important point of this hyperbolic model is that the strain-dependent tangent modulus Et (kPa) is a function of confining stress, density, and strain:

$$E_t= d\sigma/(d\epsilon_{1\ (\%)}/100)= [abc\epsilon_1^{b-1}{}_{(\%)}/(\epsilon_1^{2b}{}_{(\%)}+2c\ \epsilon_1^{b}{}_{(\%)}+c^2)]*100 \quad \text{Equation 4-14}$$

The key point in this constitutive model is that it was derived from straining (at rate of 1 mm/min) of cylindrical EPS geofoam samples with diameter and height of 50 and 100 mm, respectively.

Meguid and Hossein (2017) suggested a robust modelling procedure for numerical simulation of EPS geofoam behavior. In this model, the elastic isotropic model, Misses yield criteria and associated flow rule were considered to define the elasticity and plasticity of EPS geofoam, respectively. This method is capable of capturing the hardening of EPS material as a key factor in the response of EPS geofoam blocks. To define the plasticity, the nominal

values of strain and stress should be converted to their real values. Owing to this fact, Equation 4-15 to Equation 4-18 have been proposed for converting experimental results to numerical input values in the current study:

$$\epsilon_{true} = Ln\ (1+ \epsilon_{nominal}) \quad \text{Equation 4-15}$$

$$\sigma_{true} = \sigma_{nominal} / (1-\nu\ \epsilon_{nomimal})^2 \quad \text{Equation 4-16}$$

$$\epsilon_{true} = \epsilon_{elastic} + \epsilon_{plastic} \quad \text{Equation 4-17}$$

$$\epsilon_{elastic} = \sigma_{true} / E \quad \text{Equation 4-18}$$

Although some might use the Mohr-Coulomb model for EPS geofoam, the pivotal point in EPS blocks' response is the hardening after the 1% strain (elastic gamut). In some analyses the maximum deformations are in the threshold of elastic area, so it is viable to be mentioned that the Mohr-Coulomb is practical in the little deformation values. On the other hand, the employed model in numerical analyses is capable to see the hardening occurring over the elastic threshold (see Figure 4-15).

4.5.1 Modelling the Uniaxial Tests

In order to have a better knowledge of EPS geofoam blocks, the mentioned procedure in the above (Meguid and Hossein, 2017) was implemented in 3D finite element numerical models using ABAQUS [76, 79]. The model dimensions and loading patterns are similar to those of test samples. Figure 4-14a shows full 3D mesh of modelled sample with eight-node linear brick elements (C3D8) and Figure 4-14b shows a typical 2D side view of the models with the proposed loading. To simulate the uniaxial compressive tests, the base of EPS models was fixed and compressive loads were applied at the top of models. In all numerical analyses, the EPS blocks' tips were banned from horizontal directions, in which the symmetric response is clear (see Figure 4-16a).

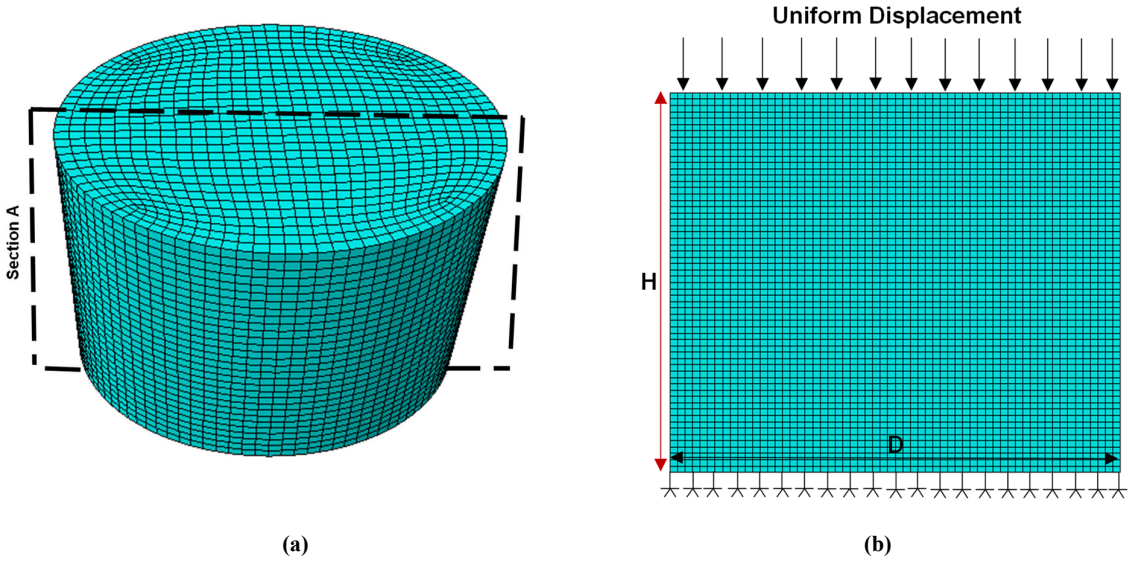

Figure 4-14: (a) Full 3D mesh of the samples EPS geofoam in ABAQUS, (b) Typical 2D side view with the boundary conditions

4.5.2 Numerical results

Results of the numerical simulation for various factors are presented in this section. Figure 4-15 show the stress strain curve for different EPS densities using the implemented methods compared to the tests. For these cases, the height and width of EPS geofoam sample is 300 mm and the strain rate is 0.001 s^{-1}. It is clear that the numerical method produces the best match with test results for all of the cases. Although Chun et al. (2004) method produces an overall reasonable trend for the whole range of strains, the values are not close to the experimental results at a great part of the stress-strain curve. Using this method, the stress strain curve for EPS with density of 21.6 kg/m^3 shows the best match with test results.

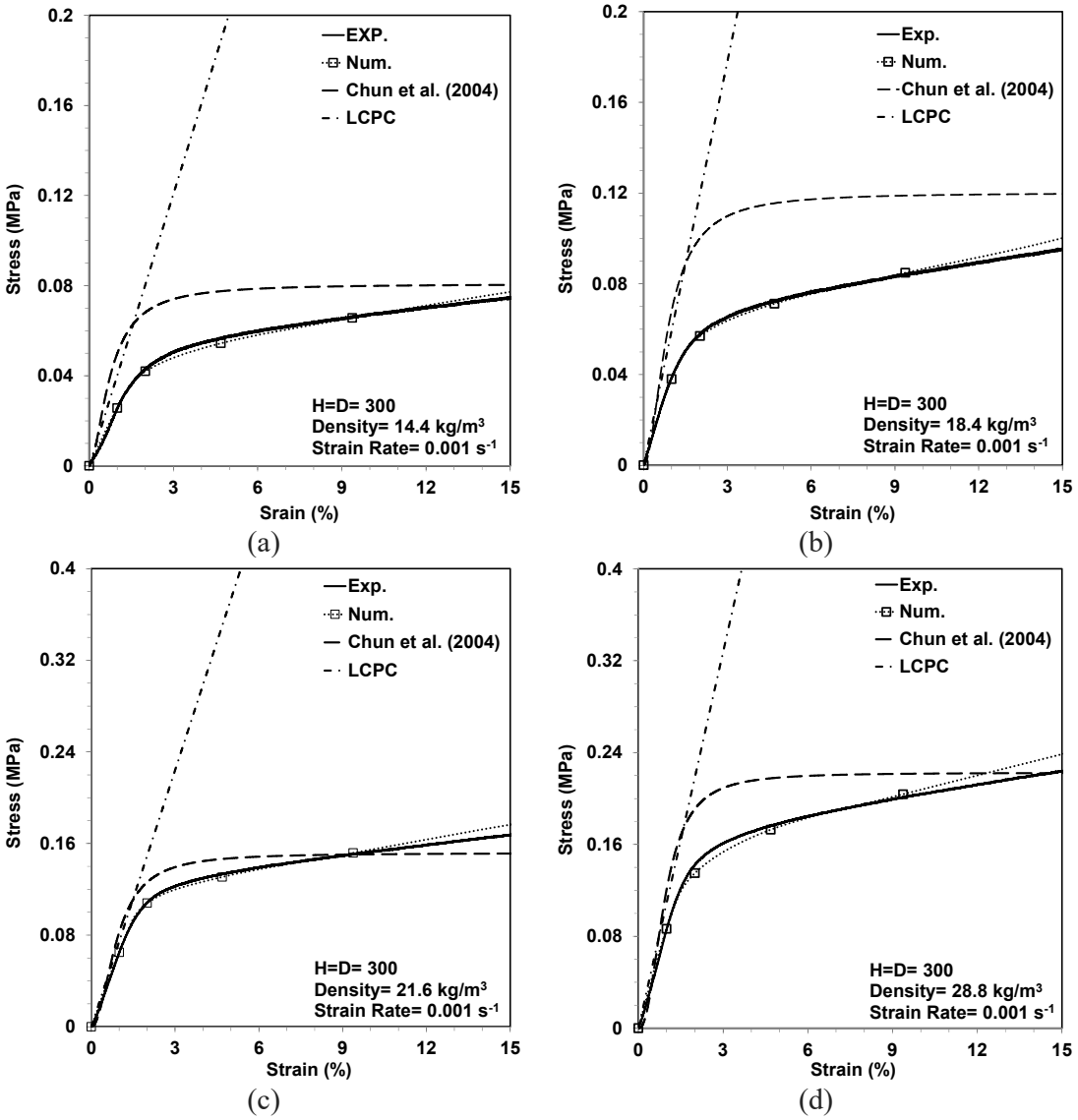

Figure 4-15: Comparison of stress-strain response for EPS densities of (a) 14.4 kg/m3, (b) 18.4 kg/m3, (c) 21.6 kg/m3, (d) 28.8 kg/m3 using various numerical methods

On the other hand, using LCPC method, the results are only valid up to strain level of 1% and beyond this point, the stress increases linearly with strain and no specific yielding point exist. Therefore, LCPC is not a reliable method for the strain values beyond 1%. The Chun method is appropriate for an initial evaluation and provides best results for intermediate EPS densities (i.e. 21.6 kg/m^3). The most reliable method for predicting stress-strain behavior of EPS is the numerical method by Meguid et al. (2017), also incorporated in this study [76].

The stress contour within the symmetric plane of EPS sample is presented in Figure 4-16a. It is clear that the stress is maximum in the middle (core) of the sample and at the outer top and bottom edges. The main portion of applied pressure is sustained by an internal core, extended diagonally to the upper and bottom of EPS sample. Thus, with this stress gradient at the two ends of the sample, and stress concentration at the external edges, the cracking of EPS sample edges under loading plate is explicable. Figure 4-16b shows stress amplitude along the central core of EPS geofoam sample height. With increase in density of EPS geofoam, the EPS strength increases and the stress amplitude at a specific height increases with increase in EPS density. Furthermore, it shows that the stress values are maximum at the center of the samples and it decrease gradually moving from the center toward the bottom and upper surface.

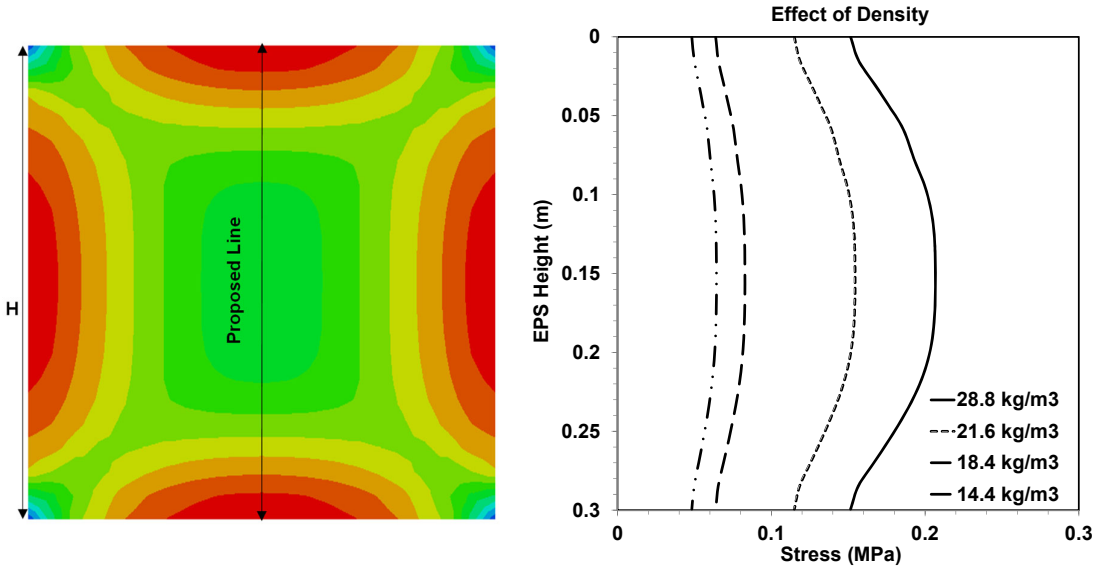

Figure 4-16: (a) Typical stress contour at sample symmetry plane for EPS block under the 5% percent axial strain, (b) stress along the centre line of different densities of EPS geofoam under The 5% axial strain

Figure 4-17 shows the effect of height to diameter ratio of EPS samples using different numerical methods compared to the test results. For all of H/D cases in the numerical analysis, the stress-strain response of H/D=1 was used. It is clear that the adopted numerical procedure yields the best fit for the experimental data for H/D=1 and H/D=1.2. For the larger H/D ratios, the numerical method somehow overestimates the applied pressure for a certain stress. This might be due to the fact that the numerical model is much more idealistic in terms of material quality and its distribution over the whole volume of the sample. In reality, the samples are not completely intact and they certainly include points of weakness

including micro-cracks etc. Furthermore, the EPS material is not evenly distributed within the sample volume, causing a varying stiffness in the sample. For these reasons, taller samples are more likely to buckle under compression. However, such fact is neglected in the numerical samples due to inherent idealization of such FEM modelling. Finally, although the overall trend is acceptable for all H/D cases using test data for H/D=1, it is best to use the stress-strain values of the specific H/D under study. Similar to previous results, it can be seen that Chun model also provides reasonable estimation for the whole strain range, while LCPC is only valid up to about 1% strain.

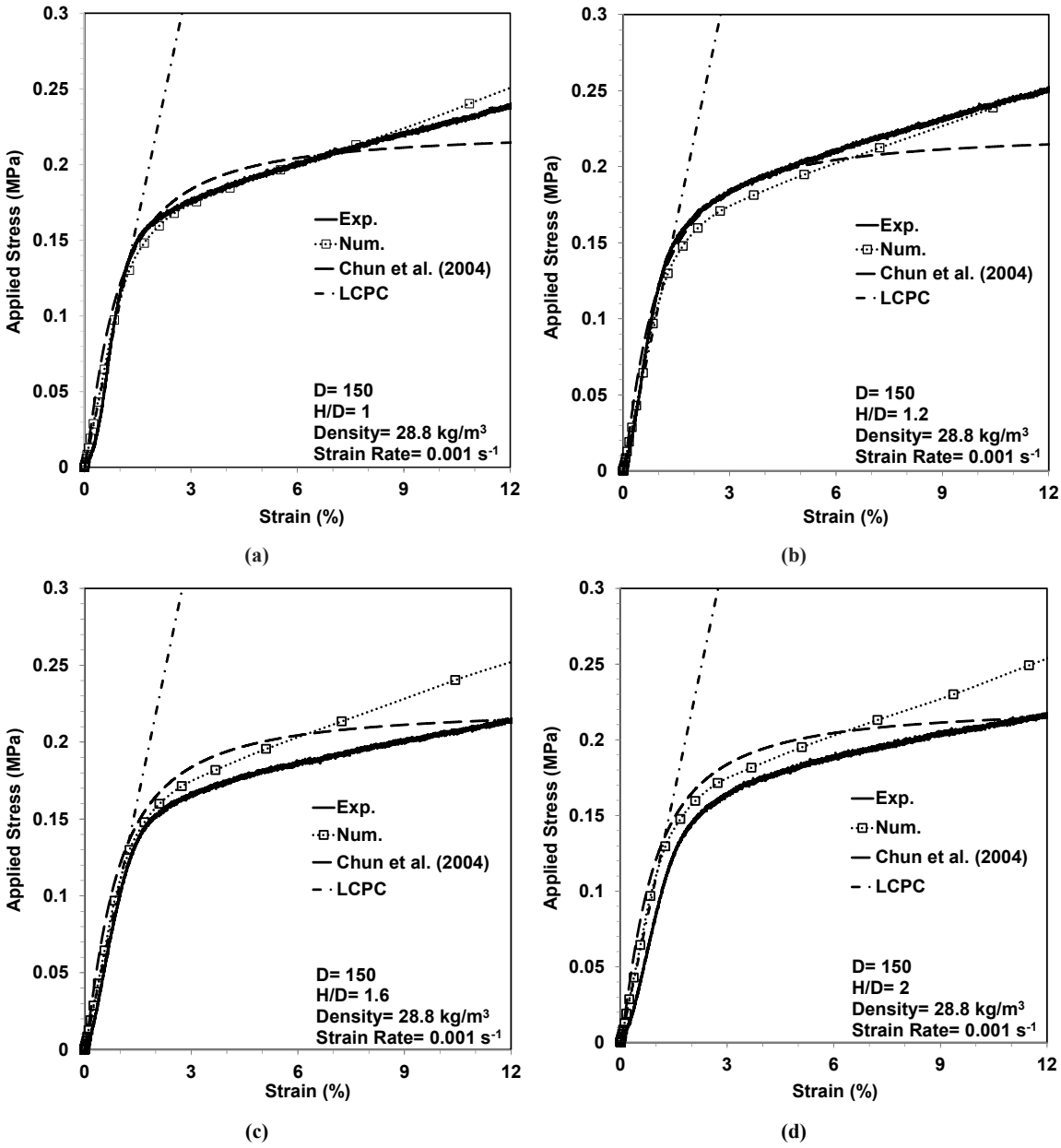

Figure 4-17: Stress-strain response of 28.8 kg/m3 EPS geofoam samples using various numerical methods for (a) H/D=1, (b) H/D=1.2, (c) H/D=1.6, (d) H/D=2

Figure 4-18a presents the typical contour of lateral deformation (in z or x direction) of EPS geofoam samples. As seen, the deformations at the side region of the samples is negligible. This phenomenon is due to the very low Poisson's ration of EPS geofoam (Stark et al., 2004). Poisson's ratio of EPS geofoam might vary depending on the applied compressive stress. Studies by Trandafir et al. (2010) have shown that the Poisson's ratio of EPS geofoam is relatively small and close to zero [27]. Normally, this slight Poisson's ratio value can be assumed zero, however it would be slightly larger than zero before yielding strain (i.e. 10%) and can become slightly negative when EPS geofoam is compressed sufficiently. The negative Poisson's ratio at this condition is the result of destruction of air bubbles and the inward collapse of the EPS structure.

For clarification, the sample diameter under loading (initial sample diameter plus the lateral deformation) vs. the value of deformation in one side is shown in Figure 4-18b. Due to very low Poisson's ratio, the difference between lateral deformation plots of different H/D ratios is insignificant. Figure 4-19a shows the effect of samples' size with numerical and experimental results. The numerical results are in good agreement with the experiments. In Figure 4-19b, the stress values at the center of the samples vs. axial strain is plotted for various sample sizes. With increase in the samples size, the stress required to generate a specific strain in the samples is increased for larger samples. At 15% axial strain, samples with D = 300 and 200 mm sustain 47% and 21% greater pressure compared to samples with D=200 mm and 100 mm, respectively. As noted before, large samples show larger strength due to the size effect of EPS geofoam.

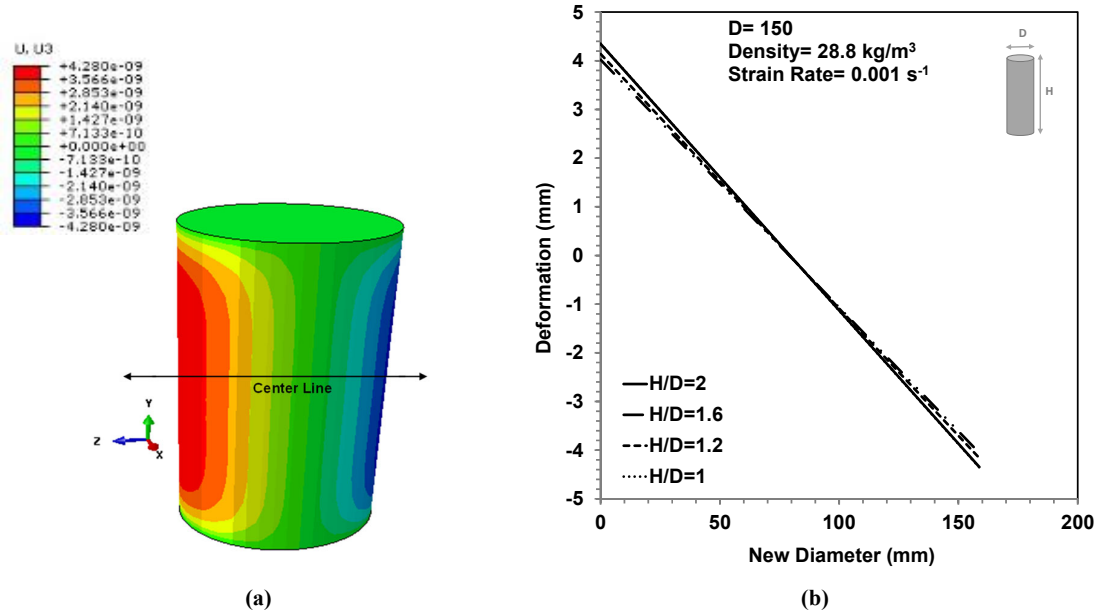

(a) (b)

Figure 4-18: (a) Typical contour of lateral strain of EPS geofoam samples along z-axis under compressive loading (b) Lateral deformation of EPS geofoam samples with different H/D ratios under the strain level of 10%

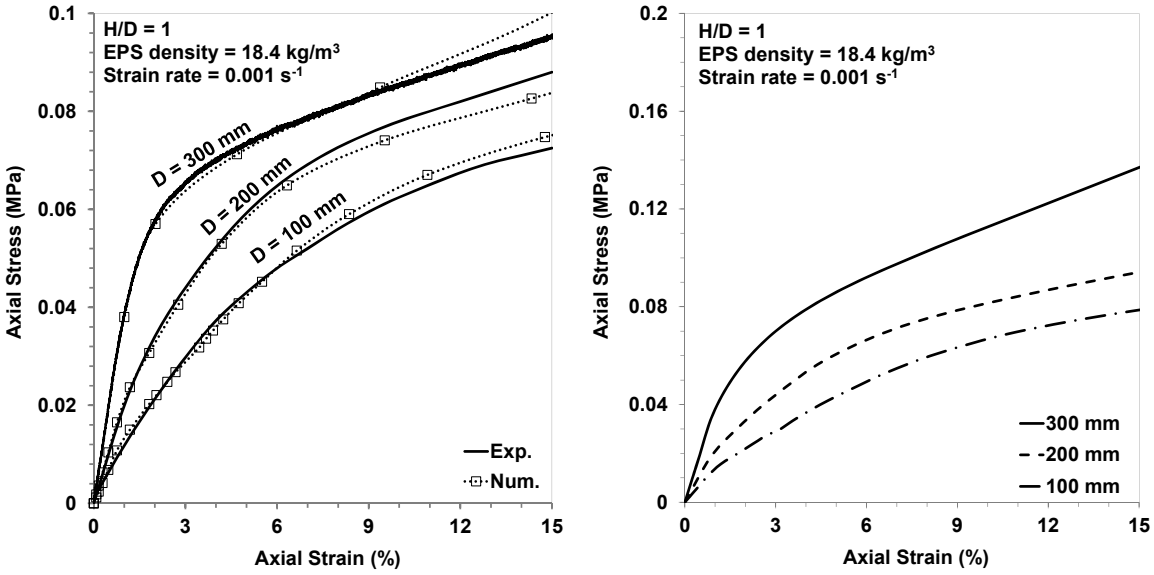

Figure 4-19: (a) Comparison of experimental and numerical methods on the effect of EPS sample size, (b) Stress at the center of EPS geofoam sample vs. axial strain for different sample dimensions

5 Behavior of EPS Backfills under Repeated Loading

5.1 Introduction

In this chapter, the results of repeated plate load tests are investigated. The overall pavement response is initially presented in Section 5.2 and then the behavior of pavement systems under repeated loading are discussed in Sections 5.3.

5.2 Overall responses

First, it would be beneficial to provide a typical comparison of reinforced and unreinforced pavement foundations in terms of surface settlement and transferred pressure on EPS geofoam in Figure 5-1a to Figure 5-1d. For the installation reported in this plot, thickness of the overlying soil layer is 400 mm and density of the top and bottom EPS layers are 22 and 19 kg/m^3, respectively (Test Series 2a and 2d in Table 3-5). During the first stage of loading (275 kPa applied pressure), variation of surface settlements for the unreinforced and reinforced cases is analogous each other, both reaching to about 5 mm after 100 load repetitions. To show the precise pressure-settlement path, Figure 5-1a was magnified for the first ten load cycles and is shown separately in the bottom-right corner of the figure. As is commonly seen in repeated loading results, the first cycle of loading shows a typically larger amount of settlement, probably due to bedding effects. Distinguishingly, the second stage of loading (550 kPa applied pressure) involves progressively increasing settlement increments during loading repetitions for the unreinforced case. Thus the development of accumulated residual and resilient deformations is evidently larger compared to the reinforced case. It is inferable that the reinforced case demonstrates stable shakedown state, while the unreinforced one shows an unstable shakedown [55] and might end up in failure due to incremental collapse after more load repetitions [80]. The final (of last cycle) peak surface settlement of the unreinforced and reinforced pavement foundations reach to 25.08 and 16.53 mm, respectively – indicating a notable reduction (34%) in surface settlement due to geocell provision.

Diagrams of the pressure transferred to EPS geofoam (Pt) can assist in explaining the described observations (see Figure 5-1c and Figure 5-1d). During the first loading stage, the peak value of Pt in unreinforced and reinforced cases remains averagely around 36 and 30 kPa, respectively. These pressures are substantially lower than the stabilizing pressure threshold of EPS 22 (Ps = 140 kPa as given in Table 3-1). With increasing the applied pressure to 550 kPa in the unreinforced case, the pressure transferred to EPS geofoam exceeds 120 kPa in the first cycle and gradually rises up to about 140 kPa, which is identical the critical threshold stress for EPS 30 – a failure is expected beyond this point. However, Pt remains below 100 kPa (significantly lower than Ps for EPS 22) for the reinforced case during this stage. The rate of change in Pt is increasing for the unreinforced case and slightly decreasing for the reinforced case, representing progressive failure of soil due to strain accumulation (Figure 5-1a) and shakedown states (Figure 5-1b), respectively. Similar performance improvement due to provision of geocell in subballast was also reported by Indraratna (2014). Thus the reinforcement acts to reduce the stress to tolerable levels, thereby

preventing strain accumulation in soil due to accumulative irrecoverable strain/damage in the underlying EPS geofoam.

Lateral resistance of the geocell walls prevents soil from early shear failure and also provides significant confinement which prevents initiation of failure surfaces. Hegde and Sitharam (2015) observed when the underlying bed is weak, geocell can resist the foundation load even after failure of the weak bed [58]. It is reported that large repeated stress applications cause progressive punching in a thinner unreinforced soil layer lying over EPS due to the weak support [68] and/or low (or even negative) Poisson's ratio of the underlying EPS geofoam [25]. Thus, it can be concluded that in a geocell-reinforced soil layer placed over an EPS geofoam bed, "vertical stress dispersion" mechanism could be the prime resistance against lower applied pressure. When the pressure is increased and the EPS layer subsequently deforms excessively below the pressurized zone, "lateral resistance" and "membrane mechanisms" would be effective. However, studies are required to confirm these predictions.

In any individual loading cycle, as the stress is applied through the loading plate, the surface settlement increases from a minimum value to a peak value. Then, during unloading, due to the elasto-plastic nature of the soil and EPS geofoam, only the elastic part of the settlement is recovered, but the plastic component remains. In other words, surface settlement increases from a minimum value to a maximum ("peak") value during each loading cycle before returning to a new minimum ("residual") value which is slightly larger than the previous minimum. It is clear that both the peak and residual settlements increase with load cycle number. Both are important, therefore the envelope formed by the peak and residual surface settlements have been plotted in Figure 5-1b and used for interpretation of results hereafter.

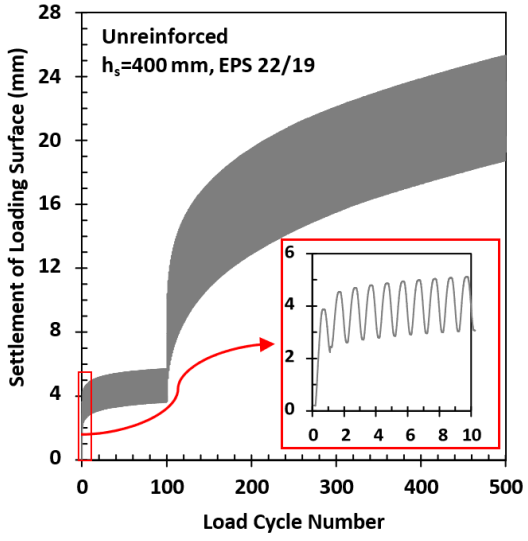

(a)

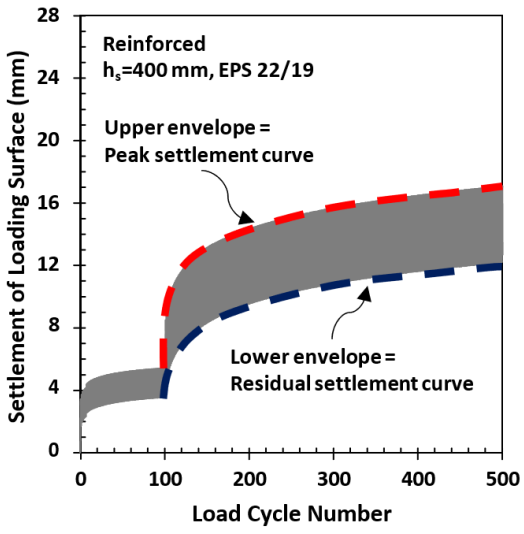

(b)

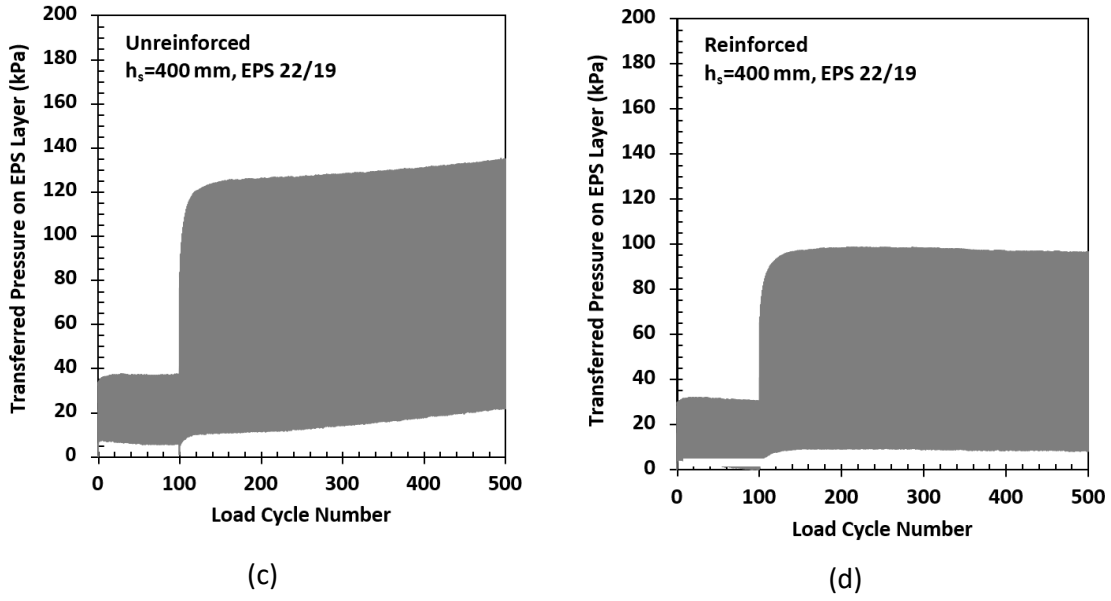

(c) (d)

Figure 5-1: Typical variation in the settlement of loading surface with load cycles for (a) unreinforced and (b) reinforced installations. Typical variation of the transferred pressure on top of EPS geofoam bed with load cycles for (c) unreinforced and (d) reinforced installations. The thickness of soil layer placed on EPS 22/19 was 400 mm

5.3 Behavior of unreinforced EPS-soil backfill

An initial set of tests were performed in the test box to identify the effect of upper soil layer density, intensity of applied pressure and distribution of stress with depth inside the EPS geofoam body. The tests also allowed the evaluation of the effects of soil thickness, upper EPS thickness and EPS geofoam density. The Test Series used in this Section are based on Table 3-5 for repeated loading in unreinforced installations.

5.3.1 The influence of backfill soil compaction

Due to the soft nature of the EPS geofoam layer, the overlying soil layer has to be compacted to its maximum achievable compaction state to reduce the effect of EPS bed and provide sufficient strength to the system. As mentioned in previous sections, the maximum compaction of a 300 to 400 mm soil cover placed over EPS blocks will not produce a dry density higher than 18.7 kN/m^3 (corresponding to 92% of maximum dry density). For 600 to 700 mm thickness, this value can reach up to 19.6 kN/m^3 (corresponding to 96% of maximum dry density). To evaluate behavior of sandy soil and its compaction (density) under repeated loading, large-scale plate load tests (will be addressed later as Test Series 1 in Table 3-4) were conducted. For this purpose, soil was placed and compacted in 12 lifts of 100 mm height to reach a total elevation of 1200 mm. To achieve a similar dry density for the soil alone, several in situ density tests were performed with various amount of compaction energy to determine appropriate compaction method of the sand alone. It was found out that only approximately half as many passes of the compactor were needed for the soil-only lifts to achieve an equal dry density as when the soil was placed over geofoam blocks.

Figure 5-2 compares hysteresis curves and settlement of loading surface for the two dry densities described in the previous paragraph. After applying 100 cycles of 275 kPa repeated pressure, the surface settlement for 18.7 kN/m^3 and 19.6 kN/m^3 cases are about 2 mm and 1.7 mm, respectively. Subsequent application of 400 cycles with 550 kPa amplitude results in a maximum settlement of 6.6 mm and 3.1 mm for these densities, respectively. Although for the low amplitude repeated pressure, the reduction of settlement with increase in dry density is only 15%, this decrease is about 53% for high amplitude load. For the lower applied pressure, the response remains in its non-plastic region under both compaction states and the settlements are similar.

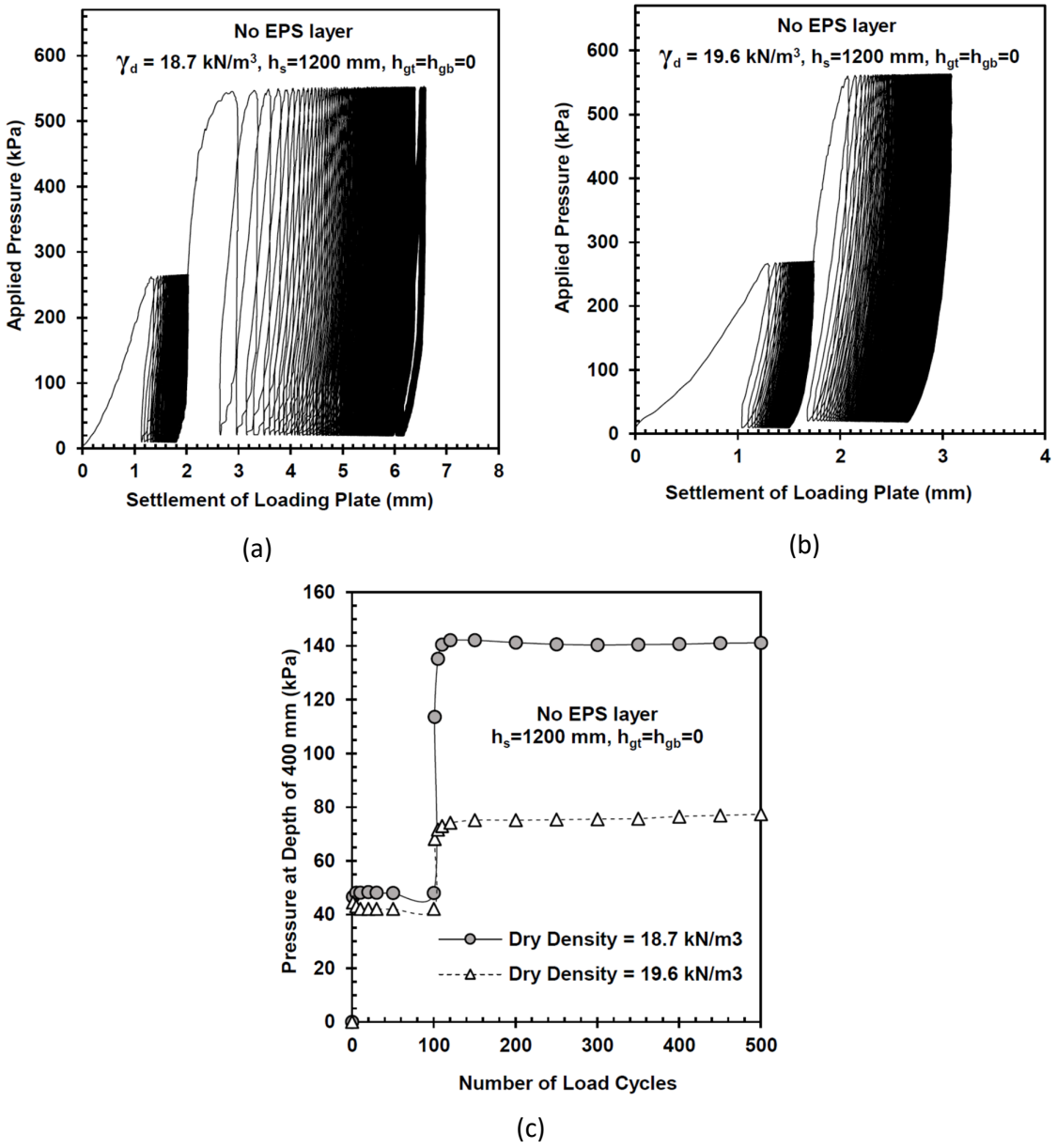

Figure 5-2: Settlement of pressure surface under 100 cycles of 275 kPa and 400 cycles of 550 kPa for (a) soil dry density of 18.7 kN/m3, (b) soil dry density of 19.6 kN/m3 and (c) Variation soil pressure with number of load cycles at depth of 400 mm

Under the large, repeated pressure, larger plastic strains and surface deformation occur in the less compacted soil due to its lower shear resistance. Consequently, application of a higher compaction energy to attain the maximum dry density can be assumed trivial in many, but not all, circumstances. Depending on the loading that the pavement will carry, special attention to compaction may have to be paid, in order to assure adequate performance.

To investigate this phenomenon in detail, it is also useful to determine the stress values in the soil as shown in Figure 5-2c. For the sake of comparability with the future tests, a pressure cell was placed at depth of 400 mm in the backfill soil. When the repeated applied pressure is 275 kPa, the measured pressure is almost identical for both dry densities, ranging between 40 and 50 kPa. By increasing the applied pressure to 550 kPa, a substantial difference shows up in the pressure levels transferred to the depth of 400 mm: the peak value of transferred pressure for low and high density cases is 140 and 80 kPa, respectively. Thus the difference in the amplitude of transferred pressure is a function of density and load level, which can be understood in terms of modulus dependency on stress level. When there is insufficient compaction and sufficient stress so that plastic deformation occurs, then modulus is low, stress is less efficiently distributed and higher peak stress levels are felt vertically beneath the load.

Accordingly, for 550 kPa stage, the stabilized resilient modulus calculated from tests [81] were approximately 270 and 230 MPa for high and low compaction cases, respectively, and were slightly lower for the 275 kPa applied pressure. These values are comparable to those of typical quarry material and, lower than those of recycled concrete aggregate [40]. The dependency of resilient modulus on the bulk stress for granular material can be simply modeled as [82]:

$$M_r = k_1 \theta^{k2} \qquad \text{Equation 5-1}$$

Where θ is the bulk stress (σ1+ σ2 +σ3), k_1 and k_2 are regression or calibration factors of this two parameter model. With increase in the bulk modulus, the resilient modulus increases. This deduction is also consistent with the fact discovered regarding the settlements of the loading surface for the two studied compaction levels.

5.3.2 The influence of applied pressure amplitude

Test Series 2 and 3 from Table 3-4aim to identify the effect of loading amplitude on settlements of the surface of pavements including EPS and to determine the pressure transferred to the upper EPS layer. A typical soil thickness of 400 mm (based on Swedish standard, 1987; Norwegian standard, 1992) was used in this Test Series. The thicknesses of upper and bottom EPS layers were selected as 200 mm and 600 mm with densities of 30 and 20 kg/m3, respectively. Each layer of soil above the EPS was compacted to its maximum achievable compaction (18.7~19.6 kN/m^3). The test was performed with load amplitudes of 400 and 800 kPa, which are the pressure amplitudes that might be applied to the pavement surface (of unpaved roads). The other pressure amplitudes were 275 and 550 kPa representing reduced pressure values anticipated on the soil beneath the asphalt cover layer in a paved road.

Figure 5-3 a and b illustrate the hysteresis curves for the specified tests. It indicates that while the reduced load (275 and 550 kPa) can hardly produce a settlement larger than 25 mm in the loading surface after a total of 500 loading cycles, the original pressure (400 and 800 kPa) can trigger up to 70 mm settlement in the loading surface after applying only 200 load cycles. The test was terminated at this surface settlement so as to prevent excessive settlement and possible damage to the pressure cell.

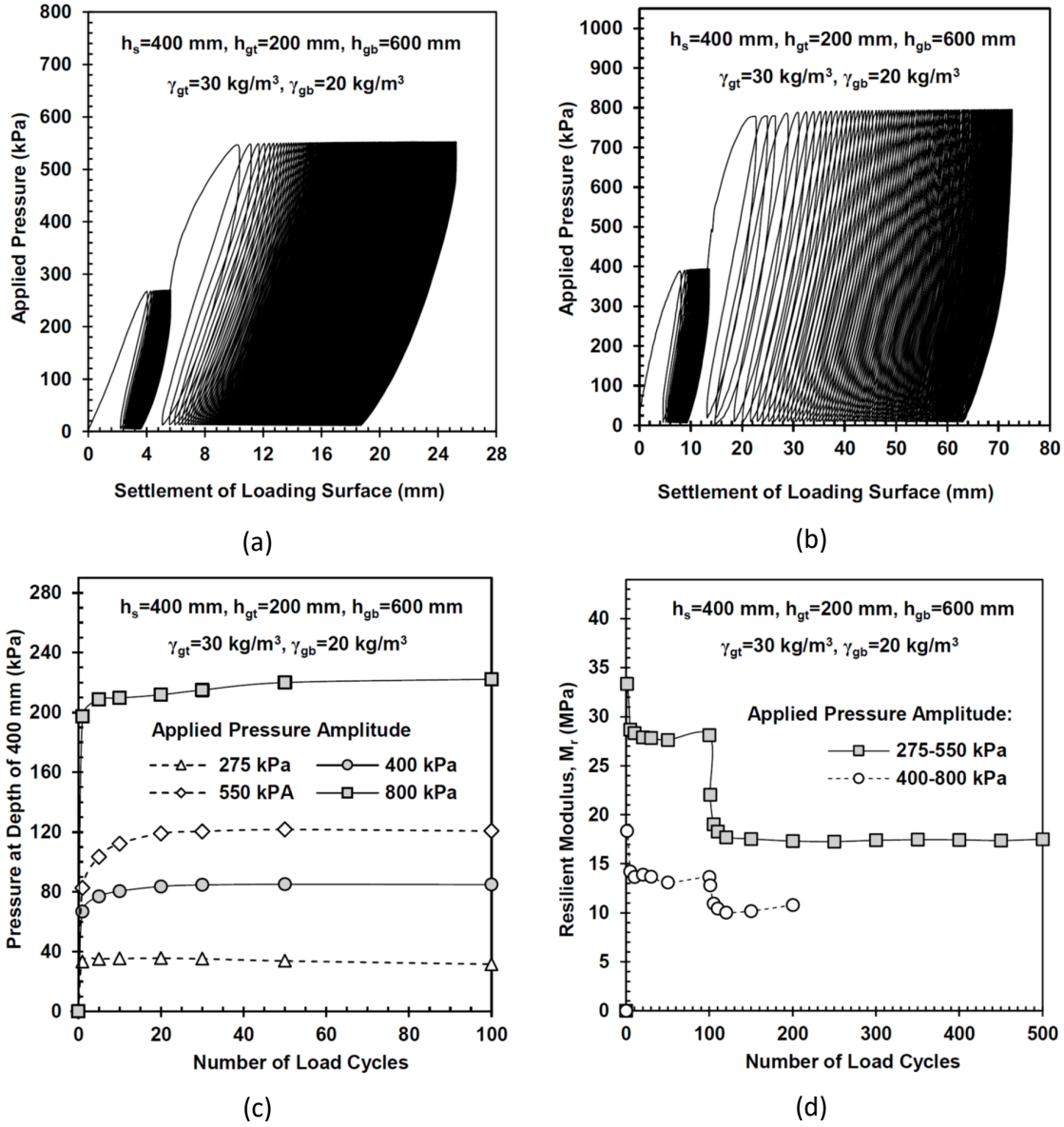

Figure 5-3: Settlement of loading surface for different pressures of repeated loading (a) after 500 cycles of reduced loading (paved road), (b) after 200 cycles of original loading (unpaved road) and (c) Measured pressure at depth of 400 mm during the first 100 cycles of each loading intensity (d) Resilient modulus of pavement for each loading intensity scenarios

Figure 5-3c depicts the value of transferred pressure on the first layer of EPS. When the applied pressure is 550 kPa, the transferred pressure is about 120 kPa which is perhaps

below the limit of unstable residual deformation of the EPS 30 as shown in Figure 5-3b. For 800 kPa, the conveyed pressure is larger than 200 kPa, which is well beyond the 150 kPa limit of instability for EPS 22. As the repeated tests on EPS samples showed, when the applied pressure over geofoam becomes excessive, the EPS very rapidly exhibits large strains with a slight increase in the pressure. Furthermore, as shown earlier in this section, the soil may not then be capable of spreading the applied load so effectively, transferring it to the EPS.

Variation of resilient modulus for soil and EPS geofoam were investigated separately in the previous sections. To deliberate resilient modulus under combined effect of soil and EPS geofoam, Figure 5-3d should be noticed. During application of 400 kPa repeated pressure (400- 800 kPa loading scenario), M_r was stabilized on 13 MPa, and it decreased to ~10 MPa under the subsequent repeated pressure of 800 kPa, until failure happened. This particular level of resilient modulus corresponds to a very short service life for the pavement, unless proper base and subbase courses to be considered above them. The other loading scenario (275-550 kPa) exhibits a better behavior, with a resilient modulus 27 and 17 MPa during the lower and higher applied pressure, respectively. While separate examination on EPS 22 and soil demonstrated resilient modulus values in orders of 5 MPa and 200 MPa for them respectively, the described assembly of these two material have resulted in a resilient modulus of 17 to 27 MPa. The reason for such low resilient modulus of the composite pavement system is the inability of EPS geofoam to provide sufficient support for the 400 mm soil above it, preventing mobilization of adequate confining pressure (bulk stress as of Eq. 5-1, to enable higher resilient moduli in soil [24].

Thus, using EPS geofoam for roads requires the designer to limit the pressure transferred to the EPS layer so as to keep the deformations of the pavement surface in a tolerable range. For unpaved systems, this implies a substantial increase in thickness of soil layer above the EPS blocks and paying attention to the density of the compacted soil. Of course, this may introduce undesirable increases in dead load and/or in construction time. For paved roads on the other hand, an asphalt layer with a typical thickness of 50 mm would deliver a definite improvement (reduction) in deformation of the system and in the pressure imposed on the EPS (46% in this study based in Figure 5-3c). In most cases, a thicker asphalt layer might be used with even greater reduction in the pressure value.

5.3.3 Variation of pressure with depth in EPS layers

Four confirmatory tests were carried out to guarantee that the pressure transmitted to the bottom of the box is negligible (Test Series 3 from Table 3-4). Similar to Section 5.3.2, the tests were performed on 400 mm of soil cover placed over four layers of EPS geofoam blocks, each with a thickness of 200 mm. The density of the uppermost EPS layer was 21.6 kg/m^3 (EPS 22) and the remaining layers were formed of EPS 19 (density of 18.4 kg/m^3). The pressure sensor was placed on the top of the top EPS layer and between the EPS layers. In this Test Series, 100 cycles of 275 kPa were followed by 400 cycles of 550 kPa load applied to loading surface. The condition and parameters' values for all of the above tests (except the location of pressure cell) were the same. As the surface settlements were closely replicated

for the all the tests (regardless of depth of the pressure cell) only the surface settlement of the test with the pressure cell at a depth of 40 mm is shown in Figure 5-3.

Figure 5-4 shows the variation of vertical pressure with depth below the loading surface. At the boundary of the soil and the first layer of the EPS (at a depth of 400 mm), the maximum pressure is about 122 kPa, about 22% of the applied surface pressure of 550 kPa. Under the first layer of EPS geofoam (at a depth of 600 mm), the pressure drops to about 15% of the surface loading pressure, a further 37% reduction from its value at the top of the EPS 22 (400mm above). By a depth of 800 mm, the pressure is only 7% of the surface pressure (a 56% decrease over the last 200mm thickness of EPS) and by a depth of 1000 mm, the stress is only 4% of the surface pressure having reduced to 18 kPa (a 47% reduction across the EPS). The role of the soil in providing the initial stress distribution is, thus, apparent. At the bottom of the box, the pressure is about 15 kPa, compared to 18kPa at the top of the lowest EPS layer – i.e. the bottom EPS layer doesn't achieve much load spreading and, at such a low stress level, won't compress much (c 1.38 mm using the EPS results presented earlier). This confirms the adequacy of the box's vertical dimensions.

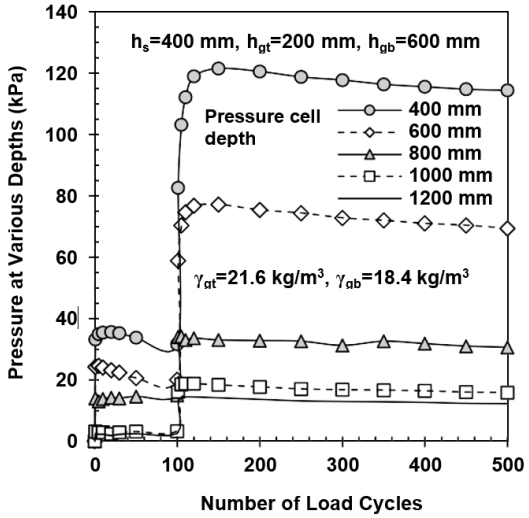

Figure 5-4: Measured pressure at different layers of EPS geofoam for 100 cycles of 275 kPa and 400 cycles of 550 kPa pressures

Yet, it appears that EPS geofoam transfers pressure vertically rather than horizontally. This can be explained with the low Poisson's ratio and non-granulated structure of this material. Granular material such as soil can effectively redistribute pressure in the horizontal direction due to interlocking of the particles, while geofoam bubbles are compressive and does not tend to expand laterally and thus, cannot appropriately transfer the pressure in the horizontal direction. Because of this characteristic, EPS geofoam undergoes very little or even zero lateral expansion (or somehow contraction unlikely) when subjected to deviator compressive pressure and induces significantly lower lateral pressures than normal earth pressures [75].

5.3.4 Combined effect of soil and upper EPS layers' thickness

Test Series 4 (see Table 3-4) was arranged so as to study the influence of variation in the soil and upper EPS layer thicknesses on the settlement of the loading surface and the pressure transferred through the soil and the top EPS layer. A layer of low-density EPS (here 400 mm of EPS 20) was placed at the bottom of test pit and the remaining part of the pavement was filled with a high-density EPS (here EPS 30) and a layer of soil. The thickness of the soil layer (hs) and thickness of the upper EPS layer (hgt) were varied within a total constant, thickness, of 800 mm.

Figure 5-5a displays total (peak) and residual deformations of the loading surface for different values of hs and hgt under 100 cycles of 275 kPa followed by 400 repetitions of 550kPa. The figure indicates that when hs is thinner than 300 mm, the pavement will undergo severe settlement after just 150 cycles. At this point, total settlement rises to 68.5 mm and the amount of residual settlement is 52.5 mm (Figure 5-5b). For larger values of hs, this rapid and unstable growth in total and residual deformation are not observed and the pavement behaves predictably for 500 load cycles. However, the degree of stability and rate of increase in total and residual settlements is not similar among them. Although the increase in rate of deformation is negligible for hs=700 mm, the remaining cases show an increase in the deformation during repeated load application. If hs is smaller than 400 mm, the pavement deformation will certainly pass 25 mm, a typical maximum allowable rutting at the surface of a low volume road [83]. On the other hand and as shown in Figure 5-5b, a maximum rut depth of 50 mm for low volume roads and 30 mm for major roads is suggested by AASHTO T 221-90, criteria that would be met for low volume roads so long as hs≥300mm whereas hs≥400mm might be needed for major roads at larger numbers of cycles.

An extended clarification can be obtained by reviewing the pressure variation over the upper layer EPS blocks. According to Figure 5-5c, for hs=600 mm and hs=700 mm, the peak pressures applied to the upper EPS layer are about 64 kPa and 37 kPa, respectively. These values are well below 100 kPa which was found as a potential upper limit for stabilized behavior of EPS 22. When the pressure transferred to the EPS is around or higher than 100 kPa (in the case of hs<=400 mm), EPS can be expected to deform at a very rapid rate, based on the earlier tests performed on the EPS specimens. Thus, from a pressure point of view, Figure 5-5c confirms that a soil thickness of >400 mm can be desirable in order to limit large EPS deformation under a surface stress of 550 kPa.

Effect of soil and upper EPS layer on the resilient modulus is presented in Figure 5-5d. As expected according to this plot, with increasing soil thickness, the resilient modulus increases. When the pavement is subjected to the first 100 cycles of 275 kPa pressure, the resilient moduli for hs=700, 600, 400, 300 and 200 mm are 115, 80, 40, 27 and 13 MPa, respectively. During the second loading stage (550 kPa applied pressure), the corresponding resilient moduli decrease to 50, 30, 21, 17 and 7 MPa, respectively. While a designer might find hs≥ 300 mm and its corresponding resilient modulus proper for subgrade under the lower pressure [81], a soil thickness of at least 600 mm might be required to satisfy typical requirement for resilient modulus of subgrade.

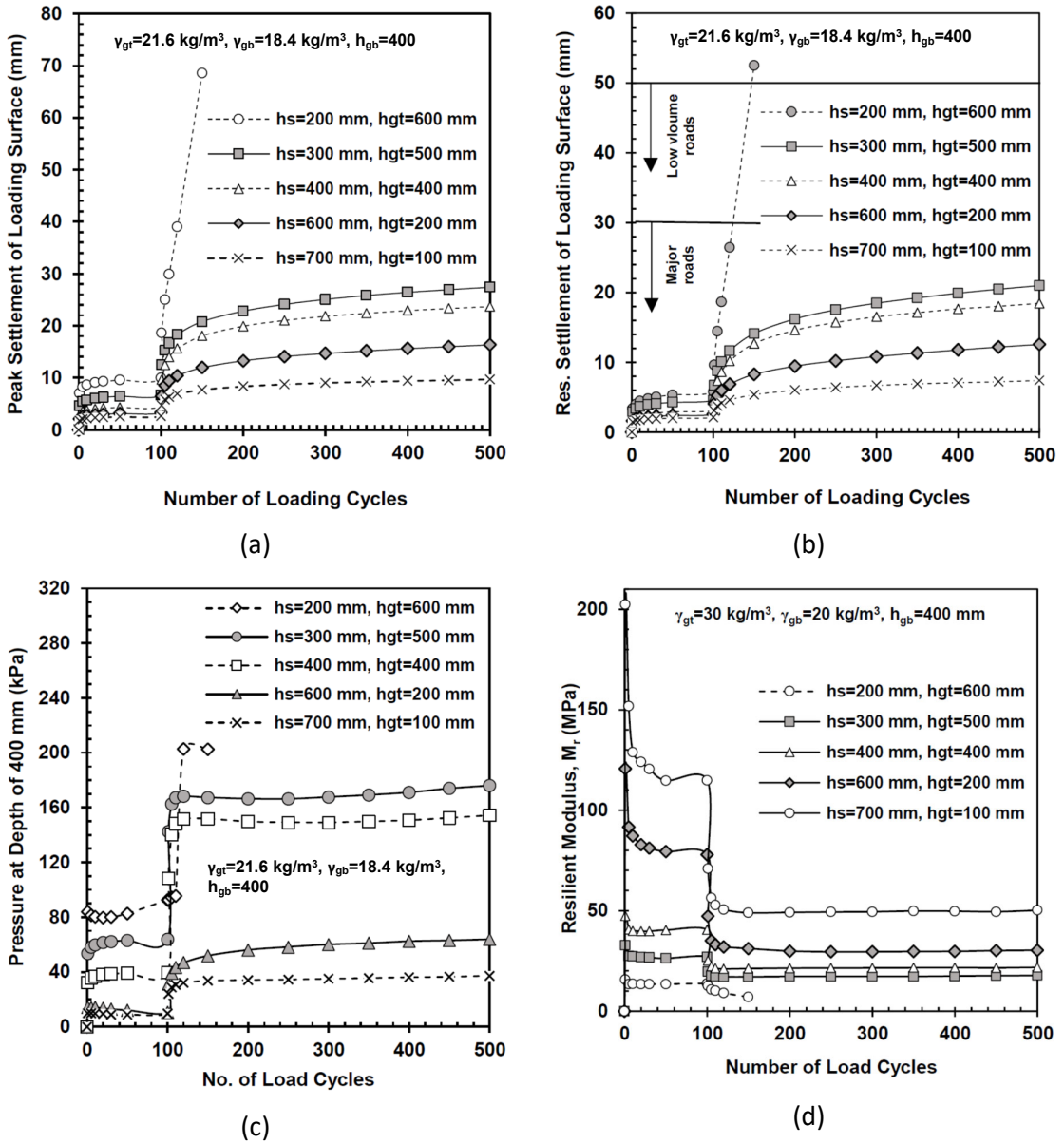

Figure 5-5: Variation of (a) total settlements and (b) residual settlements versus number of loading cycles for different values of soil and upper EPS layer thickness (hs and hgt) and, (c) Variation of transferred pressure at depth of 400 mm (top of EPS 30) for different values of hs and hgt, (d) Resilient modulus of pavements with different soil and upper EPS layers' thicknesses

Although AASHTO 1993 specifies a limit for the lower bound of resilient modules, such criterion has not been necessitated by the mechanistic-empirical (MEPDG 2008) approach and it has simply considered various cracks types and ruts as performance indicators. Nevertheless, Boone (2013) examined the effect of several factors including resilient modulus on the distress response of the pavement in Ontario area and warned that base resilient modulus and subgrade resilient modulus are among several distress indicator factors that would impact bottom-up fatigue cracking and top-down fatigue cracking,

respectively. So in terms of resilient modulus, compacted soil and EPS 22 layers with 400 and 200 mm respective thicknesses, placed on EPS 19, require a thicker asphalt layer (thicker than 50 mm of 2.5 GPa asphalt layer) in order to prevent premature failure. Otherwise, only lighter trucks should be allowed to pass, or the service life will drop significantly.

From the above figures, variation of residual (permanent) vertical strain rate against residual vertical strain is derived and shown in Figure 5-6a. When hs = 200 mm, incremental failure occurs and permanent or residual vertical strain increases rapidly, while for hs = 300, 400 mm, a mild increase in permanent vertical strain is observed, indicating plastic creep behavior. For hs = 600, 700 mm, plastic shakedown is evident. Vertical strain was calculated from the following equation [84]:

$$\varepsilon_v = \frac{4\delta_s}{\pi D(1-\upsilon^2)} I_z \qquad \textit{Equation 5-2}$$

Where δs, is the settlement of loading plate, D is the plate diameter, υ is soil's Poisson's ratio and Iz is the stress influence factor (equal to unity for circular foundation on the surface).

To prove such behaviors, the vertical stress at the middle of soil layer is plotted against the confining pressure of the soil layers in Fig. 5-6b. Range of the behavioral trends introduced by Werkmeister et al. (2001) are specified by dashed lines in this figure [31]. It is worth mentioning that the vertical stress at the middle of soil layer is calculated as the average of applied pressure on the surface and measured pressure values on EPS (shown in Figure 5-5c). The confining pressure of the layer is back-calculated from resilient modulus values (Figure 5-5d) using the simple k-θ relationship ($M_r = k1\ \theta^{k2}$). From Rada and Witczak (1981), values of k1 and k2 were interpolated as 2335 kPa and 0.59 (sum of 0.75 value for silty sands and 0.25 value for sand-gravel materials), where θ is the confining pressure at middle of the soil layer [85]. These values are also consistent with the proposed ranges by Huang (2004) [86]. The calculated stress values are presented in Table 5-1. Location of these stress points in Fig. 5-6b ascertains that hs=700 mm experiences plastic shakedown, hs=600, 400 mm demonstrate plastic creep, while hs=300, 200 mm undergo incremental failure. It should be remembered that the underlying EPS layers are neglected in this approach and the calibration factors introduced (k1 and k2) are representative of triaxial testing condition.

Table 5-1: Calibration factors for nonlinear analysis

h_s (mm)	Applied pressure (kPa)	Transferred pressure (kPa)	σ_1 (kPa)	M_r (kPa)	σ_3 (kPa)
200	550	203	376.5	9000	9.5
300	550	175	362.5	17000	27.3
400	550	154	352	22000	42.0
600	550	64	307	30000	70.5
700	550	35	292.5	50000	165.1

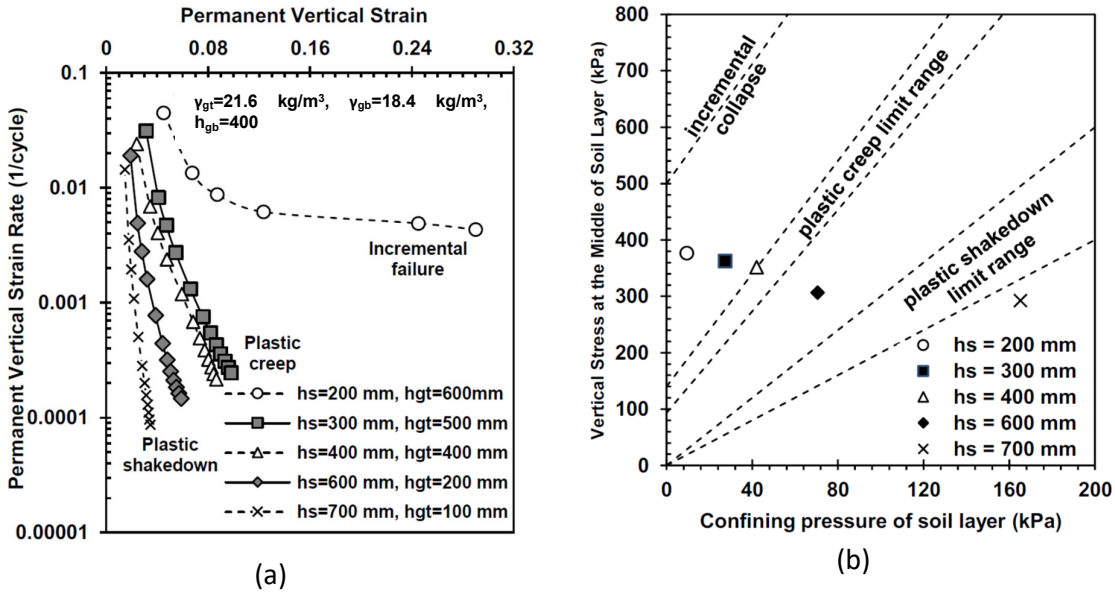

Figure 5-6: Variation of: (a) permanent vertical strain of the loading surface versus permanent vertical strain, (b) confining pressure of soil layer with the vertical stress at the middle of soil layer and behavioral limits

Additionally, ultimate values of peak and residual settlements of the loading surface are compared for different values of soil thickness in Figure 5-7.

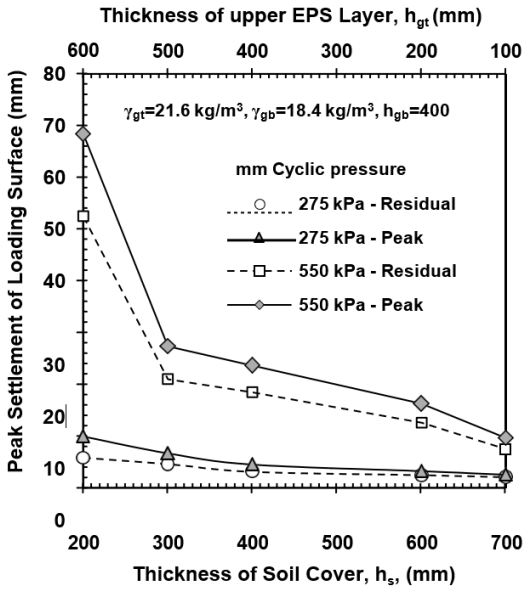

Figure 5-7: Variation of the maximum values of peak and residual settlement for different thicknesses of soil and upper EPS layers (hs and hgt)

When the lower pressure of 275 kPa is applied to the loading surface, the variation of maximum settlement does not change significantly, and it is negligible when hs is below 400 mm. It is also clear that the peak and residual deformations are very close at this point, meaning that the majority of deformation is recoverable. For a repeated load of 550 kPa, a

noticeable variation in the peak and residual deformations can be perceived with respect to hs and the difference between peak and residual deformations is clear.

Based on the peak settlement profile of loading surface shown in Figure 5-8, the maximum peak deformation of the loading surface was 75 mm for the soil layer thickness of 200 mm and the deformation for the other thicknesses of soil are, evidently, much lower. It is commonly expected that the area of soil deforming would increase with increase in depth of settlement due to the extension of the failure surface in the soil and/or the beam-type deflection of an upper foundation layer. However, in these tests, the deformation 'bowl' hardly extends beyond the edge of the loading plate for any soil thickness (Figure 5-8). This indicates a punching mechanism under the loading plate for the pavements constructed on soil-over-EPS layers.

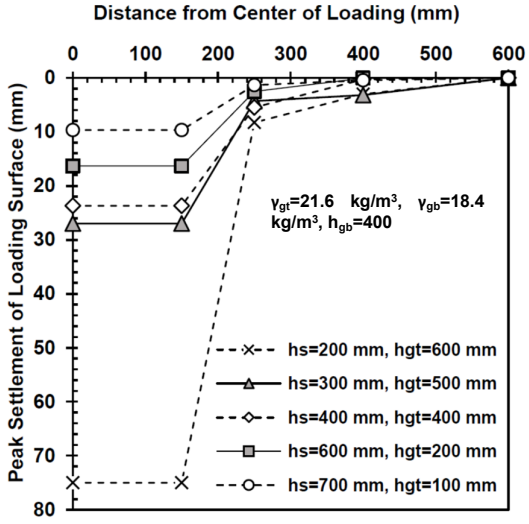

Figure 5-8: Profile of the peak settlements for different values of hs and hgt

Previous researchers [25, 87] have demonstrated that EPS geofoam shows a very small negative Poisson's ratio in its elastic region and a negative dilation angle in its plastic region. Ossa and Romo (2009) described that when the foam is compressed in three dimensions, the cellular volumes of air bubbles destruct and the internal structure of the foam buckles, resulting in lateral contraction of the material. This phenomenon leads to decrease in the strength of EPS with increase in the confining pressure and causes the material to deform in a punching manner. Therefore, it might be expected that EPS geofoam will not obey the rules of common analytical methods (at least in part), as will be discussed further in Section 5.3.7.

The larger surface settlements occurring for lower thicknesses of soil cover over the EPS layers are not exclusively a consequence of the thinner soil layers, but also due to the lower stiffnesses of those soil layers. As reported earlier, when the thickness is <400mm, the dry density of the soil reached a maximum value of 18.7 kN/m^3, whereas for 600~700 mm soil, the soil can be compacted to a dry density of 19.6 kN/m^3. This is related to the low mass and stiffness of EPS geofoam which does not provide an adequate base on which the soil mass can be compacted. Lower stiffness is expected to be associated with this lower compaction

thus achieving less load spreading and, hence, greater stress and settlements than would otherwise have been the case will be experienced immediately beneath the load.

5.3.5 Combined effect of upper and bottom EPS layers' thickness

In this section, the results of Test Series 5 are described. As discussed previously, a slight reduction in EPS usage can make a significant reduction in the cost of a highway project. Also, the cost effectiveness of an EPS backfill would be significantly affected by the thickness of the upper, higher density, EPS layer. In addition, if the thickness of such an upper EPS layer is too small, the safety of the pavement structure might be endangered due to out-of-specification deformations in the pavement. Hence, the optimum thickness of a high-density, upper, EPS layer has to be specified correctly.

Figure 5-9 illustrates the results of experiments on sections with different values of hgt and hgb. In part (a) of this diagram, it is clear that when hgt is 100 mm, settlement of the loading surface increases rapidly. It was observed that the upper EPS layer broke into two parts after the test, which can be supposed as the main reason for this dramatic increase in surface settlement in this test. However, it seems that rupture of the EPS block has not happened instantly after only a few cycles of loading, rather it happened gradually during loading. Observations from other tests suggest that when EPS blocks bend too much, invisible or very small cracks are generated in the tension region of the block (in this case, the bottom of the block), then the cracks develop under subsequent loading cycles and, eventually, the block ruptures fully or partially. For thicker blocks however, the height of the section and its moment of inertia increases. This action helps to reduce tensile stress at the bottom of the upper EPS block and, hence, will extend its bending resistance to more repetitions of loading.

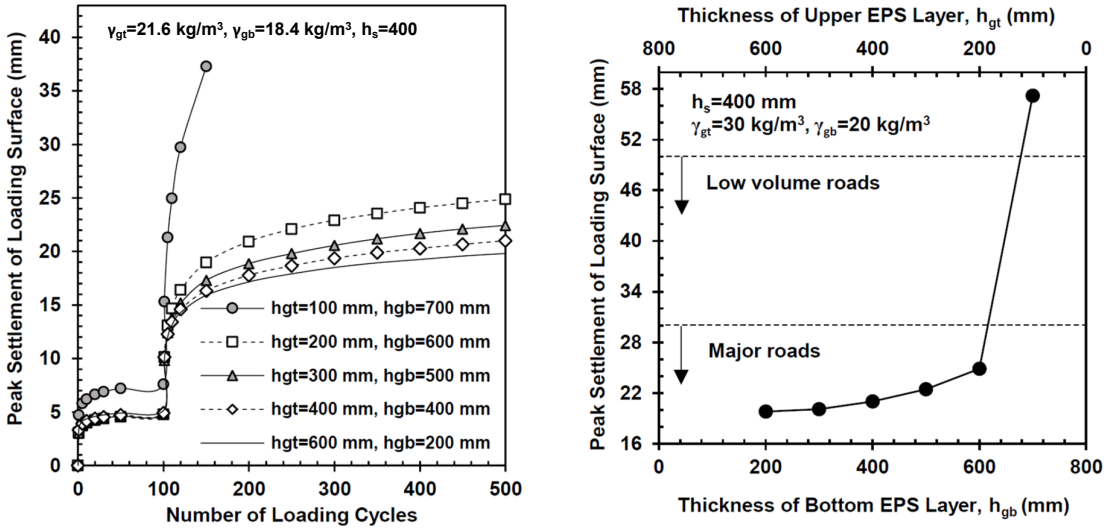

Figure 5-9: (a) Settlement of loading surface with respect to no. of load cycles for different values of hgt and hgb, (b) Peak value of surface settlements for different values of hgt and hgb

Figure 5-9b displays peak settlements extracted after 500 repetitions of low and high intensity pressures (it is extracted at load cycle of 150 for the case of hgt=100 mm and

hgb=700 mm due to that test's early failure). When hgt is less than 200 mm, peak surface settlement has increased to 57 mm. When hgt is equal to or greater than 200 mm (200 mm to 600 mm), peak value of surface settlement remains between 17.4 mm to 23.7 mm, with very small variation, and a large drop from the settlement corresponding to hgt=100 mm. Thus hgt=200 mm is approximately a minimum value for the upper EPS layer under this loading. Thickness values of the upper EPS layer larger than 200mm would increase construction costs without delivering noticeable benefit in the reduction of settlements.

5.3.6 Effect of EPS density (EPS stiffness)

The influence of EPS density on the permanent deformation was explored in Test Series 6. With this aim, the density of EPS in both the upper and lower layers was changed and the repeated plate load test was repeated for each section. Values of hs, hgt and hgb were kept equal to 400, 200 and 600 mm, respectively. Based in Figure 5-10, the amplitude of settlement in the loading surface are stabilized below 6 mm after application of several cycles of low amplitude pressure for all cases.

For the higher amplitude of applied pressure, the settlement of the loading surface rises but stabilizes quickly when the density of upper and bottom EPS layers are 28.8 kg/m^3 and 28.8 kg/m^3 or 21.6 kg/m^3 and 21.6 kg/m^3, respectively. For 29-29, maximum settlement was limited to 9.6 mm and for 22-22, this value was about 11.4 mm at the end of tests. The settlements for these two cases are significantly lower than those of EPS 22 over EPS 19. Therefore, the lower stiffness of EPS 20 is implicated as the cause of larger settlements induced in the pavement surface. As discussed previously, the initial resilient modulus of EPS 19 is about 3~4 MPa, which means that most of such EPS enters its plastic region and deforms excessively compared to EPS 22 and EPS 29 at similar depths. However, such deformation is localized and limited to a small horizontal surface of EPS and could be reduced if proper load distribution mechanisms are used. EPS 19 over EPS 19 shows extreme deformation after a limited number of pressure application and is not suitable at all.

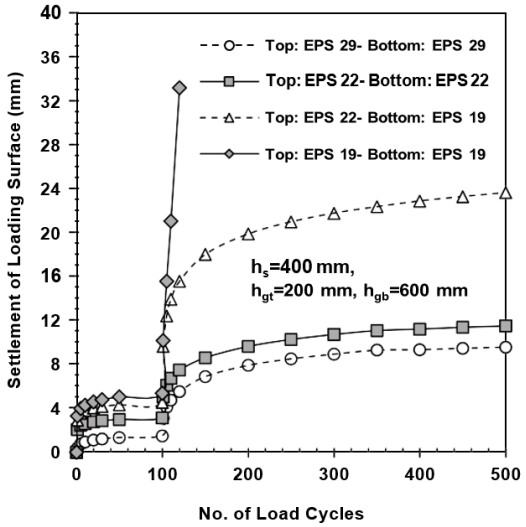

Figure 5-10: Settlement of loading surface with respect to no. of loading cycles for different values of EPS density at top and bottom layers

5.3.7 Further evaluation of results

Given that the experiments could only investigate a few of the many possible scenarios of use, the distribution of pressure in EPS layers and the likely settlement of the pavement surface, was investigated using simple analytical methods based on elasticity theory. Linear and nonlinear methods based on Burmister's layered theory, as implemented in the KENPAVE software, are available for such a purpose [86]. While a major part of the current test results (specifically those under repeated pressure of 550 kPa) are plastic in nature, the results obtained for lower repeated pressure (275 kPa) can be assumed as linear or nonlinear elastic, especially in the first cycle of loading – and it is elastic behavior that is required in a satisfactory installation. Therefore, an elastic analysis should be able to define the arrangements that deliver the limiting acceptable stresses for practical application although it would be incapable of predicting stresses and strains beyond this limit. Therefore the analysis of this section is based on these assumptions and the results might be valid for relatively smaller applied pressures. For larger applied pressure similar to Sections 5.3.4, the behavior might be different.

In both linear and non-linear methods, it is required to estimate the resilient modulus (or initial resilient modulus in the case of nonlinear method) of soil using the results of test performed on the soil alone. Simulation of the first cycle of loading of the test described in Section 5.3.1 using the linear method of KENPAVE gave a modulus of about 55 MPa for the soil alone. Moduli of upper and bottom EPS materials were equal to 2.16 and 0.81 MPa (see Table 3-1). These values were doubled based on the results of the study by Negussey (2007), so as to obtain reasonable results. Therefore, these values can represent as an equivalent elastic medium and serve as approximate implementation of the real system.

In KENPAVE, an approximate estimation of soil resilient modulus can be made based on to the first stress invariant. Although the simple k-θ model provides reasonable results when applied to triaxial test results, its application to layered system is somehow questionable. For example, while typical proposed values for k1 and k2 (which are positive) mean that soil's modulus increases with increasing confining pressure, observation by Uzan (1985) indicated that modulus for a soil can decrease with increase in the first stress invariant, θ, therefore k2 will be negative [88]. A negative value of k2 was also determined to be promising for the analysis of layered system in the current study.

A negative regression factor can be attributed to several reasons: first, the k-θ model neglects the effect of shear strain developed in the real layered system, while increase in the applied pressure generates larger confining pressure, development of shear strain might lead to decrease in the soil's modulus. It also does not take into account the effect of residual stress from compaction. Furthermore, resilient modulus values obtained from the tests indicates that for thinner soil layers, the apparent confining pressure is supposed to increase (similar to triaxial test), but in the case soft EPS geofoam underneath, the real confining pressure decreases. Therefore to match with the triaxial test results, a negative value had to be selected for k2 to match this model (that is originally obtained from laboratory triaxial tests) with the layered system of this study.

Another reason and possibly the most important reason for selecting a negative value for k2, would be the fact that the real variation of resilient modulus is decreasing until a certain vertical strain (e.g. about 0.002-0.004 in Uzan, 1985) and increasing after that. This can be the main reason for the negative value selected for the first cycle of lower amplitude pressure, where vertical strain is typically much smaller (0.016 to 0.007 on the pavement surface and much smaller in the middle of the soil layer) compared to the cases discussed in Sections 5.3.4 and 5.4.2 that resilient response is evaluated under larger applied pressures [88]. This approach was also adopted for EPS geofoam at subsequent layers, and by the use of proper calibration factors shown in Table 5-2 the desired results were obtained.

Table 5-2: Calibration factors for nonlinear analysis

Material	Calibration factors	
	k_1 (kPa)	k_2
Soil	60,000	-0.25
Upper EPS (EPS 22)	10,000	-0.01
Bottom EPS (EPS 19)	6,000	-0.01

The results for both the linear and nonlinear analyses, compared with the values measured in the experiments, are shown in Table 5-3. As shown in this table, the linear analysis gave a surface deflection of 2.5 mm and the pressures at depths of 400 mm and 600 mm were equal to 14.9 kPa and 7.5 kPa, respectively. The variation from the experimentally measured value is -38% in the case of surface settlement and equal to -55% to -66% for the transferred pressures. Using the nonlinear method, the surface settlement was calculated as 3.8 mm (-5 % deviation) and the pressures at depths of 400 mm and 600 mm were 38 kPa (+15% deviation) and 11.4 kPa (-22% deviation).

Table 5-3: Comparison of linear and nonlinear methods with those of test measurements for applied pressure of 275 kPa

Method	Surface settlement (mm)	Measured/calculated pressures (kPa) at depths			
		400 (mm)	600 (mm)	800 (mm)	1000 (mm)
Test measurement	4	33	22	14	2.5
Boussinesq	-	49	24	14	9
KENPAVE (linear)	2.5	14.9	7.5	5.4	4
KENPAVE (nonlinear)	3.8	38	17.1	10.7	7.8

Comparison of different methods for calculation of transferred pressure at different layers of EPS is also depicted in Figure 5-11. Although Boussinesq method provides reasonable estimates of stress for depths greater than 400 mm, its result is far from the measured value at a depth of 400 mm (a +49% deviation). KENPAVE linear significantly underestimated results whereas the nonlinear method already gives a much closer match from a general point of view. Overall, it is clear that a simple linear analysis is inadequate for

such a pavement system and further studies including model tests or high accuracy nonlinear analysis might be needed to determine deflections and pressure with higher reliability. For the full range of depths, the KENPAVE nonlinear method gives the most accurate result of those evaluated.

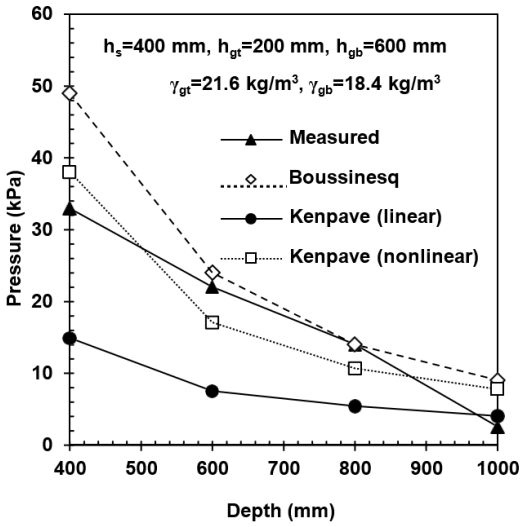

Figure 5-11: Transferred pressure at different depths obtained from analytical methods and test measurements for applied pressure of 275 kPa

Fig. 5-12a shows the effect of variation in initial soil resilient modulus (using the KENPAVE nonlinear method) on the pressure transferred to the surface of upper EPS layer, considering both EPS 22 and EPS 19 as the top layer. In this figure, the horizontal dashed lines indicate approximate threshold stress for stable response of EPS 22 and EPS 19 obtained from cubic sample tests. These values from tests were about 140 kPa and 90 kPa which were halved to provide a safety factor against unstable response of EPS geofoam. The measured point from the tests (Section 5.3.3) is close to the obtained curves, so the somewhat crude KENLAYER analysis may be useful. The figure shows that, with the EPS30, a soil with a modulus of less than 25 MPa (the vertical dashed arrow in Figure 5-12a) can't be used as the stress at the top of the EPS would be too large for that EPS, i.e. > 50kPa. With EPS19 as the upper layer (the total height composed of EPS19), none of the soil moduli deliver a safe stress when the soil thickness is 400 mm. This EPS density must be avoided from application as upper EPS layer. However, it must be remembered that the tolerable stress margins were halved. If the real stress margin (50 kPa) for EPS 19 is considered, soil with K1>30 MPa could be considered as acceptable, which is in agreement with the test results (see 5.3.6).

This approach could be easily repeated for other moduli and thicknesses of soil and EPS and for other loadings to determine the amount and quality of soil cover that is needed. To this aim, a sensitivity analysis on the effect of applied pressure, soil and upper EPS layers' thicknesses and upper and bottom EPS thicknesses analysis was performed. Figure 5-12b depicts the effect of loading intensity on the transferred pressure to the upper EPS layer with considering different k1 values. The thickness of soil, upper EPS layer and bottom EPS

layers were 400 mm, 200 mm and 600 mm, respectively and either EPS19 or EPS22 were used in the upper EPS layer. The figure indicates that for the applied pressure up to 275 kPa, all of the investigated cases are acceptable when EPS 30 is placed as the upper EPS layer. As k1 values are increased, the pressure transferred onto the EPS layers' decreases. For instance, when EPS 22 forms the upper layer, the maximum allowable applied pressure for k1=20, 40 and 60 MPa would be about 250 kPa, 310 kPa and 360 kPa, respectively. As before, using EPS 19 as the top layer failed to deliver acceptable behavior over the full range of applied pressure amplitudes.

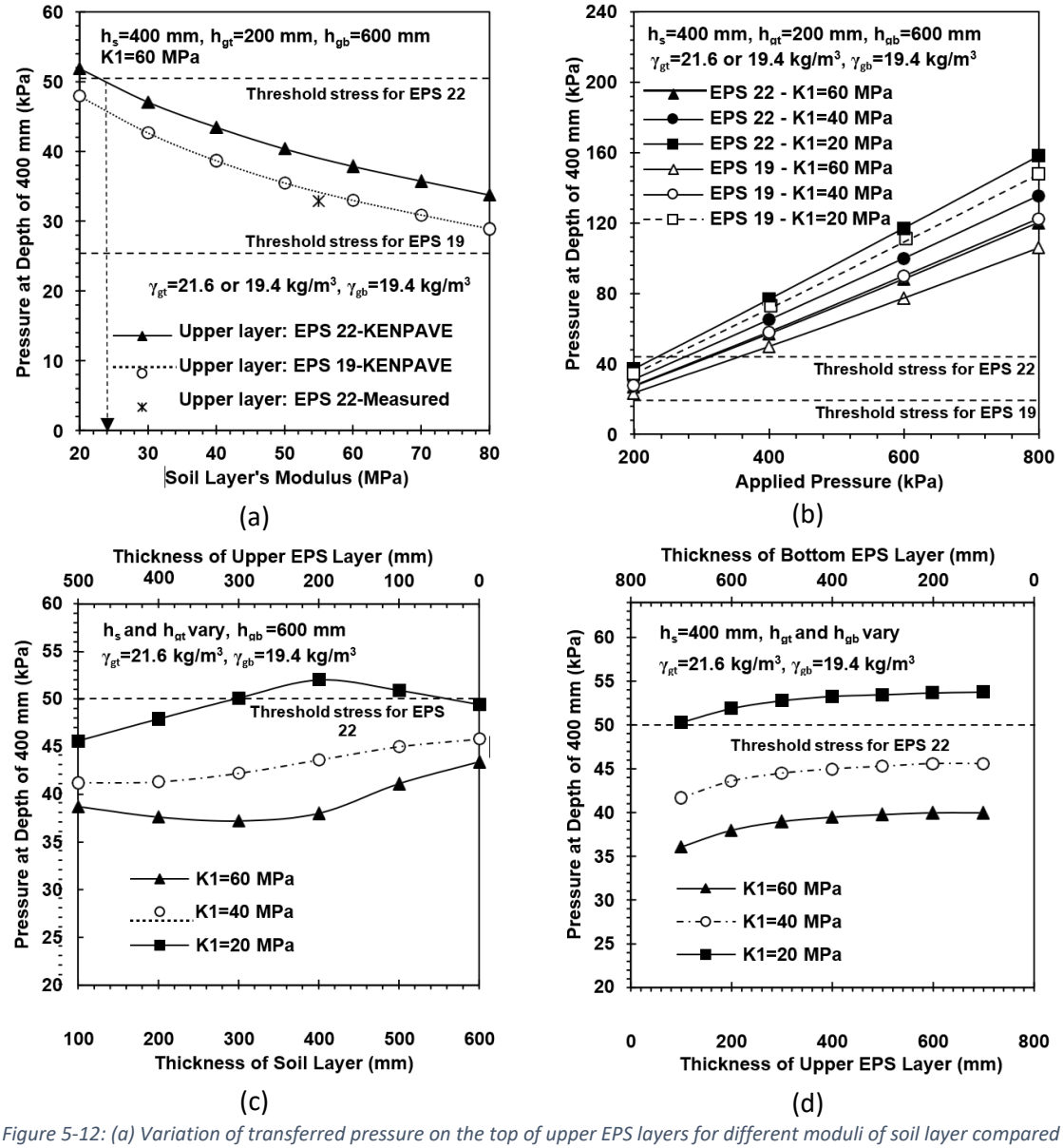

Figure 5-12: (a) Variation of transferred pressure on the top of upper EPS layers for different moduli of soil layer compared to the measured value for applied pressure of 275 kPa for the pavement with EPS 30 or EPS 20 as the top layer, (b) Effect of applied pressure intensity on the transferred pressure over the upper EPS layer, (c) Effect of soil and upper EPS layer thickness on the transferred pressure on the upper EPS layer and, (d) Effect of upper and bottom EPS layer thicknesses on the transferred pressure on the upper EPS layer

The combined effect of soil and upper EPS layer is shown in Figure 5-12c. The trend in the variation of the intensity of transferred pressure onto the upper EPS layer varies with the variation in soil stiffness (k1) and soil thickness. As a general understanding, a low value of soil stiffness (e.g. k1=20 MPa) must be avoided. For higher values of k1 though, a slight increase in the applied pressure can be observed at a depth of 400mm (i.e. poorer load spreading) with increase in soil thickness relative to upper EPS layer. Figure 5-12d displays the effect of upper and bottom EPS layers thicknesses while the thickness of soil was kept constant and equal to 400 mm. It can be seen that, when the thickness of upper EPS layer increases relative to the thickness of bottom EPS layer, the pressure slightly increases and remains constant beyond an EPS thickness of around 400mm.

The above discussion implies that for the specific kind of soil and EPS geofoam (or any similar material) used in this study, a rutting and transferred stress evaluation can be made of the effect of several factors, including soil and upper EPS layer thicknesses, density of EPS forming the top and bottom layers and applied surface pressure. A significant variation from the mentioned material characteristics might alter the predictions in a unfavorable way and hence, the application of the results must be extended with great care. Further investigation is certainly needed to discover some of the remaining issues including:

- a more rigorous characterization of the EPS's installed, as opposed to in-isolation, properties;
- the effect of the different potential EPS materials on the compaction of the covering soil layer,
- the stress distribution and the mechanism of possible failure at different amplitudes of repeated pressure.

Nevertheless, the results of this study bring deeper insight regarding the performance of pavements including EPS geofoam and improve our appreciation of the EPS-soil-load interaction effects. They show that the soil and upper EPS layer need to be considered together to ensure that the stress passed down from traffic through the soil to the EPS can be reduced to tolerable levels (i.e. sufficiently small to avoid EPS failure). Figure 5-12c suggests that, other than for light trucks, bound pavement layers will be required, perhaps with a very deliberate load spreading strategy if heavy truck loading is to be used and the weight benefit of EPS is to be obtained over a significant height of the embankment. Otherwise, there will be need for substantial thicknesses of covering soil (which opposes the purpose of using EPS) or high stress capacity EPS geofoam (with much greater load competency than EPS 22).

In general, for the tested loading amplitudes of 275 and 550 kPa, the unreinforced soil layer placed over EPS layers should not be selected thinner than 400 mm in terms of residual deformation, or 300 and 600 mm in terms of resilient modulus. Nevertheless, soil thicknesses of 400 and 600 mm can be selected as appropriate lower and upper bounds, as long as the mechanistic-empirical approach have not limited the resilient modulus. For the experiments reported above, when the thickness of soil layer is less than 400 mm, the transferred pressure on top of EPS layers increased beyond the safe stress limit of EPS 30,

which resulted in progressive increase in the strain of EPS layer. Therefore, the shear strain in the soil above the blocks increased until the soil failed in punching.

The thickness of the upper EPS layer is also influential and should not be lower 200 mm when the soil thickness is 400 mm, as the EPS block ruptures and cannot bear further pressure. The tensile strains start to grow in the soil layer above the cracked zone of EPS blocks, which results in shear or tensile failure of the whole soil layer, leading the pavement to undergo severe deformations at its surface. Therefore, the thickness of the upper EPS layer with a density of 21.6 kg/m^3 (the denser EPS) could be limited to as little as 200 mm, with a minimum covering soil thickness of 400 mm. Large thickness is not required for the upper EPS layer, as the further improvement in performance of pavement is small compared to the increase in cost of the project. Increasing the density of the bottom EPS layer significantly reduces rut depths (although, for the cases investigated, the rut would already be acceptable, before this increase), but is not recommended due to the extreme increase in project cost.

To summarize, a properly compacted layer of soil of thickness 400 mm placed above an upper EPS layer with a density of 21.6 kg/m^3 and a minimum thickness of 200 mm, in its turn placed on a bottom layer of EPS with a density 19.4 kg/m^3, would satisfy the range of settlements or rut depths for “low volume” and “major” roads (30 mm and 50 mm, respectively), as dictated by AASHTO T 221-90.

6 Summary, Conclusions and Suggestions

6.1 Introduction

To prevent EPS geofoam failure or long-term settlement of the embankment requires sufficient spreading of loads imposed at the ground surface so that the stresses on the EPS are not too large. This could be achieved by appropriate soil layers, but should be optimize, not to increases the embankment mass – while the purpose of the EPS was to reduce it. So more effective load spreading in a thin covering soil layer could be a competent method for improving the performance of the pavement foundation. Using large- scale repeated plate testing and a simplified Finite Element analysis in this study, the benefits of the soil layer overlying EPS geofoam backfill was assessed. The effect of repeated loading on the surface settlements, amplitude of the pressure transferred to the EPS geofoam and resilient modulus of the system was studied for different thicknesses of soil and different EPS densities. The following outcomes have been obtained:

6.2 Static loading

The results of the pavement foundation subjected to static loading can be extracted as:

1. To evaluate EPS properties from sample tests, a cylindrical shape might have an advantage over the cubic shape due to more uniform pressure distribution on the top and bottom surfaces of the samples.
2. A single sample is preferred to a series of samples arranged vertically in layers from top to bottom. Layered configurations tend to collapse due to instability caused by inadequate lateral support of the subsequent samples.
3. For a single sample of EPS, as the ratio of height to diameter increases, samples tend to deform in a buckling shape due to lateral instability. In such cases, the ultimate axial strain occurs at a reduced compressive strength depending on the H/D ratio.
4. With increasing strain rate, both elastic modulus and compressive strength of the EPS sample increase. The elastic modulus is more sensitive to the strain rate for denser EPS, while the overall sample strength over the plastic strain region is more sensitive to the strain rate for lighter EPS, which can be attributed to the damage to air bubbles as the applied pressure increases.
5. Increasing the EPS sample size (with constant H/D) does not considerably affect the overall stress-strain response of the EPS geofoam. However, the elastic moduli is shown to be dependent on the sample size and this dependency can be expressed in the form of a linear equation.
6. The elastic modulus of the EPS samples increases with increasing density of EPS geofoam and can be related to it using a simple linear function.
7. By implementing the stress-strain response from EPS sample tests in a numerical framework, the response of EPS geofoam samples can be reproduced with sufficient accuracy.

8. Using the numerical method, EPS samples with D=300 mm show 47% greater compressive resistance compared to samples with D=200 mm. The increase in resistance for D=200 mm compared to D=100 mm is 21%.
9. The engineering properties of the EPS of relevance can be expected to vary with supplier, EPS density and application. Therefore, the properties of the actual material to be used should be determined, as far as possible in the manner it is to be applied.
10. Compaction ability of the soil layers overlying EPS blocks depends on the proximity of the two materials. For a thickness of 100~200 mm of soil layer placed over EPS geofoam blocks, the maximum dry density of soil might be around 5% less than it would be in a layer around 400mm thick.
11. Thickness of the overlying soil layer has a considerable influence on the bearing capacity of pavement foundations supported on EPS geofoam. For instance, reducing the soil thickness from 600 to 300 mm can double the settlements observed on the pavement surface.
12. Density of EPS geofoam is another important factor that affects the performance of such pavement systems. For instance, with soil thickness of 400 mm and the applied pressure of 800 kPa, while employing a 200 mm thick EPS 29 or 22 on EPS 29 or 22 would not result in significant settlements, using EPS 30 on EPS 20 (with the same thicknesses) would trigger a punching mode failure on the pavement's surface before reaching the ultimate amplitude of applied pressure.
13. Geocell reinforcement can reduce surface settlement of the pavement foundation by up to 54% for EPS 22/19 when the ultimate magnitude pressure (800 kPa) is applied. The reduction in surface settlement by provision of geocell increases as the applied pressure increases.
14. The improvement or settlement reduction obtained from geocell would be greater when the geocell reinforced soil is used on lower density EPS beds. Furthermore, the influence of geocell is larger when thinner soil layer is employed.
15. The observed behavior in the unreinforced and reinforced pavement foundations on EPS geofoam can be attributed to the transferred pressure on the EPS geofoam (SR). The major amount of settlement initiates when the transferred pressure has approached or exceeded the compressive strength of EPS geofoam (or when SR grows further than 1.0).
16. By using geocell reinforcement, the excessive increase in surface settlement due to the gaps between EPS blocks could be almost vanished. When discontinuous EPS geofoam blocks are tightly arranged (the opening between EPS blocks is zero), load- settlement curve of the pavement foundation would be almost identical to those of the continuous formation of EPS blocks. Increasing the gap size of blocks to 5 mm in the unreinforced cases will induce 60% increase in the surface settlements at the ultimate applied pressure.
17. The settlement occurring on the surface of EPS geofoam pavement foundations could be related to the linear and nonlinear phases of the soil and underlying EPS geofoam material. Considering the interaction between these phases of soil and EPS geofoam, the resultant response could be divided into 2 or 3 phases, depending on the reinforcement status, soil thickness and EPS density.

18. The optimum embedment depth of EPS geofoam is about 0.1-0.2 times of diameter of the loading plate. However due to the practical concerns, a minimum value of u/D= 0.2 is recommended.

6.3 Repeated loading

The results of unreinforced pavement foundation subjected to repeated loading can be drawn as:

1. If an unpaved road consisting of EPS layers is subjected to the repeated loading of heavy trucks (800 kPa), deep ruts will certainly occur on the pavement surface and the operational life of the pavement will considerably decrease due to punching failure in the soil as a consequence of crushing of the EPS. However, the additional load transfers likely to be achieved by providing a bound, sealed surface, can be expected to reduce the stress in the soil and on top of the EPS to a level where the system can tolerate a large number of load repetitions.
2. The pressures likely to be applied by a light truck (275 kPa) are insufficient to produce large ruts on the surface of a pavement that includes EPS geofoam covered with 400mm of soil. However, pressure from the tires of a heavy truck (550 kPa) are likely to generate internal stresses that exceed tolerable limits unless other construction measures are introduced.
3. The thickness of the soil layer covering the EPS geofoam bed is a key factor affecting the value of settlements experienced at the loading surface. The compaction (and, hence, the shear strength) of soil placed on the EPS backfill is dependent on the thickness of soil layer placed on the top of EPS geofoam. Therefore, the value of hs affect the settlements in a duplicated way including the “thickness” itself and the achievable “compaction”. For example, when hs is equal to 200 mm, the pavement surface deforms excessively and cannot resist a large number of pressure applications.
4. In order to find an optimum thickness for soil and upper EPS layer (a cost effective and time saving solution), hs and hgt were varied in a way that their total value was kept constant. For a medium thickness of soil (hs =300mm) the surface deformation after 500 cycles of load reduced by 14, 41 and 65% as the soil thickness was increased by 33, 100 and 133%, therefore optimizing soil thickness is critical. The desired value can be selected based on the design priorities and economic factors. For all of the cases, the residual (plastic) surface settlement was about 78% of the total settlement.
5. As denser, more load resistant, EPS geofoam is costlier then the less dense type, a key design goal is to determine the thickness of upper and bottom EPS layers. With a reasonable soil cover (hs=400 m), increasing the thickness of a denser and stiffer upper EPS layer from hgt=200 mm to hgt=600 mm only caused a 20% decrease in the total settlement of loading surface. On the other hand, reduction of hgt lower than 200 mm, will induce extreme ruts on the pavement surface due to the rupture of that upper EPS layer.
6. Density of EPS in the subsequent layers has critical influence on the performance of the EPS embankment. Using EPS 29 for upper and bottom EPS layer can reduce the depth of surface ruts up to 60% after total application of 500 load cycles, with respect to EPS 22

and 19 as top and bottom layers. When the top and bottom layers are EPS 22, the mentioned reduction is 52%. However, application of upper and bottom densities of 29 kg/m^3 over 29 kg/m^3 or 22 kg/m^3 over 22 kg/m^3 and are not practical and will increase the costs of the project. The case of 19 kg/m^3 EPS placed over 19 kg/m^3 EPS is insufficient for application against 550 kPa and deforms excessively after a limited number of applications of repeated pressure.

7. An initial stress analysis was performed to investigate the sensitivity of the stress applied to the top of the EPS geofoam. It showed that there will be limiting moduli and thicknesses for the overlying soil. Therefore, it will be important to ensure a well-compacted and carefully selected overlying soil of adequate thickness to ensure that the EPS isn't overloaded and, thereby, prone to punching failure. The exact thicknesses and stiffnesses will depend on materials employed.

6.4 Suggestion for future research

Some of the highlights for the future research developments could be recommended as:

1. Using a low rate for static loading and low frequency for repeated loading, the results of this research represent the lower boundary for the performance of pavement foundations on EPS geofoam. Investigating the effect of loading rate and frequency is recommended.
2. Although from field observations, it has been proved that the effect of creep is negligible, it would be interesting to test the effect of long-term loading in the laboratory controlled condition.
3. Effect of different soil reinforcement (e.g. geocell, geotextile, planar in one or more layers) are worth investigating in the future research.
4. Development of the numerical modeling for repeated loading requires stronger hardware and can be performed for the future development of this work.

7 References

[1] A. F. Elragi, "Selected engineering properties and applications of EPS geofoam," ed: State University of New York. College of Environmental Science and Forestry …, 2000.

[2] A. Mohajerani, M. Ashdown, L. Abdihashi, M. J. C. Nazem, and B. Materials, "Expanded polystyrene geofoam in pavement construction," vol. 157, pp. 438-448, 2017.

[3] S. F. Bartlett, B. N. Lingwall, J. J. G. Vaslestad, and Geomembranes, "Methods of protecting buried pipelines and culverts in transportation infrastructure using EPS geofoam," vol. 43, no. 5, pp. 450-461, 2015.

[4] T. Stark, S. Bartlett, and D. J. T. E. I. A. Arellano, "Expanded polystyrene (EPS) geofoam applications and technical data," vol. 1298, p. 36, 2012.

[5] J. J. G. Horvath and Geomembranes, "Expanded polystyrene (EPS) geofoam: an introduction to material behavior," vol. 13, no. 4, pp. 263-280, 1994.

[6] J. S. J. G. Horvath and Geomembranes, "The compressible inclusion function of EPS geofoam," vol. 15, no. 1-3, pp. 77-120, 1997.

[7] T. D. Stark, D. Arellano, J. S. Horvath, and D. J. N. w. d. Leshchinsky, "Geofoam applications in the design and construction of highway embankments," vol. 65, p. 792, 2004.

[8] M. Duškov and W. Erkelens, "Dutch N201 road embankment with EPS geofoam," in *5th international conference on geofoam blocks in construction applications*, 2019, pp. 89-97: Springer.

[9] D. Negussey and A. W. J. U. D. o. T. Stuedlein, Rep. No. UT, "Geofoam fill performance monitoring," vol. 3, 2003.

[10] M. I. Khan, M. A. J. I. J. o. G. Meguid, and G. Engineering, "Experimental investigation of the shear behavior of EPS geofoam," vol. 4, no. 2, pp. 1-12, 2018.

[11] J. S. J. J. o. p. o. c. f. Horvath, "Emerging trends in failures involving EPS-block geofoam fills," vol. 24, no. 4, pp. 365-372, 2010.

[12] T. D. Stark, *Guideline and recommended standard for geofoam applications in highway embankments*. Transportation Research Board, 2004.

[13] V. Schaefer *et al.*, "Ground modification methods reference manual—Volume II," 2017.

[14] L. Sun, T. C. Hopkins, and T. L. Beckham, "Use of Ultra-Lightweight Geofoam to Reduce Stresses in Highway Culvert Extensions," 2005.

[15] D. Arellano, T. D. Stark, J. S. Horvath, and D. J. P. D. F. R. Leshchinsky, NCHRP Project No. 24-11, "Guidelines for geofoam applications in slope stability projects," 2011.

[16] A. O'Brien, "Design and construction of the UK's first polystyrene embankment for railway use," in *3rd international conference on EPS geofoam blocks in construction applications, Salt Lake City, USA*, 2001, pp. 9-11.

[17] A. T. Özer and E. Akınay, "First geofoam roadway embankment application in Turkey," in *5th International Conference on Geofoam Blocks in Construction Applications*, 2019, pp. 71-80: Springer.

[18] G. Athanasopoulos, P. Pelekis, and V. J. G. I. Xenaki, "Dynamic properties of EPS geofoam: an experimental investigation," vol. 6, no. 3, pp. 171-194, 1999.

[19] R. J. Bathurst, S. Zarnani, A. J. S. D. Gaskin, and E. Engineering, "Shaking table testing of geofoam seismic buffers," vol. 27, no. 4, pp. 324-332, 2007.
[20] M. S. El-kady, M. A. Alzara, and M. A. J. I. I. S. Farouk, "Reduction of lateral earth pressure using Geo-foam blocks," vol. 3, no. 1, p. 40, 2018.
[21] J. S. Tingle and S. R. J. T. r. r. Jersey, "Empirical design methods for geosynthetic-reinforced low-volume roads," vol. 1989, no. 1, pp. 91-101, 2007.
[22] M. Mengelt, T. Edil, C. J. G. E. R.-. Benson, Department of Civil, and U. o. W.-M. Environmental Engineering, Madison, Wisconsin, "Reinforcement of flexible pavements using geocells," p. 180, 2000.
[23] S. K. Pokharel, J. Han, D. Leshchinsky, R. L. Parsons, I. J. G. Halahmi, and Geomembranes, "Investigation of factors influencing behavior of single geocell-reinforced bases under static loading," vol. 28, no. 6, pp. 570-578, 2010.
[24] M. J. G. Duškov and Geomembranes, "Materials research on EPS20 and EPS15 under representative conditions in pavement structures," vol. 15, no. 1-3, pp. 147-181, 1997.
[25] A. Ossa and M. J. G. I. Romo, "Micro-and macro-mechanical study of compressive behavior of expanded polystyrene geofoam," vol. 16, no. 5, pp. 327-338, 2009.
[26] H. J. G. Hazarika and Geomembranes, "Stress–strain modeling of EPS geofoam for large-strain applications," vol. 24, no. 2, pp. 79-90, 2006.
[27] A. C. Trandafir, S. F. Bartlett, B. N. J. G. Lingwall, and Geomembranes, "Behavior of EPS geofoam in stress-controlled cyclic uniaxial tests," vol. 28, no. 6, pp. 514-524, 2010.
[28] C. Ling, J. Ivens, P. Cardiff, and M. D. J. I. J. o. M. S. Gilchrist, "Deformation response of EPS foam under combined compression-shear loading. Part I: Experimental design and quasi-static tests," vol. 144, pp. 480-489, 2018.
[29] F. Lekarp, U. Isacsson, and A. J. J. o. t. e. Dawson, "State of the art. I: Resilient response of unbound aggregates," vol. 126, no. 1, pp. 66-75, 2000.
[30] M. Mengelt, T. Edil, and C. J. G. I. Benson, "Resilient modulus and plastic deformation of soil confined in a geocell," vol. 13, no. 5, pp. 195-205, 2006.
[31] S. Werkmeister, A. R. Dawson, and F. J. T. R. R. Wellner, "Permanent deformation behavior of granular materials and the shakedown concept," vol. 1757, no. 1, pp. 75-81, 2001.
[32] A. C. Trandafir and B. A. J. J. o. m. i. c. e. Erickson, "Stiffness degradation and yielding of EPS geofoam under cyclic loading," vol. 24, no. 1, pp. 119-124, 2012.
[33] A. Ossa, M. J. G. Romo, and Geomembranes, "Dynamic characterization of EPS geofoam," vol. 29, no. 1, pp. 40-50, 2011.
[34] S. Srirajan, D. Negussey, and N. J. G. R. C. Anasthas, "Creep behavior of EPS geofoam," 2001.
[35] D. J. S. CIWMB, California, "Statewide Waste Characterization Study," 2004.
[36] T. S. Vinson, J. W. Rooney, and W. H. Haas, *Roads and Airfields in Cold Regions: A State of the Practice Report*. ASCE Publications, 1996.
[37] W. Chen *et al.*, "Static and dynamic mechanical properties of expanded polystyrene," vol. 69, pp. 170-180, 2015.

[38] S. F. Bartlett, B. N. Lingwall, and J. Vaslestad, "Methods of protecting buried pipelines and culverts in transportation infrastructure using EPS geofoam," (in English), *Geotextiles and Geomembranes,* vol. 43, no. 5, pp. 450-461, Oct 2015.

[39] M. Arshad, M. F. J. C. Ahmed, and B. Materials, "Potential use of reclaimed asphalt pavement and recycled concrete aggregate in base/subbase layers of flexible pavements," vol. 151, pp. 83-97, 2017.

[40] A. Arulrajah, J. Piratheepan, M. M. Disfani, and M. J. J. o. m. i. c. e. Bo, "Resilient moduli response of recycled construction and demolition materials in pavement subbase applications," vol. 25, no. 12, pp. 1920-1928, 2013.

[41] A. Arulrajah, J. Piratheepan, and M. M. J. J. o. M. i. C. E. Disfani, "Reclaimed asphalt pavement and recycled concrete aggregate blends in pavement subbases: laboratory and field evaluation," vol. 26, no. 2, pp. 349-357, 2014.

[42] A. Arulrajah, E. Yaghoubi, Y. C. Wong, S. J. C. Horpibulsuk, and b. materials, "Recycled plastic granules and demolition wastes as construction materials: Resilient moduli and strength characteristics," vol. 147, pp. 639-647, 2017.

[43] J. Donrak, R. Rachan, S. Horpibulsuk, A. Arulrajah, and Y. J. J. J. o. C. P. Du, "Improvement of marginal lateritic soil using melamine debris replacement for sustainable engineering fill materials," vol. 134, pp. 515-522, 2016.

[44] R. N. Georgees, R. A. Hassan, R. P. Evans, and P. J. I. J. o. P. E. Jegatheesan, "An evaluation of performance-related properties for granular pavement materials using a polyacrylamide additive," vol. 19, no. 2, pp. 153-163, 2018.

[45] A. R. Ghanizadeh, M. Rahrovan, K. B. J. C. Bafghi, and B. Materials, "The effect of cement and reclaimed asphalt pavement on the mechanical properties of stabilized base via full-depth reclamation," vol. 161, pp. 165-174, 2018.

[46] C. Gnanendran, J. Piratheepan, J. Ramanujam, and A. J. G. T. J. Arulrajah, "Accelerated laboratory pavement model test on cemented base and clay subgrade," vol. 34, no. 4, pp. 297-309, 2011.

[47] P. Jegatheesan and C. J. I. J. o. G. Gnanendran, "Permanent deformation study of pavement layers using laboratory pavement model testing," vol. 16, no. 3, p. 04015072, 2016.

[48] J. Li, M. Saberian, and B. T. J. J. o. e. m. Nguyen, "Effect of crumb rubber on the mechanical properties of crushed recycled pavement materials," vol. 218, pp. 291-299, 2018.

[49] S. Patel and J. J. J. o. M. i. C. E. Shahu, "Comparison of industrial waste mixtures for use in subbase course of flexible pavements," vol. 30, no. 7, p. 04018124, 2018.

[50] J. Piratheepan, C. Gnanendran, and A. J. J. o. m. i. c. e. Arulrajah, "Determination of c and ϕ from IDT and unconfined compression testing and numerical analysis," vol. 24, no. 9, pp. 1153-1164, 2012.

[51] M. A. Rahman, M. A. Imteaz, A. Arulrajah, J. Piratheepan, and M. M. J. J. o. C. P. Disfani, "Recycled construction and demolition materials in permeable pavement systems: geotechnical and hydraulic characteristics," vol. 90, pp. 183-194, 2015.

[52] M. Saberian, J. Li, B. Nguyen, G. J. C. Wang, and B. Materials, "Permanent deformation behaviour of pavement base and subbase containing recycle concrete aggregate, coarse and fine crumb rubber," vol. 178, pp. 51-58, 2018.

[53] J. Tavira, J. R. Jiménez, J. Ayuso, M. J. Sierra, E. F. J. C. Ledesma, and B. Materials, "Functional and structural parameters of a paved road section constructed with mixed recycled aggregates from non-selected construction and demolition waste with excavation soil," vol. 164, pp. 57-69, 2018.

[54] S. M. Tafreshi, O. Khalaj, A. J. G. Dawson, and Geomembranes, "Repeated loading of soil containing granulated rubber and multiple geocell layers," vol. 42, no. 1, pp. 25-38, 2014.

[55] J. K. Thakur, J. Han, S. K. Pokharel, R. L. J. G. Parsons, and Geomembranes, "Performance of geocell-reinforced recycled asphalt pavement (RAP) bases over weak subgrade under cyclic plate loading," vol. 35, pp. 14-24, 2012.

[56] S. M. Tafreshi, A. J. G. Dawson, and Geomembranes, "A comparison of static and cyclic loading responses of foundations on geocell-reinforced sand," vol. 32, pp. 55-68, 2012.

[57] M. DeMerchant, A. Valsangkar, A. J. G. Schriver, and Geomembranes, "Plate load tests on geogrid-reinforced expanded shale lightweight aggregate," vol. 20, no. 3, pp. 173-190, 2002.

[58] A. Hegde, T. J. G. Sitharam, and Geomembranes, "3-Dimensional numerical modelling of geocell reinforced sand beds," vol. 43, no. 2, pp. 171-181, 2015.

[59] L. Brito, A. R. Dawson, P. J. P. o. t. t. I. o. t. B. C. o. R. Kolisoja, Railways,, and C. I. Airfields , USA, "Analytical evaluation of unbound granular layers in regard to permanent deformation," pp. 187-196, 2009.

[60] J. K. Thakur, J. Han, and R. L. J. J. o. M. i. C. E. Parsons, "Factors influencing deformations of geocell-reinforced recycled asphalt pavement bases under cyclic loading," vol. 29, no. 3, p. 04016240, 2017.

[61] X. Sun, J. Han, J. Kwon, R. L. Parsons, M. H. J. G. Wayne, and Geomembranes, "Radial stresses and resilient deformations of geogrid-stabilized unpaved roads under cyclic plate loading tests," vol. 43, no. 5, pp. 440-449, 2015.

[62] E. M. Palmeira, L. G. J. G. Antunes, and Geomembranes, "Large scale tests on geosynthetic reinforced unpaved roads subjected to surface maintenance," vol. 28, no. 6, pp. 547-558, 2010.

[63] X. Yang *et al.*, "Accelerated pavement testing of unpaved roads with geocell-reinforced sand bases," vol. 32, pp. 95-103, 2012.

[64] I. Gonzalez-Torre, M. A. Calzada-Perez, A. Vega-Zamanillo, D. J. C. Castro-Fresno, and B. Materials, "Evaluation of reflective cracking in pavements using a new procedure that combine loads with different frequencies," vol. 75, pp. 368-374, 2015.

[65] P. Peralta, *Investigations on the behavior of large diameter piles under long-term lateral cyclic loading in cohesionless soil*. na, 2010.

[66] A. Shafikhani, T. V. Bheemasetti, A. J. Puppala, and A. Banerjee, "Analysis and interpretation of inclinometer and pressure cell data on a soil-geofoam embankment," in *GeoShanghai International Conference*, 2018, pp. 410-418: Springer.

[67] Y. Zou, C. Leo, and J. J. G. I. Small, "Behaviour of EPS geofoam as flexible pavement subgrade material in model tests," vol. 7, no. 1, pp. 1-22, 2000.

[68] M. J. G. Duškov and Geomembranes, "Measurements on a flexible pavement structure with an EPS geofoam sub-base," vol. 15, no. 1-3, pp. 5-27, 1997.
[69] J. C. Barrett, A. J. J. G. Valsangkar, and Geomembranes, "Effectiveness of connectors in geofoam block construction," vol. 27, no. 3, pp. 211-216, 2009.
[70] S. Moghaddas Tafreshi, O. Khalaj, and A. J. G. I. Dawson, "Pilot-scale load tests of a combined multilayered geocell and rubber-reinforced foundation," vol. 20, no. 3, pp. 143-161, 2013.
[71] R. J. T. r. r. Gandahl, "Polystyrene foam as a frost protection measure on national roads in Sweden," no. 1146, 1988.
[72] M. P. Newman, S. Bartlett, E. J. J. o. g. Lawton, and g. engineering, "Numerical modeling of geofoam embankments," vol. 136, no. 2, pp. 290-298, 2010.
[73] D. Negussey, A. Stuedlein, S. Bartlett, and C. Farnsworth, "Performance of a geofoam embankment at 100 South, I-15 reconstruction project, Salt Lake City, Utah," in *Proceedings on 3rd international conference on EPS Geofoam*, 2001.
[74] H. Hazarika, S. J. S. Okuzono, and Foundations, "Modeling the behavior of a hybrid interactive system involving soil, structure and EPS geofoam," vol. 44, no. 5, pp. 149-162, 2004.
[75] H. Wong, C. J. J. G. Leo, and Geomembranes, "A simple elastoplastic hardening constitutive model for EPS geofoam," vol. 24, no. 5, pp. 299-310, 2006.
[76] M. Meguid, M. Hussein, M. Ahmed, Z. Omeman, J. J. G. Whalen, and Geomembranes, "Investigation of soil-geosynthetic-structure interaction associated with induced trench installation," vol. 45, no. 4, pp. 320-330, 2017.
[77] B. S. Chun, H.-S. Lim, M. Sagong, K. J. G. Kim, and Geomembranes, "Development of a hyperbolic constitutive model for expanded polystyrene (EPS) geofoam under triaxial compression tests," vol. 22, no. 4, pp. 223-237, 2004.
[78] J.-P. Magnan and J.-F. J. B. d. l. d. l. d. p. e. c. Serratrice, "Propriétés mécaniques du polystyrène expansé pour ses applications en remblai routier," no. 164, pp. 25-31, 1989.
[79] D. S. J. D. S. Simulia, Providence, RI, "ABAQUS 6.13 User's manual," vol. 305, p. 306, 2013.
[80] X. Yang, J. Han, R. L. Parsons, D. J. F. o. A. Leshchinsky, and C. E. i. China, "Three-dimensional numerical modeling of single geocell-reinforced sand," vol. 4, no. 2, pp. 233-240, 2010.
[81] B. Christopher, C. Schwartz, and R. J. N. H. I. Boudreau, Federal Highway Administration, US Department of Transportation, Washington, DC, "Geotechnical Aspects of Pavements FHWA NHI-05-037," 2006.
[82] R. Hicks, "Factors influencing the resilient properties of granular materials," Thesis submitted to the University of California, Berkeley for the degree of …, 1970.
[83] Y. Qiu, N. DENNIS, R. J. S. ELLIOTT, and foundations, "Design criteria for permanent deformation of subgrade soils in flexible pavements for low-volume roads," vol. 40, no. 1, pp. 1-10, 2000.
[84] D. Kim and S. Park, "Relationship between the subgrade reaction modulus and the strain modulus obtained using a plate loading test," in *9th World Congress on Railway Research, Lille-France*, 2011.

[85] G. Rada and M. W. Witczak, *Comprehensive evaluation of laboratory resilient moduli results for granular material* (no. 810). 1981.
[86] Y. H. Huang, "Pavement analysis and design," 2004.
[87] B. N. Lingwall, *Development of an expanded polystyrene geofoam cover system for pipelines at fault crossings*. The University of Utah, 2011.
[88] J. J. T. r. r. Uzan, "Characterization of granular material," vol. 1022, no. 1, pp. 52-59, 1985.

8 Publication

1) **Khalaj, Omid**, Sohan, Abedin Nejad, and Tomas, Janda. "Multi Elements Simulation of Biaxial Test with Two Different Soil Layers Using Hypoplastic Constitutive Model." In IOP Conference Series: Materials Science and Engineering, vol. 1161, no. 1, p. 012001. IOP Publishing, 2021.
2) **Khalaj, Omid**, Naser Joz Darabi, Seyed Naser Moghaddas Tafreshi, and Hana Jirková. "Assessment the Role of Expanded-Polysterene Block and Grogrid Layer on Behavior of Buried Pipeline." In IOP Conference Series: Earth and Environmental Science, vol. 609, no. 1, p. 012014. IOP Publishing, 2020.
3) **Khalaj, Omid**, S. Abedin Nejad, and Stepan Jenicek. "The Effect of Geocell Reinforced Embankment Construction on the Behaviour of Beneath Soil Layers Using Numerical Analysis." In IOP Conference Series: Earth and Environmental Science, vol. 609, no. 1, p. 012015. IOP Publishing, 2020.
4) **Khalaj, Omid**, Mehran Azizian, Naser Joz Darabi, Seyed Naser Moghaddas Tafreshi, and Hana Jirková. "The Role of Expanded Polystyrene and Geocell in Enhancing the Behavior of Buried HDPE Pipes under Trench Loading Using Numerical Analyses." Geosciences 10, no. 7 (2020): 251.
5) **Khalaj, Omid**, Seyed Mohammad Amin Ghotbi Siabil, Mehran Azizian, Seyed Naser Moghaddas Tafreshi, Bohuslav Masek, Miloslav Kepka, Tomas Kavalir, Michal Krizek, and Hana Jirkova. "Experimental and numerical investigation of expanded polystyrene (EPS) geofoam samples under monotonic loading." Geomechanics and Engineering 22, no. 6 (2020): 475-488.
6) **Khalaj, Omid**, Seyed Mohammad Amin Ghotbi Siabil, Seyed Naser Moghaddas Tafreshi, Miloslav Kepka, Tomáš Kavalir, Michal Křížek, and Štěpán Jeníček. "The experimental investigation of behaviour of expanded polystyrene (EPS)." In IOP Conference Series: Materials Science and Engineering, vol. 723, no. 1, p. 012014. IOP Publishing, 2020.
7) **Khalaj, Omid**, Seyed Mohammad Amin Ghotbi Siabil, Seyed Naser Moghaddas Tafreshi, and Hana Jirkova. "Performance evaluation of pavements constructed on EPS geofoam backgill using repeated plate load test." In IOP Conference Series: Earth and Environmental Science. Institute of Physics Publishing, 2019.
8) **Khalaj, Omid**, Naser Joz Darabi, Seyed Naser Moghaddas Tafreshi, and Štěpán Jeníček. "Damping Ratio of Foundation Bed with Multi-layered Rubber-Soil Mixtures." In IOP Conference Series: Earth and Environmental Science, vol. 221, no. 1, p. 012008. IOP Publishing, 2019.
9) **Khalaj, Omid**, N. Joz Darabi, SN Moghaddas Tafreshi, and Bohuslav Mašek. "Protection of buried pipe under repeated loading by geocell reinforcement." In IOP Conference Series: Earth and Environmental Science, vol. 95, no. 2, p. 022030. IOP Publishing, 2017.
10) **Khalaj, Omid**, Azizian mehran, Seyed Naser Moghaddas Tafreshi, and Bohuslav Mašek. "Laboratory investigation of buried pipes using geogrid and EPS geofoam block." In IOP conference series: earth and environmental science, vol. 95, no. 2, p. 022002. IOP Publishing, 2017.

11) **Khalaj, Omid,** Shervin Davarifard, Seyed Naser Moghaddas Tafreshi, and Bohuslav Mašek. "Cyclic Response of Footing with Embedment Depth on Multi-Layered Geocell-Reinforced Bed." In IOP Conference Series: Earth and Environmental Science, vol. 44, no. 2, p. 022015. IOP Publishing, 2016.
12) **Khalaj, Omid,** Tafreshi, SN Moghaddas, A. R. Dawson, and B. Mašek. "Repeated load response of soil reinforced by two layers of geocell." Procedia Earth and Planetary Science 15 (2015): 99-104.
13) **Khalaj, Omid**, Zakeri, Reza, Seyed Naser Moghaddas Tafreshi, Masek, Bohuslav and Stadler, Ctibor. " The Effect of a Rubber Sheet on the Dynamic Response of a Machine Foundation Located over a Small Thickness of Soil Layer." In IOP Conference Series: Earth and Environmental Science, In Press.
14) **Khalaj, Omid**, Zakeri, Reza, Seyed Naser Moghaddas Tafreshi, Masek, Bohuslav and Stadler, Ctibor. "The Experimental Investigation of the Repeated-Loading Behaviour of the Sand-Rubber-Mixture (SRM)." In IOP Conference Series: Earth and Environmental Science, In Press.